



**Tomas Bata University in Zlín**  
**Faculty of Technology**

**Doctoral thesis**

**Properties and behaviors of polymeric systems  
containing mineral fillers**

Vlastnosti a chování polymerních systémů s bílými  
plnivy

Ing. Zdeněk Závorka

Programme: Chemistry and Materials Technology  
Course: Technology of Macromolecular Substances  
Supervisor: doc. Ing. Jiří Maláč, CSc.

Zlín, 2013

## **ACKNOWLEDGEMENTS**

I would like to express my appreciation to my supervisor doc. Ing. Jiří Maláč, CSc. for his guidance and support throughout the completion of this work. I would also like to thank Brian Cardwell for his great advice, suggestions and critical evaluation of my work; as well as Jana Pinkasová of Gumárny Zubří for her help with materials preparation and testing. In addition I would like to express my gratitude to everyone who, in some way, contributed to the completion of this work and my graduate studies. I would like to acknowledge my wife Jitka and our children Natálie, Vojtěch, Ondřej and Berenika for their love, patience, support and encouragement; and my mother, grandmother and friends for their help and support. Finally, I would like to thank our Lord for his blessing in helping me combine my studies with my work and family life.

## **ABSTRACT**

Compounds of acrylonitrile-butadiene rubber (NBR) and various fillers including silica, nanoclays, and other common white fillers, were prepared. The performance of these compounds was assessed for gas permeation resistance, static mechanical properties (tensile strength, elongation, hardness) and dynamic mechanical properties ( $G'$ ,  $G''$ ,  $\tan \delta$ ). Morphology of the compounds prepared was investigated using XRD, TEM and FTIR techniques. The addition of nanoclay fillers improved all tested mechanical properties. Compounds with nanoclay fillers also exhibited a significant decrease in permeation rate for refrigerant R-134a. Presence of silica in NBR compound improved exfoliation of nanoclay.

Keywords: acrylonitrile-butadiene rubber, NBR, nanoclay, exfoliation, silica, refrigerant, diffusion, permeation, R-134a, HFO-1234yf

## **ABSTRAKT**

Byly připraveny akrylonitril-butadienové (NBR) kaučukové směsi s různými typy minerálních plniv - silikou, nanojílly, kaolínem a talkem. Vlastnosti těchto směsí byly zkoumány testem plynopropustnosti, statickými mechanickými testy (pevnost v tahu, prodloužení, tvrdost) a dynamickými mechanickými testy ( $G'$ ,  $G''$ ,  $\tan \delta$ ). Morfologie připravených směsí byla studována pomocí analýz XRD, TEM a FTIR. Přídavek nanojílu do směsi zlepšil všechny testované parametry. Směsi s nanojílly také vykazovaly snížení plynopropustnosti refrigerantu R-134a. Přítomnost siliky ve směsi zvýšila exfoliaci nanojílu.

Klíčová slova: akrylonitril-butadienový kaučuk, NBR, nanojíl, exfoliace, silika, refrigerant, difúze, R-134a, HFO-1234yf

# CONTENTS

<b>LIST OF FIGURES .....</b>	<b>7</b>
<b>LIST OF TABLES .....</b>	<b>11</b>
<b>LIST OF ABBREVIATIONS.....</b>	<b>12</b>
<b>INTRODUCTION .....</b>	<b>13</b>
<b>1 CURRENT SITUATION OF THE STUDIED PROBLEM .....</b>	<b>15</b>
<b>1.1 Rubber.....</b>	<b>15</b>
1.1.1 Acrylonitrile-butadiene rubber .....	15
<b>1.2 Gas diffusion.....</b>	<b>16</b>
1.2.1 Factors contributing to gas diffusion.....	18
<b>1.3 Mineral fillers .....</b>	<b>20</b>
<b>1.4 Silica .....</b>	<b>22</b>
<b>1.5 Clay minerals.....</b>	<b>23</b>
1.5.1 Kaolinite.....	24
1.5.2 Talc.....	25
1.5.3 Montorillonite .....	25
1.5.4 Clay surface modification .....	27
<b>1.6 Polymer nanocomposites .....</b>	<b>28</b>
1.6.1 Nanocomposite preparation .....	29
1.6.2 Mechanical properties .....	31
1.6.3 Barrier properties .....	32
<b>1.7 Elastomer - refrigerant compatibility .....</b>	<b>33</b>
<b>2 THE AIMS OF RESEARCH WORK .....</b>	<b>35</b>
<b>3 TEST METHODS AND MATERIALS .....</b>	<b>37</b>
<b>3.1 Measurement of dynamic – mechanical properties .....</b>	<b>37</b>

<b>3.2</b>	<b>Measurement of tensile stress - strain.....</b>	<b>38</b>
<b>3.3</b>	<b>Measurement of tear strength .....</b>	<b>39</b>
<b>3.4</b>	<b>Measurement of hardness .....</b>	<b>40</b>
<b>3.5</b>	<b>Measurement of compression set .....</b>	<b>40</b>
<b>3.6</b>	<b>Measurement of permeation .....</b>	<b>41</b>
3.6.1	Description of test method.....	42
3.6.2	Calculation of permeation .....	42
3.6.3	Test method .....	43
<b>3.7</b>	<b>Nanocomposite structure analysis.....</b>	<b>45</b>
3.7.1	X-ray diffraction (XRD) .....	45
3.7.2	Transmission electron microscopy .....	47
<b>3.8</b>	<b>Measurement of FTIR.....</b>	<b>48</b>
<b>3.9</b>	<b>Materials.....</b>	<b>48</b>
<b>3.10</b>	<b>Preparation of rubber compounds.....</b>	<b>49</b>
<b>3.11</b>	<b>Vulcanization of rubber compounds .....</b>	<b>50</b>
<b>4</b>	<b>RESULTS AND DISCUSSION.....</b>	<b>51</b>
<b>4.1</b>	<b>Nanoclays performance investigation.....</b>	<b>51</b>
4.1.1	Vulcanization characteristics .....	51
4.1.2	Hardness testing.....	53
4.1.3	Tensile testing.....	54
4.1.4	Tear strength .....	56
4.1.5	Compression set.....	57
4.1.6	Barrier properties .....	58
4.1.7	Dynamic-mechanical properties .....	59
4.1.8	XRD analysis .....	66
4.1.9	FT-IR analysis .....	69
4.1.10	TEM analysis .....	72
4.1.11	Summary.....	73
<b>4.2</b>	<b>Nanoclay / silica mixture optimization .....</b>	<b>75</b>
4.2.1	Vulcanization characteristics .....	75

4.2.2	Hardness testing .....	76
4.2.3	Tensile testing .....	77
4.2.4	Tear strength.....	79
4.2.5	Barrier properties .....	80
4.2.6	XRD analysis .....	81
4.2.7	TEM analysis .....	84
4.2.8	Dynamic-mechanical properties.....	88
4.2.9	Summary .....	97
<b>4.3</b>	<b>Investigation of silica and influence of viscosity on nanoclay intercalation .....</b>	<b>99</b>
4.3.1	Rubber compound composition .....	99
4.3.2	XRD analysis .....	100
4.3.3	Summary .....	100
<b>CONCLUSION .....</b>		<b>102</b>
<b>REFERENCES .....</b>		<b>104</b>
<b>PUBLICATION.....</b>		<b>111</b>
<b>CURRICULUM VITAE .....</b>		<b>112</b>

## LIST OF FIGURES

Figure 1: NBR structure [17].....	15
Figure 2: HNBR structure [22].....	16
Figure 3: Diffusion of gas through a polymeric membrane .....	17
Figure 4: Mineral filler classification [36] .....	21
Figure 5: Basic particle shapes and aspect ratios[36].....	21
Figure 6: Surface activity of the particle [36] .....	22
Figure 7: Surface of silica [38].....	22
Figure 8: Basic clay structures [41].....	23
Figure 9: Structure of kaolinite [41].....	24
Figure 10: Structure of talc [41] .....	25
Figure 11: Structure of montorillonite [41].....	26
Figure 12: Ion-change intercalation method [48].....	27
Figure 13: Ion-dipole intercalation method [50] .....	28
Figure 14: Structures of polymer / clay composites [53] .....	29
Figure 15: The in-situ polymerization method [48] .....	30
Figure 16: The solution polymerization method [48].....	30
Figure 17: Melt intercalation process [48] .....	31
Figure 18: Scheme of gas diffusion through the nanocomposite [20].....	32
Figure 19: Orientation of nanoplatelets relative to the diffusion direction [64] .....	33
Figure 20: Die configuration of RPA 2000 [74] .....	37
Figure 21: Dynamic mechanical properties of rubber compound [38].....	37
Figure 22: Scheme of trapped rubber in the filler particle network [86].....	38
Figure 23: Rubber dumbbell sample [18].....	38
Figure 24: Typical stress strain curve of rubber [18] .....	39
Figure 25: Shape of standard tear specimens [18].....	40
Figure 26: Compression set [76] .....	41
Figure 27: Scheme of mass spectrometer test stand .....	41
Figure 28: Scheme of photoacoustic spectrometer INOVA 1314 [85] .....	42
Figure 29: Test stand Maximator with mass spectrometer INOVA 1314.....	44
Figure 30: Record of measurement .....	44
Figure 31: Approximation of measured data.....	44
Figure 32: Principle of X-ray diffraction [48].....	46
Figure 33: XRD visualization of mechanisms of clay intercalation and exfoliation [53] .....	46
Figure 34: Description of a transmission electron microscope [80].....	47
Figure 35: Scheme of FTIR [90] .....	48
Figure 36: Comparison of maximum torque (MH) .....	52

Figure 37: Comparison of maximum torque (MH) .....	52
Figure 38: Comparison of hardness obtained for the tested samples .....	53
Figure 39: Comparison of tensile strength .....	54
Figure 40: Comparison of elongation.....	55
Figure 41: Comparison of modulus $M_{100}$ .....	55
Figure 42: Comparison of tear strength.....	56
Figure 43: Compression set comparison .....	58
Figure 44: R-134a permeation comparison .....	59
Figure 45: Dependence of dynamic storage shear modulus $G'$ on temperature at strain amplitude 1% and frequency 0,3 Hz.....	60
Figure 46: Dependence of loss factor $\tan \delta$ on on temperature at strain amplitude 1% and frequency 0,3 Hz.....	61
Figure 47: Dependence of real part of dynamic modulus $G'$ on strain amplitude from 0,5 to 250 % at temperature 40 °C and oscillation frequency 0,1 Hz.....	62
Figure 48: Dependence of real part of dynamic modulus $G'$ on strain amplitude from 0,5 to 250 % at temperature 70 °C and oscillation frequency 0,1 Hz.....	62
Figure 49: Dependence of real part of dynamic modulus $G'$ on strain amplitude from 0,5 to 250 % at temperature 120 °C and oscillation frequency 0,1 Hz....	63
Figure 50: Dependence of loss dynamic modulus $G''$ on strain amplitude from 0,5 to 250 % at temperature 40 °C and oscillation frequency 0,1 Hz.....	64
Figure 51: Dependence of loss dynamic modulus $G''$ on strain amplitude from 0,5 to 250 % at temperature 70 °C and oscillation frequency 0,1 Hz.....	64
Figure 52: Dependence of loss dynamic modulus $G''$ on strain amplitude from 0,5 to 25% at temperature 120 °C and oscillation frequency 0,1 Hz.....	65
Figure 53: Dependence of loss factor $\tan \delta$ on strain amplitude from 0,5 to 250 % at temperature 40 °C and oscillation frequency 0,1 Hz .....	65
Figure 54: Dependence of loss factor $\tan \delta$ on strain amplitude from 0.5 to 250 % at temperature 70 °C and oscillation frequency 0,1 Hz .....	66
Figure 55: Dependence of loss factor $\tan \delta$ on strain amplitude from 0,5 to 250 % at temperature 120 °C and oscillation frequency 0,1 Hz .....	66
Figure 56: XRD pattern for compound No. 6 – Cloisite Na+ .....	67
Figure 57: XRD pattern for compound No. 2 – Cloisite 93A .....	67
Figure 58: XRD pattern for compound No. 5 – Cloisite 20A .....	68
Figure 59: XRD pattern for compound No. 4 – Cloisite 25A .....	68
Figure 60: XRD pattern for compound No. 8 – Kaolin P05 .....	69
Figure 61: XRD pattern for compounds No.1 silica.....	69
Figure 62: FTIR spectra for NBR and silica .....	70
Figure 63: FTIR spectra for compounds No. 4 - Cloisite 25A and No. 6 - Cloisite Na+ .....	70



Figure 64: FTIR spectra for compound No. 8 – Kaolin P05 .....	71
Figure 65: FTIR spektra for compound No. 1 - Silica .....	71
Figure 66: TEM analysis of compound No. 4 Cloisite 25A .....	73
Figure 67: Comparison of hardness.....	77
Figure 68: Comparison of tensile strength .....	78
Figure 69: Comparison of elongation.....	78
Figure 70: Comparison of modulus $M_{100}$ .....	79
Figure 71: Comparison of tear strength.....	80
Figure 72: R-134a permeation comparison .....	81
Figure 73: XRD pattern for compounds with Cloisite 25A / KS 300 .....	82
Figure 74: XRD pattern for compounds with Cloisite 25A / KS 408 .....	83
Figure 75: XRD pattern for compounds with 10 phr of silica.....	83
Figure 76: XRD pattern for compounds with 30 phr of silica.....	84
Figure 77: TEM analysis - Cloisite 25A / KS 300 (10 phr / 30 phr) .....	85
Figure 78: TEM analysis - Cloisite 25A / KS 408 (10 phr / 30 phr) .....	86
Figure 79: TEM analysis - Cloisite 25A / KS 408 (5 phr / 30 phr) .....	87
Figure 80: TEM analysis - Cloisite 25A / KS 408 (15 phr / 30 phr) .....	88
Figure 81: Dependence of dynamic storage shear modulus $G'$ on strain amplitude at temperature 70°C - Cloisite 25A / Perkasil KS 300 .....	90
Figure 82: Dependence of dynamic storage shear modulus $G'$ on strain amplitude at temperature 70°C - Cloisite 25A / Perkasil KS 408 .....	90
Figure 83: Dependence of loss dynamic modulus $G''$ on strain amplitude at temperature 70°C - Cloisite 25A / Perkasil KS 300 .....	91
Figure 84: Dependence of loss dynamic modulus $G''$ on strain amplitude at temperature 70°C - Cloisite 25A / Perkasil KS 408 .....	92
Figure 85: Dependence of loss factor $\tan \delta$ on strain amplitude at temperature 70°C - Cloisite 25A / Perkasil KS 300 .....	93
Figure 86: Dependence of loss factor $\tan \delta$ on strain amplitude at temperature 70°C - Cloisite 25A / Perkasil KS 408 .....	93
Figure 87: Dependence of dynamic storage shear modulus $G'$ on temperature - Cloisite 25A / Perkasil KS 300.....	94
Figure 88: Dependence of dynamic storage shear modulus $G'$ on temperature - Cloisite 25A / Perkasil KS 408.....	95
Figure 89: Dependence of loss factor $\tan \delta$ on temperature - Cloisite 25A / Perkasil KS 300 .....	95
Figure 90: Dependence of loss factor $\tan \delta$ on temperature - Cloisite 25A / Perkasil KS 408 .....	96
Figure 91: Dependence of loss dynamic modulus $G''$ on temperature - Cloisite 25A / Perkasil KS 300 .....	97

Figure 92: Dependence of loss dynamic modulus $G''$ on temperature - Cloisite 25A / Perkasil KS 408 .....	97
Figure 93: XRD pattern for compounds with various viscosity .....	100

## LIST OF TABLES

Table 1: Formulation of NBR compounds with various mineral fillers.....	49
Table 2: Types of tested nanoclay, kaolin and talc.....	49
Table 3: Formulation of NBR compounds with various ratio of silica KS 300 and Cloisite 25A .....	50
Table 4: Formulation of NBR compounds with various ratio of silica KS 408 and Cloisite 25A .....	50
Table 5: Vulcanization parameters .....	51
Table 6: Hardness – testing results .....	53
Table 7: Tensile testing results .....	54
Table 8: Tear strength results .....	56
Table 9: Compression set results .....	57
Table 10: Permeation results .....	59
Table 11: Comparison of average particle size and surface area of silica.....	75
Table 12: Vulcanization parameters .....	75
Table 13: Hardness results.....	76
Table 14: Tensile strength, elongation and $M_{100}$ results.....	77
Table 15: Tear strength results .....	79
Table 16: Permeation results .....	81
Table 17: Recipe of experimental compounds .....	99

## LIST OF ABBREVIATIONS

NBR	Nitrile butadiene rubber
R-134a	Hydro-fluorocarbon refrigerant 1,1,1,2-Tetrafluoroethane
GWP	Global warming potential
HFO-1234yf	Hydro-fluoroolefin refrigerant 2,3,3,3-Tetrafluoropropene
A/C	Air conditioning
PVC	Poly-vinyl chloride
HNBR	Hydrogenated acrylonitrile butadiene rubber
IIR	butyl rubber
BIIR	Bromo-butyl rubber
CIIR	Chloro-butyl rubber
ECO	Epichloro-hydrin rubber
SBR	Styrene-butadiene rubber
BR	Butadiene rubber
NR	Natural rubber
EV	Efficient sulfur vulcanization system
CV	Conventional sulfur vulcanized system
CEC	Cation exchange capacity
PAG	Polyalkyle-glycol
POE	Polyol-ester
RPA	Rubber process analyser
ShA	Shore A hardness unit
IRHD	International rubber hardness durometer unit
EC	European Union Commission Regulation
XRD	X-ray diffraction
TEM	Transmission electron microscopy
FTIR	Fourier Transform Infra-Red spectroscopy
IR	Infra-red

## INTRODUCTION

Mineral fillers have been used in various rubber compounds since the beginning of industrial rubber production. The first generation of these fillers was natural minerals such as calcium carbonate, magnesium carbonate, baryte, zinc oxide, talc and kaolin. The modest property improvement and reinforcing effects gained from these mineral fillers was sufficient in the 1930's and 1940's, because only natural rubber and small volumes of chloroprene materials were commercially available.

Newer synthetic rubbers developed in the 1950's required mineral fillers to provide higher levels of reinforcement due to the lack of strain crystallization in these materials. One revolutionary active reinforcing filler introduced was based on silicon dioxide and is generally called "silica". Utilization of silica filler allowed the creation of light colors in rubber compounds without the deterioration of mechanical properties. The use of silica had a positive impact on the environment and for the automotive industry by decreasing hysteresis and rolling resistance in green type tires improving automotive fuel efficiency [1].

The latest generation of mineral fillers has been introduced over the last few years. New mineral fillers are comprised of layered nanoclays which have also been commercially used as effective reinforcing fillers in thermoplastic polymers. Layered nanoclays offer a significant improvement in mechanical properties when compared to conventional fillers. Currently montmorillonite is the most commonly used nanoclay from the smectite clay group. After exfoliation montmorillonite has a very large surface area, up to  $700 \text{ m}^2 / \text{g}$ . High surface area in combination with a high aspect ratio, delivers highly effective mechanical reinforcement. This filler also has the potential to provide an effective gas permeation barrier. Optimal addition levels of exfoliated nanoclay fillers is about 5 %, which is a much lower level than required for standard mineral fillers or carbon black [2].

Successful application of nanoclays as a filler in thermoplastic polymers suggests further investigation for use in elastomer nanocomposites. Significant decrease of gas diffusion with improvement of mechanical properties of elastomers suggest nanoclays would be an ideal filler for special gas sealing applications, where extremely low permeation of gas molecules through the elastomeric matrix is required.

One of the possible applications for nanoclay fillers is elastomeric sealing between refrigerant transport parts in automotive air conditioning systems. The cooling effect offered by air conditioning systems is typically achieved by utilizing a hydrofluorocarbon refrigerant 1,1,1,2-Tetrafluoroethane (R-134a). However, R-134a has a very high relative global warming potential (GWP) and therefore the European Union has issued a directive restricting the use of refrigerant R-134a in new vehicle models

introduced after January 2011 that will be produced in 2016 and beyond [3]. The proposed replacement for refrigerant R-134a is 2,3,3,3-Tetrafluoropropene (HFO-1234yf) developed by E.I. duPont deNemours and Honeywell International [4]. Modest changes in rubber tensile strength, elongation, hardness, and volume after exposure to this new refrigerant suggests good material compatibility with rubbers. However, permeation of the new refrigerant through sealing components increases by about 30% when compared to the current R-134a due to differences in molecular composition and size between R-134a and HFO-1234yf molecules [5]. This demonstrates the importance of improving permeation behavior of rubber compounds for future use with low GWP refrigerants without sacrificing the mechanical properties necessary for sealing performance. Improving permeation resistance of these rubber materials can be achieved by proper selection of the mineral fillers added to the rubber compound. Specifically, permeation resistance can be improved by utilizing common fillers with plate-like structure, such as kaolin clay and talc. While these fillers tend to be cost effective, they may cause unacceptable deterioration of the mechanical properties of the rubber compound [1]. Addition of nanoclay fillers offers both reduced permeation rates for refrigerant and improvement of mechanical properties.

Most of published research papers on rubber nanocomposites investigate the use of nanoclay as the only active filler in the rubber compound. However, the commercial application of this type of compound is complicated by the relatively high price of nanoclays. In automotive applications, the introduction of new materials is typically hindered by the requirement that new materials maintain or reduce the price of materials currently being used. This leads to the necessity to offsetting the cost of higher priced fillers by combining them with lower priced ones.

Only a few researchers have investigated combination of nanostructured silica or carbon black and nanoclay fillers [6], [7], [8], [9], [10], [11], [12], [13], [14], [15]. These hybrid filler systems of nanoclay and nanostructured conventional fillers improved mechanical properties of the rubber nanocomposites investigated. One very important output of these investigations was the synergy experienced between layered nanoclays and silica or carbon black [7], [9], [14]. Combination of silica and nanoclay was also the subject of our study and our effort to identify the most cost effective A/C rubber compounds which optimize both mechanical properties and permeation resistance. Combinations of silica, kaolin and talc were investigated in parallel as low cost solutions and compared with silica and nanoclay combinations in their effect on property modification.

# 1 CURRENT SITUATION OF THE STUDIED PROBLEM

## 1.1 Rubber

Rubber is a type of polymer which exhibits very high elongation, low elastic modulus and high yield strain compared with other materials. The structure of rubber is amorphous which allows considerable segmental motion due to low glass transition temperature ( $T_g$ ). The long elastomer chains are physically cross-linked during “vulcanization” with significant improvement in mechanical properties and allows for their practical use at temperatures above  $T_g$ . Vulcanized elastomers can be reversibly extended by relatively low stress up to several times their original length, depending on the specific type of elastomer [16].

### 1.1.1 Acrylonitrile-butadiene rubber

NBR is the abbreviation for the unsaturated copolymer of butadiene and acrylonitrile (ACN). Acrylonitrile content in commercially practical NBR typically ranges between 18 to 45 %. Increasing ACN level improves oil resistance due to its high polarity but reduces low temperature flexibility due to its more “plastic” like behavior. Butadiene content improves flexibility at low temperatures due to its more elastomeric behavior [16].

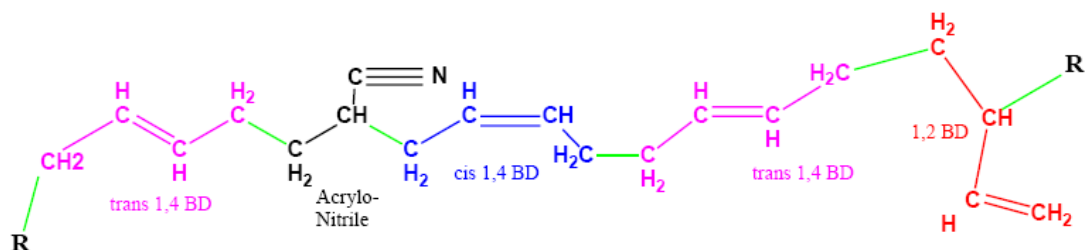


Figure 1: NBR structure [17]

NBR is produced by emulsion polymerization. NBR producers vary polymerization temperature to manufacture “hot” and “cold” polymers. Hot NBR materials are highly branched and provide significant improvement in tear strength and shape retention for thin wall and complex extrusions. Linear polymer chains of cold NBR are less viscous and contribute to less power consumption during mixing, extruding or molding processes. Most NBR manufactures make at least 20 conventional elastomer variations, with one global manufactures now offering more than 100 grades [18]. NBR is used in a wide variety of application areas requiring oil, fuel and chemical resistance. Maximum long term operating temperature of NBR is 110°C. NBR is not resistant to ozone, due to unsaturation of main chain. Ozone resistance can be

improved by addition of PVC, but low temperature flexibility of this blend is reduced. The main applications for NBR include hydraulic hose and seal elements, conveyor belting, oil field and automotive applications.

NBR is the least expensive oil resistant elastomer and its global consumption is approximately 400.000 metric tons.

Hydrogenated NBR (HNBR) is utilized for applications over the temperature limit of NBR or when additional chemical and environmental resistance is required. The hydrogenation process removes most of the residual unsaturation in the polymer and significantly improves resistance to ozone, oxygen and heat aging [18].

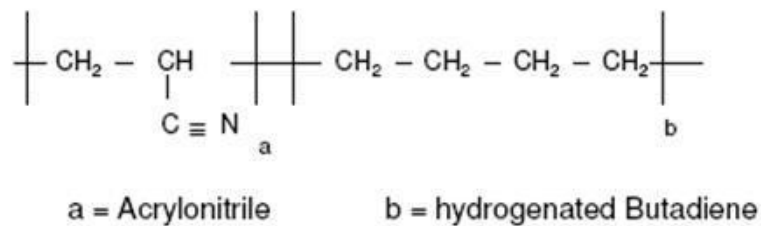


Figure 2: HNBR structure [22]

## 1.2 Gas diffusion

The diffusion or permeation of gases through polymeric membranes and seal elements can be described by four associated processes [20], [21]:

- Sorption of gas molecules on the surface of the polymer
- Dissolution of the gas in to the polymer
- Diffusion through the polymer
- Desorption of gas from the opposite surface of polymer membrane



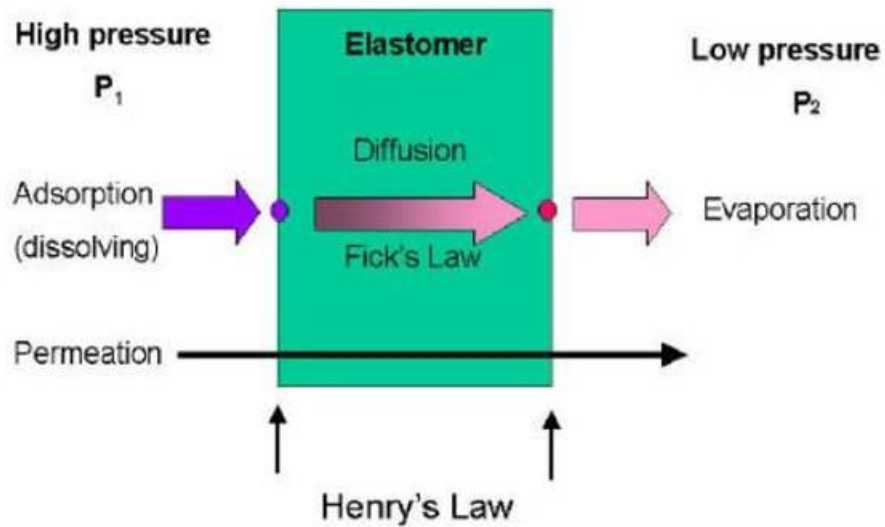


Figure 3: Diffusion of gas through a polymeric membrane

This process is described by Fick's first law of diffusion [21]:

$$J = -D \left( \frac{\partial c}{\partial x} \right) \quad (1)$$

Where:  $J$  .....diffusion flux [ $\text{mol. m}^{-2} \cdot \text{s}^{-1}$ ]

$D$  ..... diffusion coefficient [ $\text{m}^2 \cdot \text{s}^{-1}$ ]

$c$  ..... concentration of the penetrant [ $\text{mol. cm}^{-3}$ ]

$x$  .....thickness of the membrane [cm]

This steady state diffusion function is applicable when the concentration of gas does not vary with time. When the gas concentration varies with time, the diffusion process is described by Fick's second law:

$$\frac{\partial c}{\partial t} = D \left( \frac{\partial^2 c}{\partial x^2} \right) \quad (2)$$

If steady state diffusion flow is constant and the diffusion coefficient is independent of the concentration, then equation (1) can be re-written:

$$J = D \left( \frac{c_1 - c_2}{h} \right) \quad (3)$$

where:  $c_1, c_2$  ..... sorbent concentration [ $\text{mol. cm}^{-3}$ ]

$h$  ..... thickness of membrane [cm]

Partial pressures  $p_1$  and  $p_2$  are used in place of surface concentrations  $c_1$  and  $c_2$  in the case of transport of gases and vapors. According to a form of Henry's law at constant temperature [21], [23]:

$$c = Sp \tag{4}$$

where:  $S$  ..... solubility coefficient [mol. cm<sup>-3</sup>. Pa<sup>-1</sup>]  
 $p$  ..... partial pressure [Pa]

The permeation flux is given by combination of equations (3) and (4):

$$J = DS \left( \frac{p_1 - p_2}{h} \right) \tag{5}$$

where  $p_1$ ,  $p_2$  are the partial pressures on the two sides of the membrane. The permeability coefficient,  $P$ , is described by the equation:

$$P = DS \tag{6}$$

Equation (5) can be written in terms of permeability as:

$$J = P \left( \frac{p_1 - p_2}{h} \right) \tag{7}$$

### 1.2.1 Factors contributing to gas diffusion

Gas diffusion through a rubber matrix is influenced by the nature of the polymer, type of cross-links, effect of plasticizers, properties of penetrant, fillers present and by temperature [21].

#### *Nature of the polymer*

Free volume between molecules within the polymeric matrix and segmental mobility of the polymer chains are factors influencing gas diffusion. Segmental mobility is affected by degree of cross-linking, degree of unsaturation, degree of crystallinity, nature of constituents and by glass transition temperature. Lower glass temperature of rubbers allows higher segmental mobility of polymer chains than in plastics and therefore gas diffusivity in rubbers is higher than diffusivity in plastics. Increase in saturation of the main chain by hydrogenation restricts segmental mobility and decreases diffusivity. Diffusivity linearly decreases with increasing density of cross-links at low levels of cross-link density. At higher levels of cross-linking, the rate of decrease of diffusivity levels off. Large numbers of substituent methyl groups on the main chain of the polymer decreases diffusivity by restriction of segmental mobility [21] - [26]. Therefore butyl rubber (IIR), bromo-butyl rubber (BIIR), chloro-butyl

rubber (CIIR) and epichloro-hydrin rubber (ECO) possess the best gas barrier properties. However, the most commonly used rubbers styrene-butadiene rubber (SBR), butadiene rubber (BR) and natural rubber (NR) have less resistance to gas diffusion, due to their structures containing higher segmental mobility [19], [27], [28].

### ***Type of cross-links***

Different vulcanization systems exhibit different levels of gas diffusivity in the same polymeric matrix with the same degree of cross-linking. The lowest gas permeability occurs in the presence of stable carbon - carbon bonds provided by peroxide vulcanization, followed by efficient sulfur vulcanization system (EV) with mono or disulfidic linkages. The highest diffusivities are seen in conventional sulfur vulcanized system (CV) with polysulfidic linkages, due to high chain flexibility of the network [21].

### ***Effect of plasticizer***

Diffusivity is increased by the addition of plasticizers into the polymer because they raise the segmental mobility and decrease cohesion force between chains. Solubility coefficient of the penetrant is lowered by plasticizer and therefore concentration of dissolved gas in the polymeric matrix is increased [21], [29].

### ***Nature of penetrant***

The size and shape of gas molecule influences the level of permeability. Diffusivity increases with decreasing size of the gas molecules. Flat or elongated molecules of gas have higher diffusion coefficients than spherical molecules of equal molecular volume [21], [30], [31].

Polarity of gas molecules influences solubility in the polymeric matrix. Gas molecules with similar polarity to the polymer in which diffusion is occurring increase the solubility coefficient [32], [33].

### ***Fillers***

Gas diffusion in filled polymers is influenced by the nature of the fillers as well as the degree of adhesion and compatibility between filler and the polymeric matrix. Compatibility is the ability of the filler to bond to the rubber matrix [35]. Compatible fillers decrease the free volume between molecules of polymeric matrix and create a tortuous diffusion path for permeating molecules of gas. Tortuous path level is influenced by shape and orientation of particles and by volume fraction of filler particles. Incompatibility between fillers and polymer by low adhesion increases free

volume of the polymer composite along the interface between filler and polymer and thus increases gas permeability [21], [29]. Permeation resistance of polymers is improved by utilizing fillers with plate-like structure which tend to increase a tortuous diffusion path for the permeating molecules.

### **Temperature**

Temperature influence of gas diffusion through polymeric materials is described by the Arrhenius equation [21], [23], [25]:

$$D = D_0 \exp\left(-\frac{E_D}{RT}\right) \quad (8)$$

$$S = S_0 \exp\left(-\frac{\Delta H_s}{RT}\right) \quad (9)$$

$$P = P_0 \exp\left(-\frac{E_P}{RT}\right) \quad (10)$$

- where:
- $E_D$  ..... Activation energy of diffusion
  - $E_P$  ..... Activation energy of permeation
  - $\Delta H_s$  ..... heat of solution of the penetrant in the polymer
  - $D_0, S_0, P_0$  ..... pre-exponential factors
  - $R$  ..... universal gas constant
  - $T$  ..... absolute temperature [°K]

Gas diffusion exponentially increases with temperature.

### **1.3 Mineral fillers**

A wide range of mineral fillers are used in rubber compounds. Fillers are added into the polymeric matrix to improve physical and mechanical properties, reduce cost or create colors for the final rubber product [34].

Particulate fillers are classified into three main categories according to their effect on the physical and mechanical properties of the rubber compound [18]:

1. Non-reinforcing or degrading fillers
2. Semi-reinforcing fillers
3. Reinforcing fillers

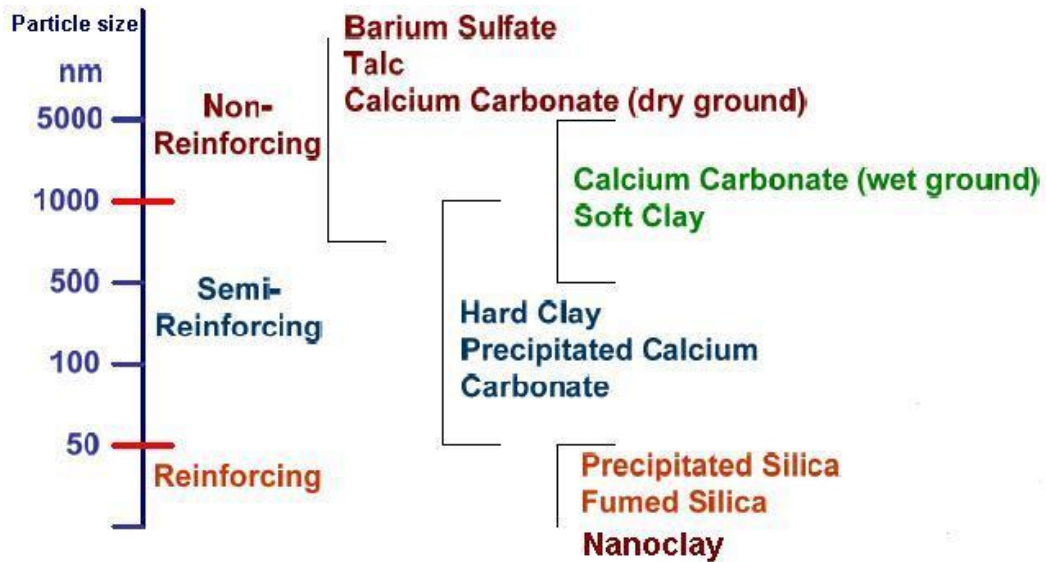


Figure 4: Mineral filler classification [35]

Reinforcing effects of fillers are related to [35]:

1. Average particle size – smaller size imparts better reinforcement to polymers
2. Surface area of particle – fillers with higher surface area have more surface area available for contact and higher potential to reinforce the polymer
3. Shape of particle – fillers with high aspect ratios or plate shapes provide greater reinforcement and barrier to diffusion than low aspect ratios or spherical shapes.

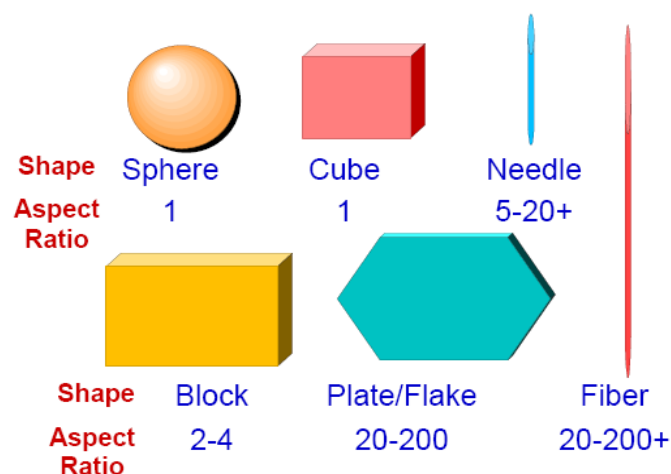


Figure 5: Basic particle shapes and aspect ratios[35]

4. Surface activity – fillers with higher surface activity reinforce the polymer more effectively. Surface chemistry of the filler determines the ability of the rubber

matrix to wet filler surface and effectively reinforce the rubber. No bonding between rubber and filler can produce an air gap along the filler surface increasing permeability and reducing strength [35].

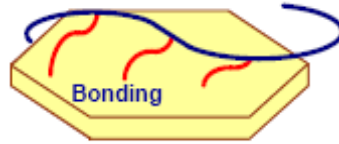


Figure 6: Surface activity of the particle [35]

## 1.4 Silica

Amorphous silica is derived from particles of the inorganic compound  $(\text{SiO}_2)_n$ , where a silicon atom is covalently bonded in a tetrahedral arrangement with four oxygen atoms [18]. Precipitated silica is produced by the controlled neutralization of sodium silicate solution by either concentrated sulphuric, hydrochloric or carbonic acid. Variation in the reaction conditions can create different particle size according to the requirements of the final application. Spherical particles form clusters or aggregates by hydrogen bonding and aggregates are bonded to form agglomerates. The surface of precipitated silica contains about 6% adsorbed free water, siloxane groups and reactive silanol groups. Silanol groups influence hydrophilic nature of silica and its reactivity with rubber, water, soluble zinc and other compounding ingredients. Free water ensures that the silica particle is saturated with active silanols and provides a barrier to the reaction of silanols with soluble zinc and accelerators [35], [36].

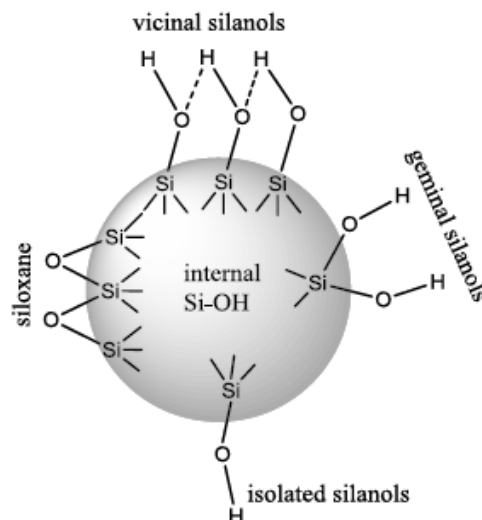
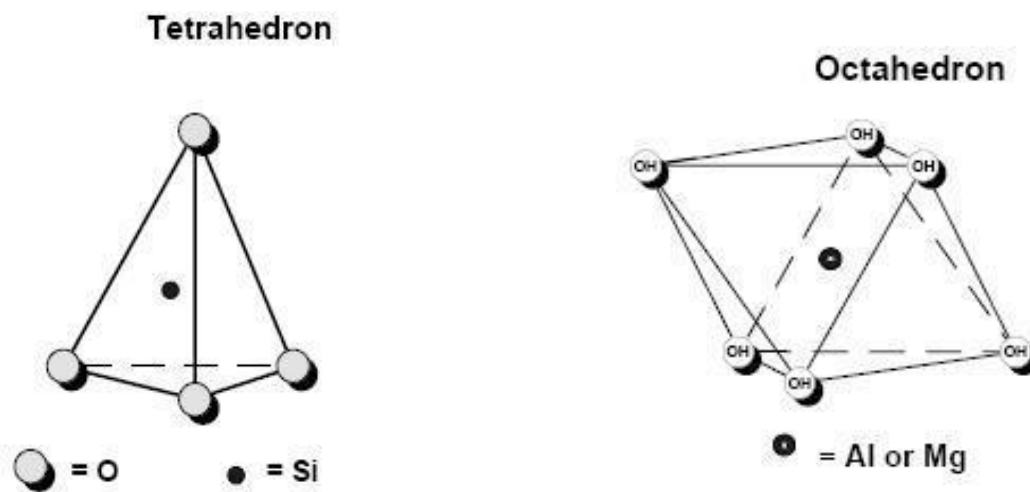


Figure 7: Surface of silica [37]

Interaction between silica and the rubber matrix is significantly improved by surface treatment of the silica. This modification is accomplished using chemical reactions which create a bond between organo-silane and silanol groups on the silica surface. Once the silica is reacted with silane, it produces an organo-philic or organo-functional surface which improves adhesion between silica and rubber matrix as can be seen in the Figure 7 [35].

## 1.5 Clay minerals

Clay minerals are hydrous aluminum phyllosilicates with the occasional addition of potassium, calcium, magnesium or iron [38]. Layered mineral clays are based on two basic units. These units are the tetrahedron and octahedron shown in Figure 8:



*Figure 8: Basic clay structures [40]*

Tetrahedral and octahedral structures are bonded together into the basic structure of clay minerals by different interaction links (mainly van der Waals forces).

Layered clays are classified according to their structures into two basic categories - 1:1 and 2:1. Structure of 1:1 clay minerals is a combination of one tetrahedral and one octahedral sheet. Structure of 2:1 clay is created by one octahedral sheet sandwiched between two tetrahedral sheets [39].

The most important characteristics of clay are [41], [42]:

- Purity level
- Cation exchange capacity (CEC)
- Aspect ratio

### ***Purity level***

High purity is critical to achieve the maximum improvement in mechanical properties. Impurities have to be eliminated before the clay is surface modified, because these are source of stress concentration, which negatively influences impact resistance of composite material. [42]

### ***Cation exchange capacity (CEC)***

CEC refers to the number of  $\text{Al}^{3+}$  ions that can be substituted by cations of other metals. It is measured in milliequivalents per gram (meq/g) or more frequently per 100 g (meq/100g) [43]. Larger CEC values increase the ability of the clay surface to be modified through ion exchange reactions making this a key parameter for manipulating surface activity and resulting properties of the filler [44].

### ***Aspect ratio***

The aspect ratio of a clay particle shape is the ratio of its longer dimension to its shorter. Plate like structure of clay together with high value of aspect ratio is assumed to be highly effective reinforcing filler at low addition level, due to very large total surface area of clay [42].

## **1.5.1 Kaolinite**

Kaolinite is a platy aluminosilicate with the general chemical composition  $\text{Al}_2\text{Si}_2\text{O}_5(\text{OH})_4$ . The structure of kaolinite is shown in the Figure 9.

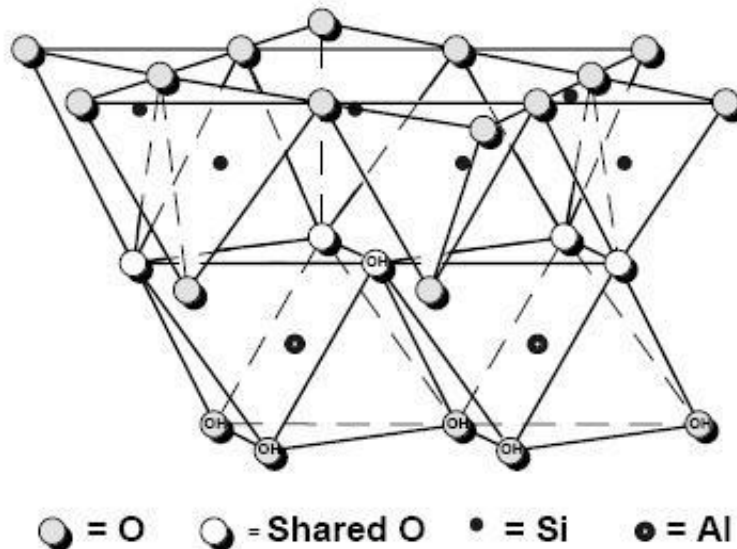


*Figure 9: Structure of kaolinite [40]*



It is 1:1 dioctahedral structure created by tetrahedral sheets of  $\text{SiO}_4$  and octahedral sheets  $\text{Al}_2(\text{OH})_4$  bonded by hydroxyl groups. The continuous sheet structure of kaolinite creates thin particles which exist in nature as overlapping flakes.

Kaolinite is an important filler for a wide range of rubber compounds including materials that demand high levels of adhesion to reinforcement materials, good processability, low price and adequate reinforcement properties [1]. CEC of kaolinite is between 3 to 15 meq/100 g, which is low in comparison to other layered clay minerals [43].

### 1.5.2 Talc

Talc is a mineral composed of hydrated magnesium silicate. The chemical formula is  $\text{H}_2\text{Mg}_3(\text{SiO}_3)_4$  or  $\text{Mg}_3\text{Si}_4\text{O}_{10}(\text{OH})_2$ . Talc has 2:1 structure created by one octahedral and two tetrahedral sheets as shown in Figure 10.

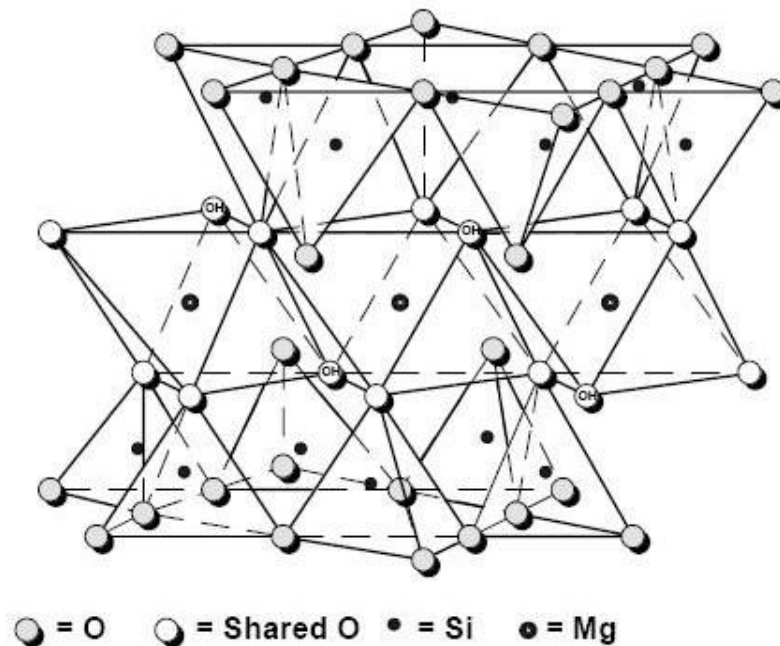


Figure 10: Structure of talc [40]

Individual talc plate layers are held together by weak van der Waals forces. Sliding and delamination of talc layers is not difficult and this gives talc its characteristic soft, slippery feel [40].

### 1.5.3 Montmorillonite

Montmorillonite was discovered in 1847 in France (Montmorillon) by Damour and Salvétat [39]. Its general formula is  $(\text{OH})_4\text{Si}_8(\text{Al}_{x-4}\text{Mg}_x)\text{O}_{20}$ . Montmorillonite is a

mineral with an anisotropic, plate-like, high aspect-ratio morphology, composed of fine lamellar particles arranged in triple 2:1 layers (Figure 11).

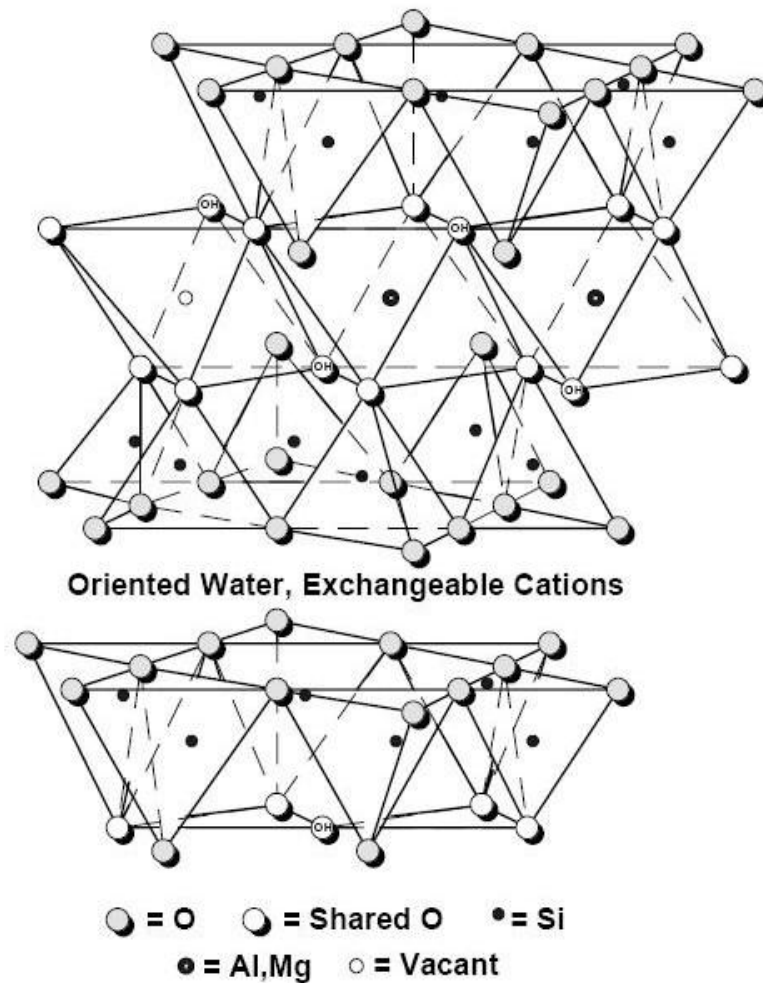


Figure 11: Structure of montmorillonite [40]

A central octahedral layer is enclosed between two tetrahedral layers. Silicon in the tetrahedral layers is surrounded by six atoms of oxygen. In the octahedral layer, two aluminum atoms are surrounded by six oxygen atoms. The triple layers are joined by chemical bonds to common oxygen atoms. Small amount of the octahedral  $\text{Al}^{3+}$  are replaced by  $\text{Mg}^{2+}$ . This substitution generates negative charge on the surface of the platelets, which is compensated for by exchangeable cations, usually  $\text{Na}^+$  or  $\text{Ca}^{2+}$ , between the laminar layers. In addition to these counter ions, oriented water occupies the interlaminar space, due to the hydrophilicity of clay. When  $\text{Ca}^{2+}$  is the exchangeable cation, there are two water layers. While a  $\text{Na}^+$  counter ion usually produces just one water layer [40], [2]. Cation exchange capacity (CEC) of montmorillonite is in the range of 80 to 150 meq/100 g and is much higher than kaolinite. Aspect ratios are between 300 to 1500. Total surface area of completely

exfoliated montmorillonite is up to  $700 \text{ m}^2/\text{g}$ . High aspect ratio and surface area of the exfoliated montmorillonite are required for highly effective reinforcement and effective gas barrier properties at low addition levels in the polymer [45].

#### 1.5.4 Clay surface modification

Mineral layered clay and most of conventional polymers are immiscible in one another and have poor physical interaction between the organic polymer and the inorganic filler. This lack of interaction causes reduced mechanical and thermal performance. Modification of the minerals is therefore necessary to form effective layered clay / polymer composites. Compatibility of silicate clay with standard polymers is improved by conversion of the normally hydrophilic silicate surface to organophilic. This change allows intercalation of the clay in the polymeric matrix using such modifiers as alkyl ammonium or alkyl phosphonium salts. Alkyl ammonium and alkyl phosphonium cations decrease the surface energy of the clay, improve wetting characteristics with the polymeric matrix and extend the interlayer spacing. Interlayer spacing is extended with increased polymer chain length and the percentage of intercalation agent [46]. This modification method is called the “ion-change intercalation method” (Figure 12).

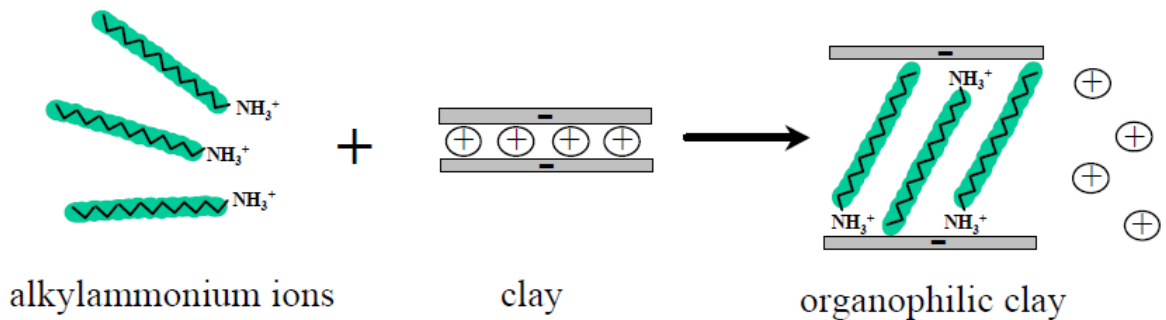


*Figure 12: Ion-change intercalation method [47]*

A second and more recent method of intercalation is the “ion-dipole method”. This intercalation principle depends on the interaction between the dipole of the organic compound and cation of interlayer. Interlayer distance increases by an intercalation process and depends on the type and concentration of the organic compound. Different amounts of intercalant agents create mono and bilayer intercalante molecule arrangements with various inclinations to the surface of montmorillonite as can be seen in the Figure 13 [48], [49], [50].

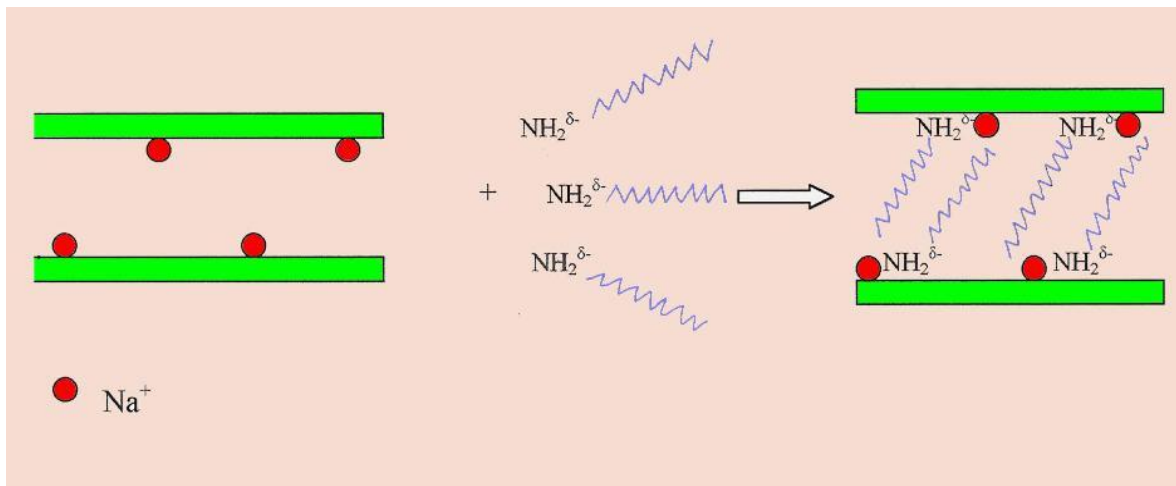


Figure 13: Ion-dipole intercalation method [49]

## 1.6 Polymer nanocomposites

Polymer nanocomposites are described as a new class of material alternative to standard polymers filled by conventional fillers. In this new class of material, inorganic fillers with at least one dimension in the nano-meter size ( $10^{-9}$  m) are dispersed in a polymer matrix and offer significant improvement in the properties of the polymer. Property improvement typically focuses on a change in the modulus, strength, heat aging, chemical resistance, gas diffusion or flammability. These improved results are ideally achieved by nano-fillers with much lower additions in comparison to conventional fillers [2].

Polymer nanocomposites are materials with a homogenous distribution of nano filler particles in the polymeric matrix.

Incorporation of clay into polymeric matrices can generate the three structures shown in Figure 14 [51]:

1. Conventional microcomposites
2. Intercalated nanocomposites
3. Exfoliated nanocomposites

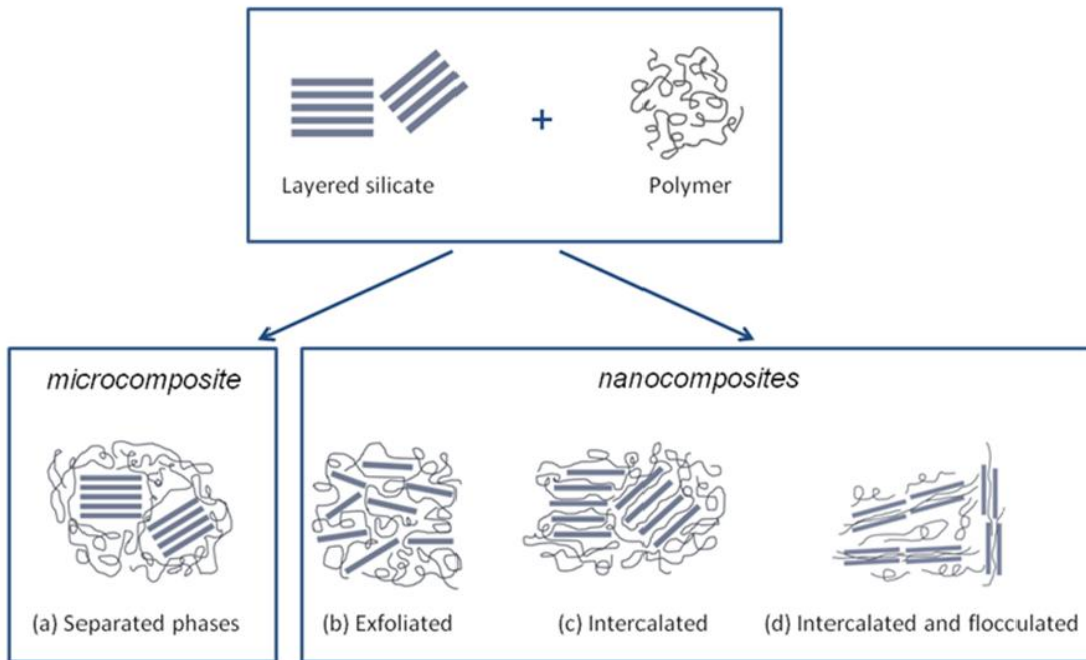


Figure 14: Structures of polymer / clay composites [52]

Typically smectite-type clays with layered structures were investigated as nanofillers for polymer / clay applications. Smectite clays have unique properties due to large chemically active surface areas, a high cation exchange capacity, and interlamellar surfaces with hydration characteristics [53]. Currently, montmorillonite is the most widely used filler from the smectite clays group. The first commercial applications of polymer nanocomposites were introduced in by Toyota in clay/PA 6 nanocomposites utilized for serial production of timing belt covers with improved mechanical parameters and durability [54].

### 1.6.1 Nanocomposite preparation

Polymer layered silicate nanocomposites are prepared by four different methods: in-situ polymerization, solution method, melt intercalation and the latex method [55], [56]

#### *In-situ method*

In-situ polymerization is the current typical process used to synthesize thermoset-clay nanocomposites. This method is described in Figure 15. Monomer is inserted into interlayer spaces which results in swelling. Monomer is then dispersed during polymerization [54], [56].

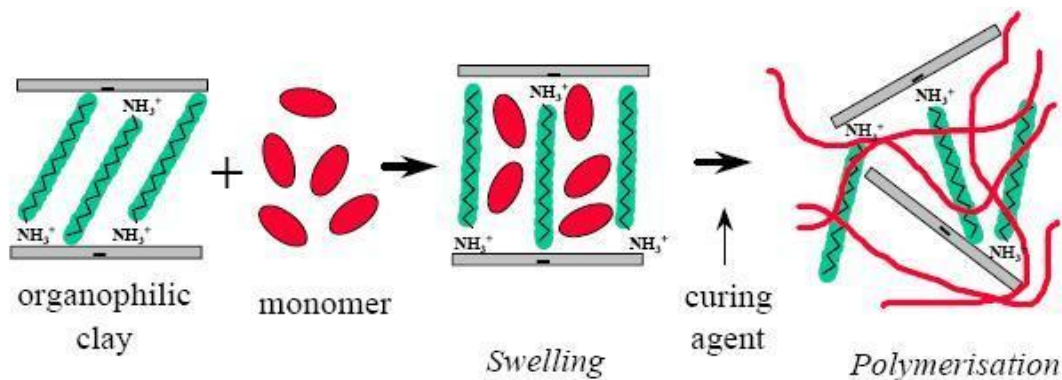


Figure 15: The in-situ polymerization method [47]

The first synthesized polymer-clay nanocomposites based on polyamide 6 were prepared by this method.

### Solution method

The solution method uses polar solvents to synthesize intercalated polymer-layered silicate nanocomposites. Clay is dispersed in the polar solvent, and after expansion, is added into a polymer solution. Polymer chains intercalate between the silicate layers. Excess solvent is usually removed by evaporation under vacuum. A schematic of this method is shown in Figure 16.

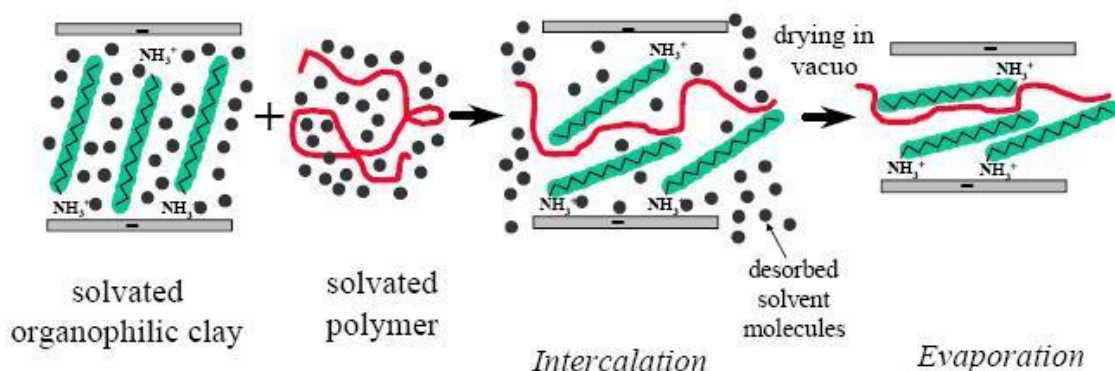


Figure 16: The solution polymerization method [47]

### Melt intercalation method

The third method of nanocomposites preparation is based on direct compounding of polymer and modified nanoclay. Advantages of this method over previous in-situ and solution intercalation methods are its environmental friendliness due to the absence of organic solvent and its ability to utilize standard industrial processing equipment for extrusion, injection molding, and mixing of rubber-clay and thermoplastic-clay nanocomposites [42].

Requirements of the compounding are perfect nanoclay particle homogenization and the highest exfoliation level, combined with no degradation of polymer. Polar type of polymers such as NBR and HNBR are optimal for preparation of nanocomposites with these requirements.

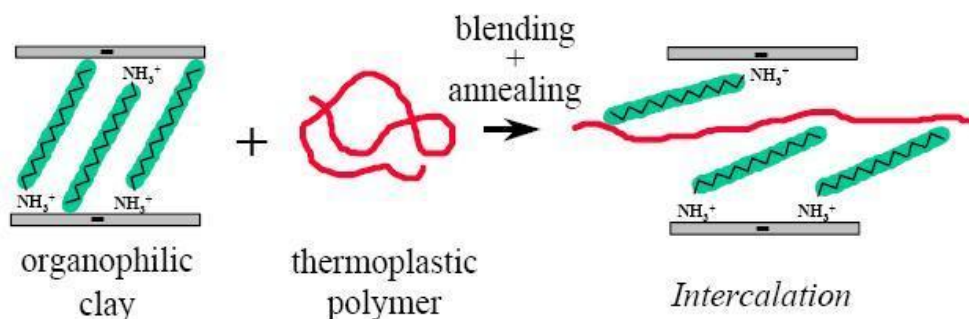


Figure 17: Melt intercalation process [47]

### ***Latex method***

This method is convenient for the preparation of rubber nanocomposites since most types of rubber are available in a latex form. Layered clay is dispersed in deionized water and is then mixed with latex rubber. This mixing is then followed by coagulation by flocculants. Rubber molecules penetrate and swell between extended or exfoliated layers of clay. An advantage of this method is coexistence of intercalation with exfoliation with the presence of no volatile solvent [57].

### **1.6.2 Mechanical properties**

Properties of elastomers with nanofiller additions are improved in comparison to conventional composites. Research shows strong improvement in the mechanical properties of elastomers including hardness, tensile strength, elongation and modulus [10], [11], [58], [59], [60]. Improvement was investigated for the thermal properties and flame retardancy as well and results show better performance of rubber nanocomposite for these characteristics [56], [61].

Montmorillonite provides an increase in modulus and tensile strength at a 3-5% loading compared to 20-60% loading for conventional reinforcing filler such as silica, and carbon black [2]. On the other hand, results show deterioration in the tear resistance in comparison to elastomers filled by carbon black or silica. This is caused by the plate like shape of particles with sharp edges on the interface between particle and polymeric matrix [62].

### 1.6.3 Barrier properties

The mass transport mechanism of gas permeation in the polymer nanocomposite resides within the permeable phase polymer matrix in which is dispersed non-permeable nanoplatelets. Permeability of nanocomposites is influenced by three key factors:

- Volume fraction of the nanoplatelets
- Orientation of nanoplatelets relative to the diffusion direction
- Aspect ratio of nanoplatelets

Transport mechanisms within polymer nanocomposites follow Fick's law. The polymeric matrix maintains the same properties and behaviors as a virgin non-filled polymer. Reduction of free volume within polymeric matrix decreases the solubility, as well as diffusion, by creating a tortuous diffusion path through which molecules of gas must travel in the polymeric matrix as shown in Figure 18 [20].

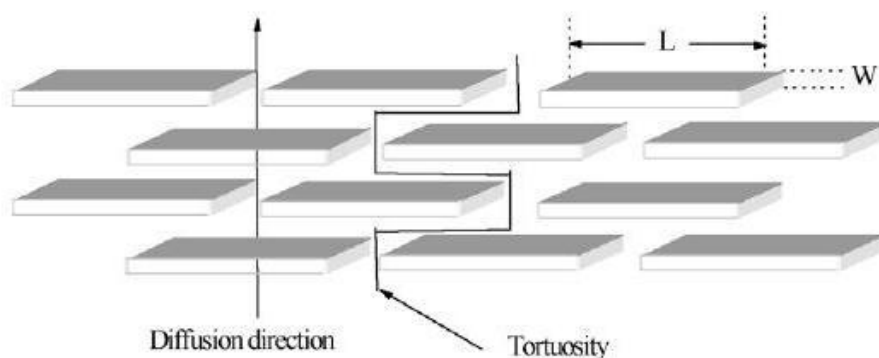


Figure 18: Scheme of gas diffusion through the nanocomposite [20]

Loading of nanoclays is typically up to 5 weight %, thus reduction of the polymeric matrix volume is small due to low volume fraction of nanoplatelets. Therefore tortuous diffusion path is the major factor, which is influenced by the shape and the degree of dispersion of the nanoplatelets. The tortuosity factor and aspect ratio of fully exfoliated nanocomposite are much higher than intercalated nanocomposite and results in a more effective barrier membrane for gasses [20].

Perpendicular orientation of exfoliated nanoplatelets to the diffusion direction provides the highest tortuosity and therefore the greatest reduction of the gas permeation as can be seen in Figure 19 [20].



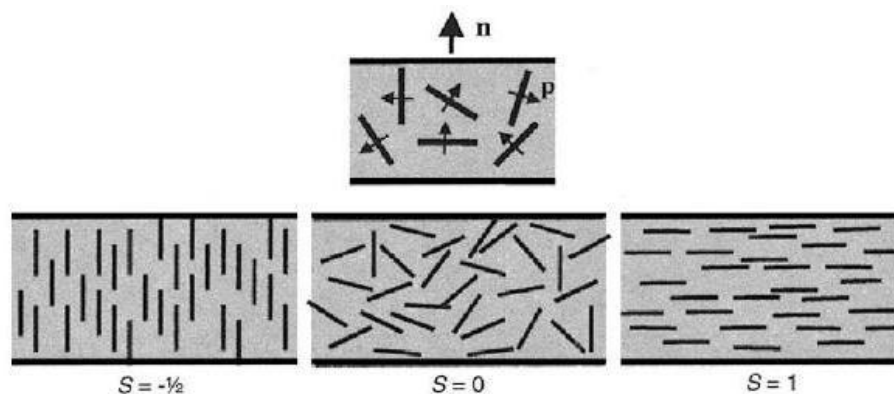


Figure 19: Orientation of nanoplatelets relative to the diffusion direction [63]

Improvement of the gas barrier properties of rubber compounds filled by modified nanoclay was reported by several studies for EPDM, NBR, HNBR SBR, IIR, NR nanocomposites [58], [59], [64], [65], [66], [67], [68], [69].

## 1.7 Elastomer - refrigerant compatibility

Material compatibility with refrigerant is one of the most important requirements for polymeric components used in mobile air conditioning (A/C) systems. In addition to the refrigerant compatibility, a further requirement is compatibility with compressor lubricants. These lubricants are based on polyalkyle-glycol (PAG) for standard compressors or on polyol-ester (POE) based lubricant for electric compressors in hybrid vehicles. The cooling effect offered by A/C systems is typically achieved using closed-loop vapor compression refrigeration cycles utilizing a hydro-fluorocarbon refrigerant such as 1,1,1,2-Tetrafluoroethane (R-134a). However, R-134a has a very high relative global warming potential (GWP) of about 1300 times that of an equivalent mass of carbon dioxide over a 100 year time horizon with roughly 14 year lifetime once released into the atmosphere [70]. Therefore the European Union has issued a directive restricting the use of refrigerants with high GWP (such as R-134a) in new car models introduced after January 2011 that will be produced after 2016 [3]. One of the proposed replacements for R-134a is 2,3,3,3-Tetrafluoropropene (HFO-1234yf) developed by E.I. duPont deNemours and Honeywell International. HFO-1234yf possesses a more modest GWP of 4 times that of carbon dioxide with an atmospheric lifetime of only 11 days [4].

Due to differences in molecular composition and size, it was desired to assess the compatibility and permeation rates of the new HFO-1234yf with rubber compounds utilized in current A/C systems [5]. Changes in rubber tensile strength, elongation, hardness, and volume suggest good compatibility after exposure to the new refrigerant.

However, permeation of HFO-1234yf through sealing components increases by about 30% when compared to the current R-134a.

Elastomers used in the A/C applications are EPDM, HNBR, CR and IIR due to their good compatibility with refrigerant, compressor lubricant and their temperature range [71].

## 2 THE AIMS OF RESEARCH WORK

### Objective:

- Investigate the effect of hybrid filler systems of silica and nanoclay on a NBR compound with emphasis on morphology, mechanical properties and gas diffusion
- Develop a rubber compound with optimized morphology and mechanical properties with decreased refrigerant R-134a diffusion

### Application:

- Refrigerant sealing elements in automotive air conditioning systems

### Investigation plan

#### 1. Proposal of rubber compound

- Rubber type NBR
- Vulcanization system – peroxide
- Modification of basic recipe by different type and amount of mineral fillers
- Targets:
  - Tensile strength: 8 MPa min.
  - Elongation: 150 % min.
  - Hardness: 70 to 80 ShA
  - Tear strength: 2.5 N/mm min.
  - Compression set: 20 % (110°C / 24 hrs) max.
  - Permeation: 25 % reduction (R-134a, 70°C) min.

#### 2. Investigation of mineral filler influence to permeation

- Selection of mineral fillers
  - Nanoclays, silica, kaolin, talc
  - Combination of silica / nanoclay, silica / kaolin, silica / talc

#### 3. Investigation of hybrid filler system silica / nanoclay

- Interaction between filler particles
- Interaction between filler particles and polymeric matrix
- Influence to static - mechanical and dynamic – mechanical properties
- Influence to intercalation and exfoliation of nanoclay

#### **4. Testing facility**

- FT UTB (static - mechanical and dynamic – mechanical parameters, rheology)
- Halla Visteon Climate Control (permeation of R-134a)

### 3 TEST METHODS AND MATERIALS

#### 3.1 Measurement of dynamic – mechanical properties

Dynamic mechanical properties were measured by a rubber process analyzer RPA 2000 produced by Alpha technologies. The RPA 2000 is dynamic mechanical rheological tester designed to test raw elastomers, mixed rubber compound or cured compounds. As can be seen in Figure 20, the RPA strains a sample in shear by oscillation of a lower die in a pressurized sealed cavity. The lower die can oscillate from 0,05 to 90° and oscillation frequency can be varied between 0.1 to 2000 cycles per minute [72].

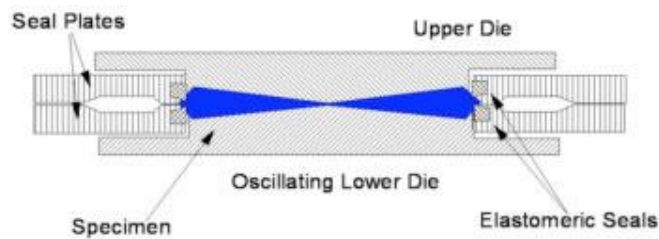


Figure 20: Die configuration of RPA 2000 [73]

The RPA 2000 provides measurement of elastic torque  $S'$ , viscous torque  $S''$ , storage modulus  $G'$ , loss modulus  $G''$ , complex dynamic viscosity  $\eta^*$ , real dynamic viscosity  $\eta'$ , loss factor  $\tan \delta$ , vulcanization characteristics (minimal torque ML, maximal torque MH) and other responses.

Elasticity of rubber material is measured by storage elastic modulus  $G'$  which shows ability of material to store energy. Loss of energy as heat is measured by loss viscous modulus  $G''$  which determines the ability to dissipate energy. Loss factor  $\tan \delta$  measures dissipation of energy relative to the stored energy during deformation and is determined by ratio of storage modulus  $G'$  and loss modulus  $G''$  [37]:

$$\tan \delta = G'' / G' \quad (11)$$

Typical charts of dynamic mechanical properties are shown in Figure 21.

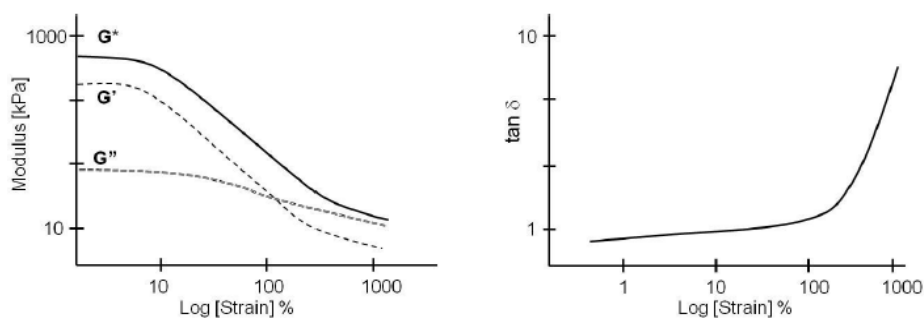


Figure 21: Dynamic mechanical properties of rubber compound [37]

Storage modulus  $G'$  shows typical non-linear behavior, which was observed by Warring [85]. This phenomenon is called the Payne effect according to A. R. Payne which is thoroughly studied and described as a non-linear behavior of filled rubber compounds [86], [87]. Payne effect describes difference between low-strain ( $\approx 10\%$  strain) and high-strain modulus ( $\approx 10\%$  strain).  $G'$  is not strain dependent at low-strain, while non-linear dependence is shown at high-strain over 10%. Decrease in elastic modulus upon increasing strain is caused by breakdown of filler particle networks [86].

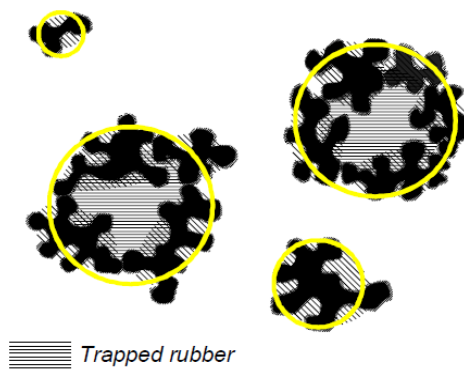


Figure 22: Scheme of trapped rubber in the filler particle network [85]

The Payne effect is mainly related to the filler network created in the rubber matrix. Chains of rubber can be trapped in filler particle networks as shown in Figure 22 and lose elastomer identity, because their behavior is similar to filler under stress-strain. Thus the effective volume of rubber is reduced by filler structure and influences increases in the  $G'$  modulus. Trapped rubber is released by breakdown of the filler structure at increased strain amplitude [85].

### 3.2 Measurement of tensile stress - strain

Tensile stress – strain is the most fundamental mechanical test used for measuring the mechanical behavior of elastomers. This data is collected using a uni-axial testing machine pulling used vulcanized dumbbell-shaped rubber samples in tension while recording loads and displacements. Figure 23 shows typical shape of test sample [18].



Figure 23: Rubber dumbbell sample [18]

Ultimate tensile strength, ultimate elongation and tensile stress at different elongations are typically determined by this test. Figure 24 shows typical stress-strain curve for a vulcanized rubber compound. As can be seen, this curve is non-linear making calculation of Young's modulus not practical [18].

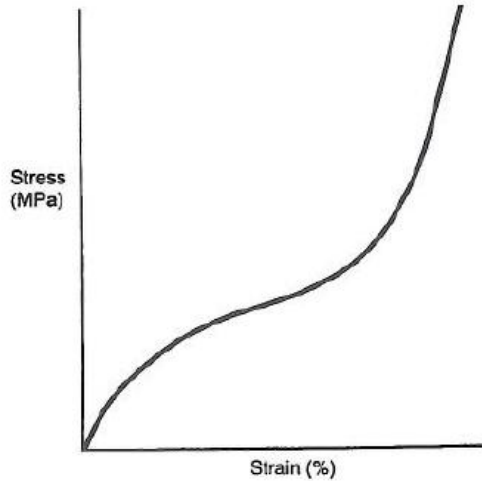


*Figure 24: Typical stress strain curve of rubber [18]*

The elongation at break is the elongation measured at the point which the sample ruptures under the increasing tensile load. Elongation at break is an important indicator of the rubber compound's suitability for seal elements which are stretched by a large percentage during assembly [75].

The tensile strength is the force necessary to rupture a standard test piece at a given rate of elongation and is calculated as the ratio of the force (F) applied to the rubber material at break to original cross-sectional area of test sample. Tensile strength is usually expressed in megapascals (MPa) [80].

Instantaneous tensile stress at different elongations is often referred to as "modulus" and is defined as tensile strength at a particular elongations (100%, 200, %, 300%) [75].

Tensile stress – strain properties were measured in this investigation by a Tensometer 2000 produced by Alpha technologies according to test methods defined in ISO 37.

### **3.3 Measurement of tear strength**

Tear strength is defined as the maximum force which causes a "nick" or "stress concentration" in a defined test sample to propagate into a tear. Tear resistance measures sensitivity of cured rubber to surface defects. Tear resistance of different rubber compounds depends on the crosslink density, state of vulcanization, filler types and filler loadings [18], [75].

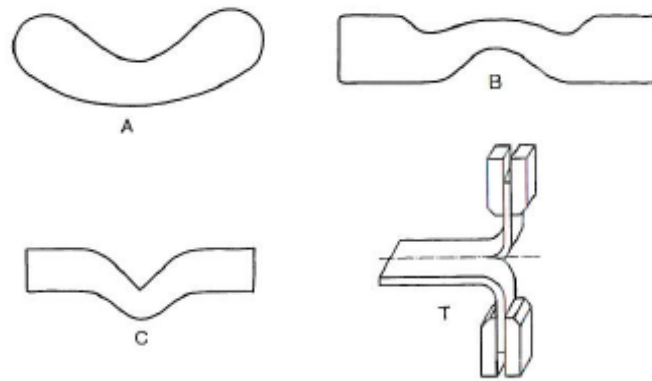


Figure 25: Shape of standard tear specimens [18]

Tear strength was measured by a Tensometer 2000 Alpha technologies according to test methods defined in ČSN ISO 6383-1. A “trouser” tear specimen (similar in geometry to sample “T”) was used in the test.

### 3.4 Measurement of hardness

Hardness is the most useful parameter for the characterization of elastomers. It is very fast, inexpensive and simple test method. Hardness measures an elastomer’s resistance to deformation. Deformation is applied by forcing a rigid indenter with defined shape into the surface of a rubber sample in a specified time. Hardness is typically measured in units Shore A or International Rubber Hardness Durometer (IRHD) [18].

Hardness was measured by a durometer HBA 100-0 according to ČSN ISO 7619-1 (Shore A) and by a Barreis durometer according to ISO 48 (IRHD).

### 3.5 Measurement of compression set

Compression set describes loss of elastic memory of elastomers and is measured as percentage of original deformation of the test sample. Typically better elastomeric memory results in lower compression set. Compression set depends on the elastomer base, test time, test temperature, deformation of test sample and contact medium [75].

Compression set (CS) is calculated:

$$CS = \frac{h_0 - h_1}{h_0 - h_2} \cdot 100 \quad \% \quad (12)$$

Where:  $h_0$  original height of the test piece [mm]  
 $h_1$  height of deformed test piece [mm]  
 $h_2$  height of released test piece (after a definite time delay) [mm]



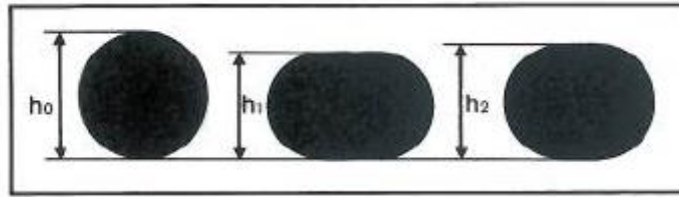


Figure 26: Compression set [75]

Compression set testing in this investigation was performed according to specification ČSN ISO 815-1 at temperature 110°C for 24 hrs.

### 3.6 Measurement of permeation

Permeation of refrigerant R-134a was measured by mass spectrometer. A schematic of the mass spectrometer test stand is shown in Figure 27. A fixture with the test sample to be measured is placed in the bottom of a chamber and is connected to a tank of liquid R-134a refrigerant placed outside of the test chamber. Refrigerant permeates through test sample and flows into test chamber. An analyzer in the chamber can then sample the chamber gasses non-destructively and return the tested gasses back into the test chamber for continuous measurement.

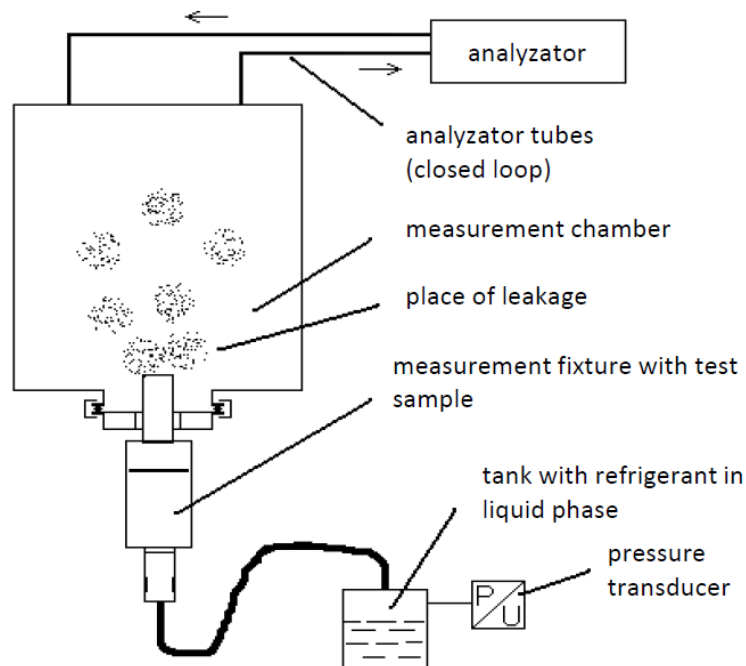


Figure 27: Scheme of mass spectrometer test stand

### 3.6.1 Description of test method

Photoacoustic spectroscopy is based on the absorption of electromagnetic energy by analyzed molecules. A schematic of a photoacoustic spectrometer is shown in Figure 28.

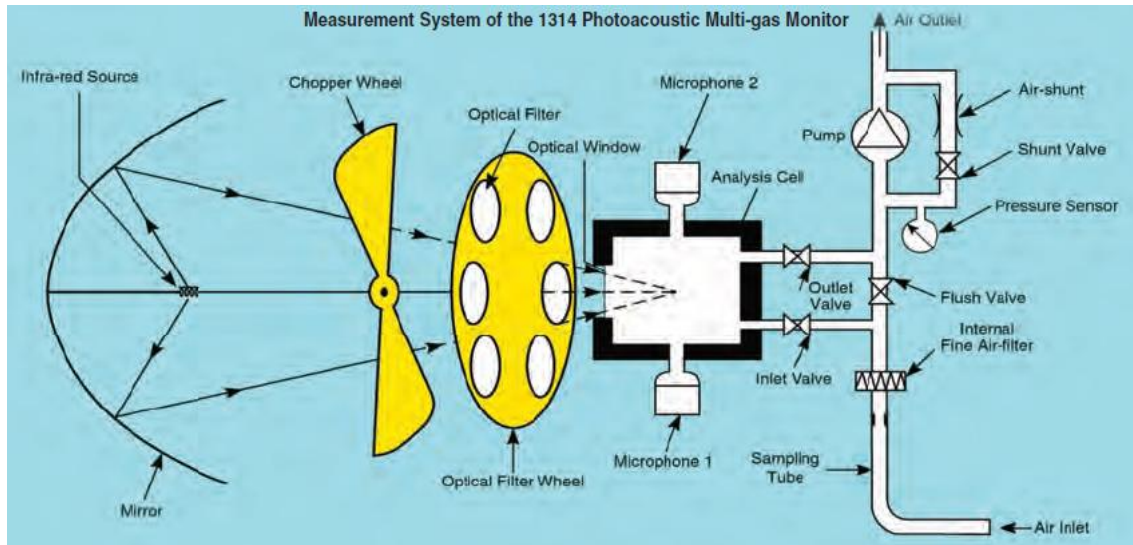


Figure 28: Scheme of photoacoustic spectrometer INOVA 1314 [84]

Collision of gas molecules with others leads to local warming and an increase of pressure of gas within the closed test chamber. Fluctuations of pressure are generated by thermal expansion, which is detected in the form of acoustic waves. Modulated electromagnetic energy generates periodic thermal energy within the measured gas and thermal and the pressure wave of the gas being measured will have same frequency as this electro-magnetic energy modulation. Change in pressure depends on the concentration of measured gas. The periodic variation in the temperature and pressure generates acoustic waves in the gas and these waves propagate through the volume of the gas to the microphone detector. A microphone photoacoustic signal gives a spectrum proportional to the absorption spectrum of the sample [76], [77].

### 3.6.2 Calculation of permeation

Permeation is calculated using the initial and final HFC-134a concentrations, temperatures and pressures within the test the enclosure, together with the net measurement of enclosure volume [74]:

$$m_{HFC-134a} = M_{HFC-134a} \cdot V_{shed} \cdot \frac{P_{shed}}{R \times T_{shed}} \cdot c \cdot 10^{-6} \quad (13)$$

$$c = \frac{m_{HFC-134a} \cdot R \cdot T_{shed}}{P_{shed} \cdot M_{HFC-134a} \cdot V_{shed} \cdot 10^{-6}} \quad (14)$$

The total leakage-mass of HFC-134a is calculated by means of the following formula [74]:

$$\dot{m}_{HFC-134a} = M_{HFC-134a} \cdot (V_{shed} - V_{AC}) \cdot \frac{P_{shed}}{R \cdot T_{shed}} \cdot \frac{(C_{HFC-134ae} - C_{HFC-134ai}) \cdot 10^{-6}}{(t_e - t_i)} \quad (15)$$

where:	$\dot{m}_{HFC-134a}$	leak flow rate of HFC-134a	[kg/s]
	$m_{HFC-134a}$	weight of refrigerant	[kg]
	$c$	concentration of refrigerant	[ppm]
	$V_{shed}$	SHED-chamber net volume	[m <sup>3</sup> ]
	$V_{AC}$	gross volume of test sample	[m <sup>3</sup> ]
	$T_{shed}$	absolute temperature in the chamber	[K]
	$P_{shed}$	absolute pressure in the chamber	[kPa]
	$C_{HFC-134ae}$	value of final concentration	[ppm]
	$C_{HFC-134ai}$	value of initial concentration	[ppm]
	$t_e$	final time	[s]
	$t_i$	initial time	[s]
	$M_{HFC-134a}$	molar mass of HFC-134a	[g/mol]
	$R$	gas constant	[kJ/(kmolK)]

### 3.6.3 Test method

Permeation of refrigerant R-134a through samples of vulcanized rubber was measured utilizing test equipment supplied by Maximator with a photoacoustic spectrometer (Innova model 1314) at a pressure 2 MPa and temperature 70°C. The Maximator test stand is shown in the Figure 29. The test was done according to European Union Commission Regulation (EC) No 706/2007 [74]. Refrigerant concentration in the test chamber was recorded over the test duration. Permeation was calculated in g/year for test samples with thickness of 2 mm and area of 238 mm<sup>2</sup>.



Figure 29: Test stand Maximator with mass spectrometer INOVA 1314

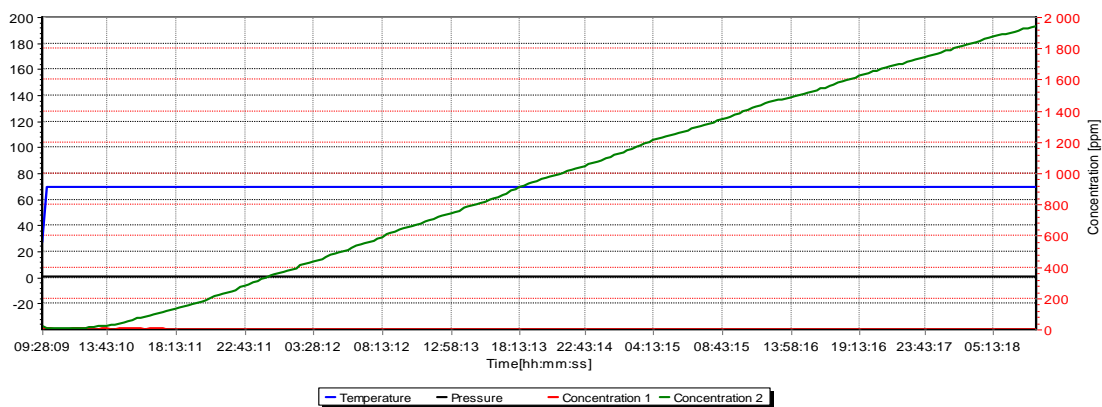


Figure 30: Record of measurement

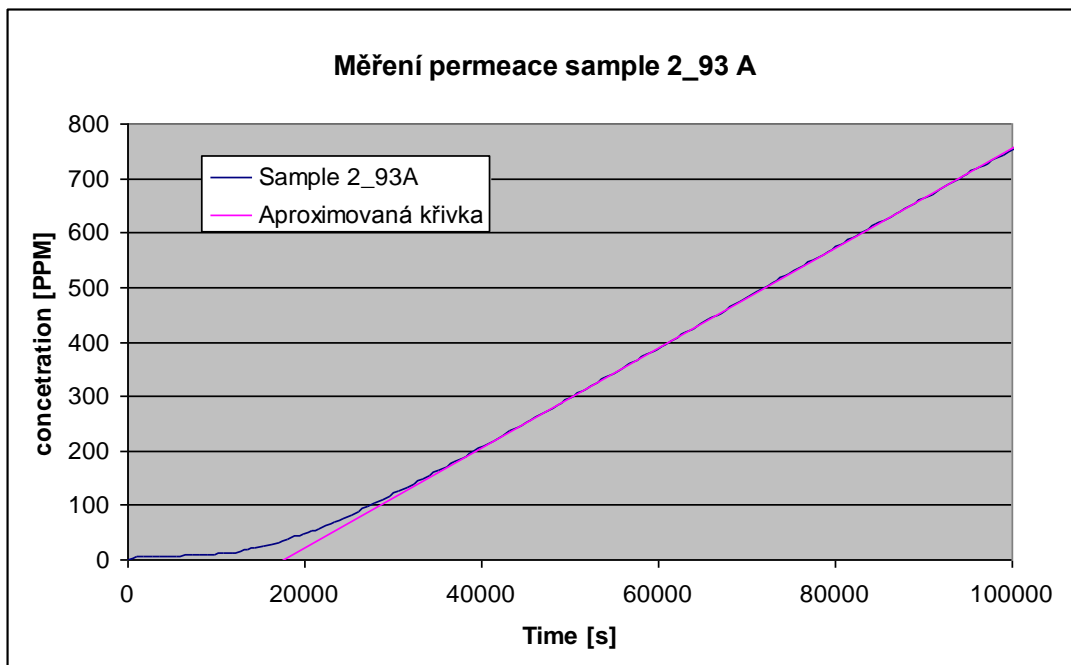


Figure 31: Approximation of measured data

### 3.7 Nanocomposite structure analysis

Two test methods were used for characterization of the structure of rubber / clay nanocomposites – X-ray diffraction (XRD) and Transmission electron microscopy (TEM).

XRD is a relatively simple method to investigate the spacing between the nanoclay layers. Simple sample preparation and a rapid test rate are very advantageous for this test method. XRD yields data in less than 1 hour on a simple slab sample. Interpretation of the results must be performed properly, because of the lack of analysis sensitivity and limits of the XRD test equipment can cause incorrect conclusions regarding the rubber nanocomposite structure. Therefore, additional analysis using TEM is necessary to complement the XRD results. TEM provides a direct analysis of the nanoclay distribution and exfoliation in polymeric matrix, but requires substantial skill in test sample preparation and analysis.

#### 3.7.1 X-ray diffraction (XRD)

XRD analysis detects the regular spacing of the clays and organoclays due to their layered structures. Type and size of this peak indicates level of platelet separation in clay structure.

Diffraction from two scattering separated clay layers by a distance  $d$  (interlamellar spacing or  $d$ -spacing) with incident X-rays of wavelength  $\lambda$  at incident angle  $\theta$  is known as Bragg diffraction. Description of Bragg diffraction is based on the idea that the diffracted beam rises by "reflection" from a system of parallel platelets of organoclays. The incident and diffracted beams form the same angle  $\theta$  with the system of parallel platelets, thus corresponding to the law of reflection as it shown in Figure 32 [47].

It is apparent that the radiation diffracted by platelet of nanoclay is superimposed with the same phase, as is the case with ordinary reflection at a planar interface. In contrast, radiation diffracted by an adjacent parallel plane at a distance  $d$  has a path difference  $2d \sin\theta$ . Radiation diffracted different planes thus superimposed with the same phase, if is valid condition [78]:

$$2d \sin\theta = n\lambda \quad (16)$$

This equation is known as Bragg's Law, where  $n$  is an integer number representing the order of diffraction, and  $\lambda$  is the wavelength of the incident radiation.

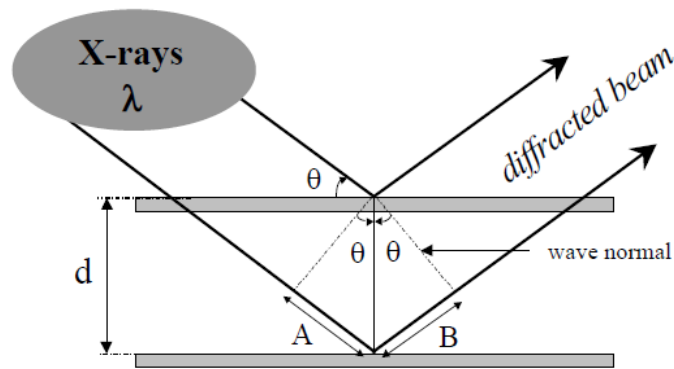


Figure 32: Principle of X-ray diffraction [47]

XRD analysis of polymer-clay nanocomposites is influenced by two factors. The first factor is the quite small amount of clay in nanocomposite structure, therefore XRD analysis must be sensitive enough to detect the crystalline structure of the clay in the polymeric matrix. The second factor is the analysis performance at low angle. This means that the sample holder can be present in the analysis together with irradiated surface. Therefore it is recommended that the test configuration should consist of a thin sample with large surface area [47].

XRD analysis visualizes status and level intercalation and exfoliation of nanoclay. Intercalation of polymer chains into clay interlayer space is reflected by XRD by shift of reflection to the left to lower values of the  $2\theta$  angle (Figure 33a). Reflexion of exfoliation of nanoclay remains at same value of  $2\theta$  angle and intensity is decreased as it shown in Figure 33b [52].

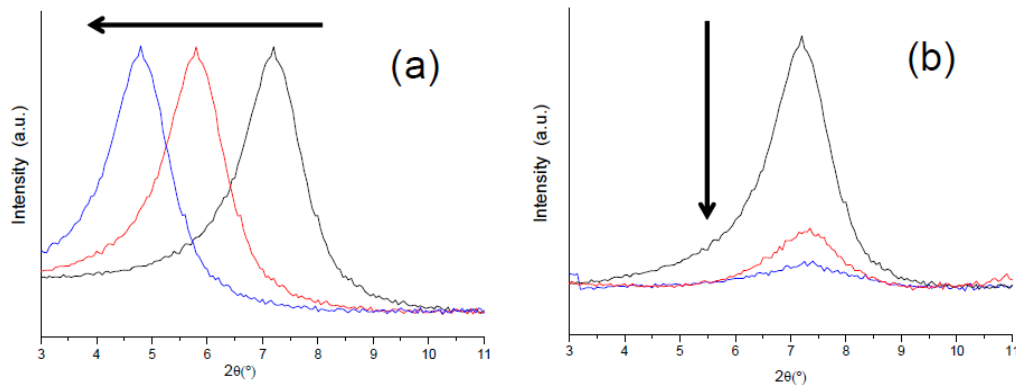


Figure 33: XRD visualization of mechanisms of clay intercalation and exfoliation [52]

X-Ray Diffraction analysis (XRD) of the cured NBR rubber samples was obtained using PANalytical X'Pert PRO diffracto-meter equipped with a Cu-K $\alpha$  radiation source ( $\lambda= 0,154$  nm) at room temperature. The scans were collected in the  $2\theta$  range from  $1,0^\circ$  to  $30^\circ$  at a step of  $0,02^\circ$  and the counting time of one scan 5 s. Samples were in  $1\text{cm}^2$  pieces cut from 2 mm rubber slab.

### 3.7.2 Transmission electron microscopy

Transmission electron microscopy (TEM) is an effective technique to analyze structures at and below the nanometer distance scale. Therefore TEM can confirm and supplement results obtained by XRD for clay layer spacing [47].

TEM operates on the same basic principles as the light microscope but uses electrons instead of light and magnetic lenses instead of glass ones. The TEM uses a focused beam of electrons as an "illumination" source and the much lower wavelength of an electron makes it possible to obtain resolutions thousands of times better than with a transmission light microscope.

The electron gun at the top of the microscope emits a beam of electrons that travels through vacuum in the column of the microscope. The TEM uses electromagnetic "lenses" to focus the electron beam into a very small spot size. The electron beam then travels through the test sample. Some of the electrons are scattered and disappear from the beam, depending on the density of material through which they pass. The unscattered electrons strike a fluorescent screen at the bottom of the TEM which creates an image of the tested sample in varied levels of darkness according to their density [79].

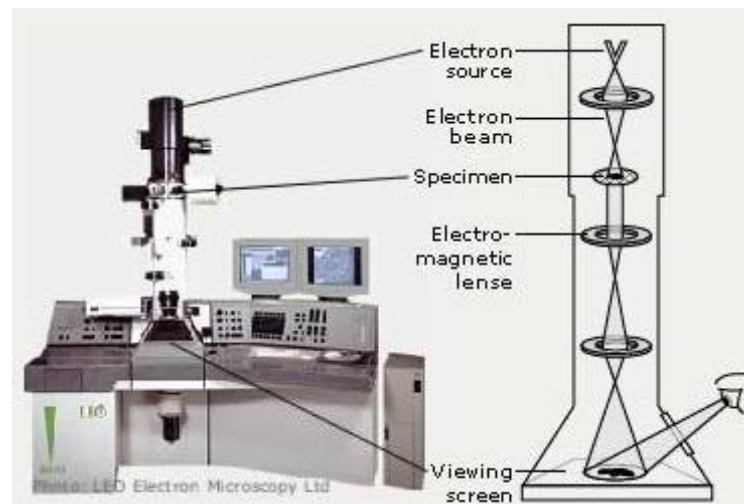


Figure 34: Description of a transmission electron microscope [79]

Specimen preparation is very important and constitutes a major difficulty in TEM analysis. Samples are prepared by ultramicrotomy and the thickness of test sample must be less than 100 nm [47].

Samples of vulcanized NBR rubber compounds for TEM analysis were cut by ultra cryomicrotomy using a Leica Ultracut UCT at cryo-conditions at thicknesses of approximately 50 nm. Temperature of sample was  $-70^{\circ}\text{C}$  and temperature of knife -

45°C. Microscopy observation was performed by a Tecnai G2 Spirit transmission electron microscope, operating at an acceleration voltage of 120 kV.

### 3.8 Measurement of FTIR

Fourier Transform Infra-Red spectroscopy (FTIR) is an important tool of the organic chemistry to study chemical changes in the materials. This method provides an advantage over conventional infrared systems by higher sensitivity, speed and improved data processing.

Scheme of FTIR principle is shown in Figure 35. A broad band of different wavelengths of infrared radiation are emitted by an infrared source. Infrared radiation is modulated by an interferometer and passes through the tested sample, where it is absorbed by various molecular bonds present in the tested sample. Subsequently the intensity of IR beam is registered by a detector and the signal transformed by computer to generate the IR spectrum of measured sample [89].

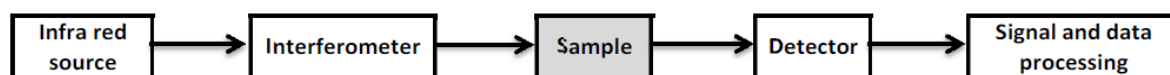


Figure 35: Scheme of FTIR [89]

FTIR analysis was performed using an attenuated total reflectance (ATR) technique at room temperature, 32 scans (Nicolet, AVATAR 320).

### 3.9 Materials

Acrylonitrile-butadiene rubber used in the study was Krynac<sup>®</sup> 33.45, Krynac<sup>®</sup> 49.75 from Lanxess Corporation and Europrene<sup>®</sup> N33.45 from Enichem. The active silica fillers Perkasil<sup>®</sup> KS 300 and Perkasil<sup>®</sup> KS 408 were produced by Akzo Nobel. Nanoclays Cloisite<sup>®</sup> 15A, 20A, 25A, 93A, Na<sup>+</sup> were prepared by Rockwood Additive and Nanofil<sup>®</sup> 5 by Sud-Chemie. Standard kaolin, type KKAKA was supplied by LB Minerals Kaznejov and calcined type PO5 by Ceske lupkove zavody. The supplier of talc, type 1.A was Demerska Hnusta. Vulcanization was achieved using the peroxide (Norperox BIPB 40) in combination with an activator (RheinChemie Rhenofit TAC/GR 70).



### 3.10 Preparation of rubber compounds

Rubber compounds were prepared in two stages. A masterbatch of NBR, silica and oil was first compounded in a Pomini Farell (2,5 liters) laboratory mixer for 6 minutes at a temperature of 150°C. The plate-like inorganic fillers were then added to the masterbatch together with the vulcanization system on a two-roll mill and mixed for 11 minutes at a temperature of about 40°C. Formulations of the rubber compounds with various mineral fillers are shown in Table 1. Types of tested nanoclay, kaolin and talc are summarized in Table 2.

Table 1: Formulation of NBR compounds with various mineral fillers

<b>Chemical</b>	<b>Compound No. 1 [phr]</b>	<b>Compounds No. 2 to 10 [phr]</b>
NBR Krynac <sup>®</sup> 33.45	100	100
Silica Perkasil KS 300	30	30
Diocetyl adipate oil	20	20
Nanoclay, kaolin or talc	-	10
Peroxide Norperox BIPB 40	7	7
Rhenofit TAC/GR 70	2	2
Total	159	169

Table 2: Types of tested nanoclay, kaolin and talc

<b>Compound</b>	<b>White filler</b>
No. 2	Cloisite 93A
No. 3	Cloisite 15A
No. 4	Cloisite 25A
No. 5	Cloisite 20A
No. 6	Cloisite Na+
No. 7	Nanofil 5
No. 8	Kaolin calcinated P05
No. 9	Kaolin
No. 10	Talc

Formulation of rubber compounds with various ratios of silica and nanoclay are shown in Table 3 and Table 4.

Table 3: Formulation of NBR compounds with various ratio of silica KS 300 and Cloisite 25A

	Compounds KS 300									
	0/10	5/10	10/10	15/10	0/30	5/30	10/30	15/30	7,5/20	12,5/20
NBR Krynac <sup>®</sup> 33.45	100	100	100	100	100	100	100	100	100	100
Silica KS 300	10	10	10	10	30	30	30	30	20	20
Cloisite 25A	-	5	10	15	-	5	10	15	7,5	12,5
Diocetyl adipate oil	20	20	20	20	20	20	20	20	20	20
Peroxide Norperox BIPB 40	7	7	7	7	7	7	7	7	7	7
Rhenofit TAC/GR 70	2	2	2	2	2	2	2	2	2	2

Table 4: Formulation of NBR compounds with various ratio of silica KS 408 and Cloisite 25A

	Compounds KS 408									
	0/10	5/10	10/10	15/10	0/30	5/30	10/30	15/30	7,5/20	12,5/20
NBR Krynac <sup>®</sup> 33.45	100	100	100	100	100	100	100	100	100	100
Silica KS 408	10	10	10	10	30	30	30	30	20	20
Cloisite 25A	-	5	10	15	-	5	10	15	7,5	12,5
Diocetyl adipate oil	20	20	20	20	20	20	20	20	20	20
Peroxide Norperox BIPB 40	7	7	7	7	7	7	7	7	7	7
Rhenofit TAC/GR 70	2	2	2	2	2	2	2	2	2	2

### 3.11 Vulcanization of rubber compounds

All prepared rubber compounds were vulcanized in a hydraulic press at a temperature 175°C for optimum cure time t<sub>90</sub> and 2 mm thick samples for testing of mechanical properties were obtained.

## 4 RESULTS AND DISCUSSION

Testing and investigation was performed in three steps. First, the six different types of nanoclays (Cloisite<sup>®</sup> 15A, 20A, 25A, 93A, Na<sup>+</sup> and Nanofil<sup>®</sup> 5) were investigated in combination with silica Perkasil<sup>®</sup> KS 300 filler. The second step involved the investigation of the optimal mix ratio of nanoclay Cloisite<sup>®</sup> 25A with two types of silica – Perkasil<sup>®</sup> KS 300 and Perkasil<sup>®</sup> KS 408. The last step of investigation compared difference in influence of polymer viscosity and load of silica to morphology of NBR nanocomposites.

### 4.1 Nanoclays performance investigation

Combinations of silica and nanoclay mixed in an NBR matrix were the subject of this study. An effort was made to identify the most cost effective rubber compounds which optimize both mechanical properties and permeation resistance. Combinations of silica, kaolin and talc were investigated in parallel as low cost solutions and compared with silica and nanoclay combinations in their effect on property modification.

#### 4.1.1 Vulcanization characteristics

Vulcanization characteristics of the rubber compounds were determined by a rubber process analyzer (Alpha Technologies RPA 2000) at a temperature of 175°C.

As can be seen in Table 5, the addition of all the types of mineral fillers investigated does not influence vulcanization times  $t_{90}$  and  $ts_2$ .

Table 5: Vulcanization parameters

Compound	ML [dN.m]	MH [dN.m]	$ts_2$ [min]	$t_{90}$ [min]	$\tan \delta$ max. S'
1 - silica	0,51	27,77	0,71	7,13	0,019
2 - 93A	0,90	24,66	0,74	6,64	0,044
3 - 15A	0,73	24,75	0,74	7,05	0,025
4 - 25A	1,08	26,30	0,73	6,98	0,035
5 - 20A	0,80	25,25	0,74	7,10	0,028
6 - Na <sup>+</sup>	0,61	30,92	0,69	7,15	0,017
7 - Nano5	0,78	25,71	0,73	7,10	0,025
8 - P05	0,56	29,86	0,71	7,18	0,015
9 - kaolin	0,54	29,67	0,71	7,19	0,020
10 - talc	0,63	29,92	0,71	7,22	0,018

Differences between the behavior of nanoclays and standard mineral fillers (kaolin and talc) are shown in torque measured (ML and MH). While compounds with nanoclays show lower maximum torque (MH) as shown in Figure 36, compounds with standard mineral fillers show lower minimum torque (ML) as can be seen in Figure 37. Difference between compounds with nanoclay and compounds with talc or kaolin are shown in the results of loss tangent ( $\tan \delta$ ). Cloisite Na<sup>+</sup> was observed to be an exception within the nanoclays tested showing similar values as talc or kaolin. The cause for this difference can be difference in stability of filler particle networks at different temperatures. While temperature inside of test samples at time of ML measurement should be lower than temperature of die, at time of MH measurement is temperature of test sample 175°C.

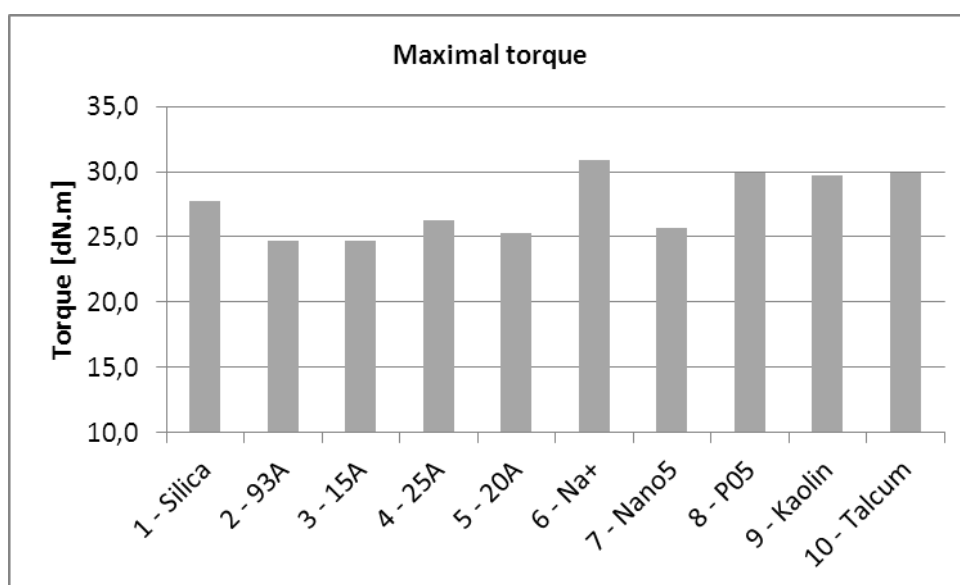


Figure 36: Comparison of maximum torque (MH)

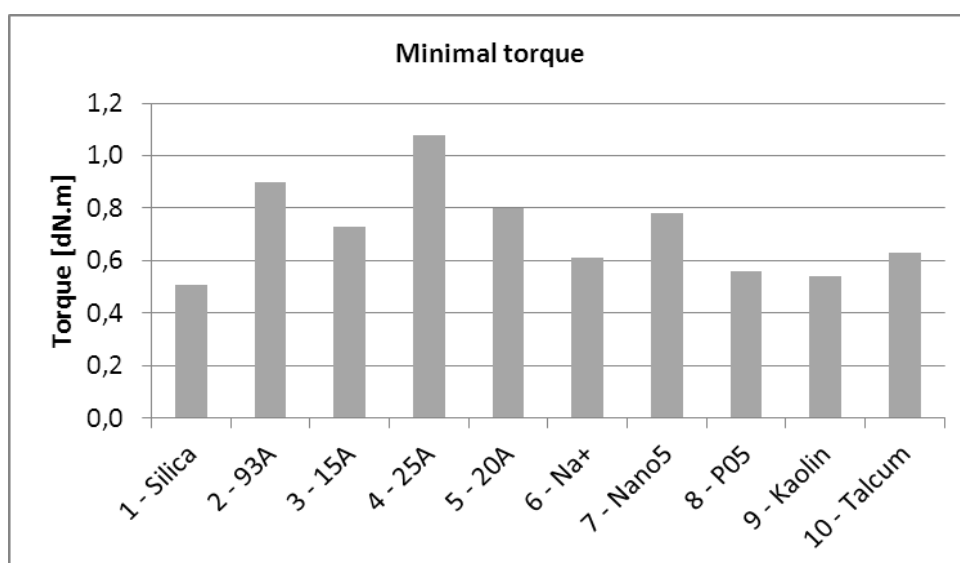


Figure 37: Comparison of minimum torque (MH)

### 4.1.2 Hardness testing

As it is shown in Table 6 and Figure 38, the addition of all types of tested nanoclay fillers resulted in significant increases in hardness. All compounds which contained nanoclay met the project hardness target of 70 to 80 ShA.. The largest hardness increases were achieved by Cloisite 20A, Cloisite 25A and Cloisite Na<sup>+</sup> with a typical increase of 11 to 13 Shore A in comparison to base compound No. 1. These results indicate that good distribution of the nanoclay was achieved in the NBR matrix. However, some increase in hardness was also observed in compounds containing kaolin and talc. This increase of hardness is likely result of the plate-like structure of filler particles and their parallel orientation to the surface of test samples.

Table 6: Hardness – testing results

Compound	Hardness (ShA)
1 - Silica	66
2 - 93A	72
3 - 15A	73
4 - 25A	79
5 - 20A	76
6 - Na <sup>+</sup>	77
7 - Nano5	73
8 - P05	67
9 - Kaolin	70
10 - Talc	68

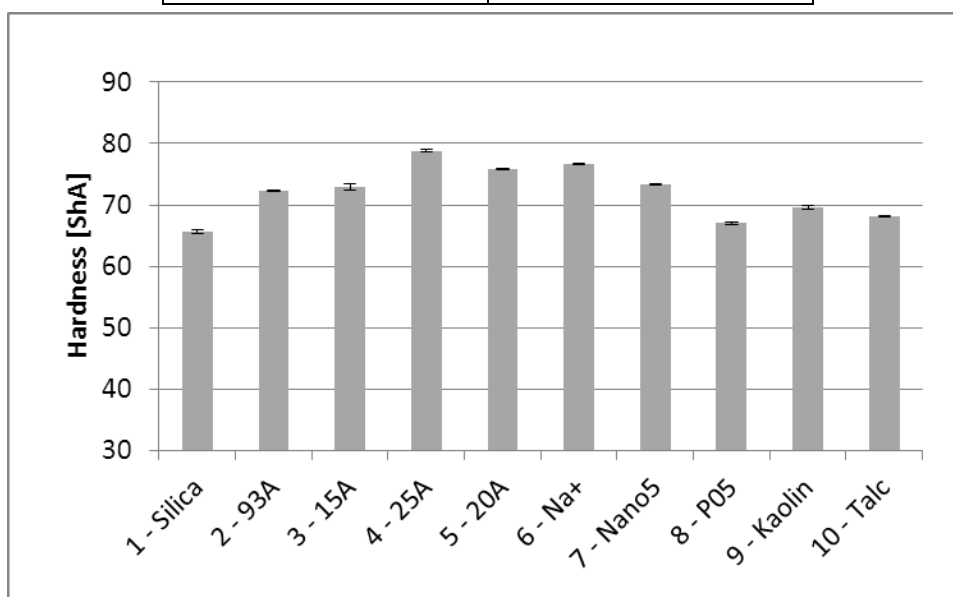


Figure 38: Comparison of hardness obtained for the tested samples

### 4.1.3 Tensile testing

Figure 39, Figure 40, Figure 41 and Table 7 show results for measured tensile strength, elongation and modulus  $M_{100}$ .

Table 7: Tensile testing results

Compound	Tensile strength [MPa]	Elongation [%]	$M_{100}$ [MPa]
1 - Silica	4,3	125	3,4
2 - 93A	9,2	191	5,2
3 - 15A	8,2	181	4,7
4 - 25A	9,8	182	5,9
5 - 20A	8,8	182	5,1
6 - Na+	6,8	134	5,3
7 - Nano5	9,3	189	5,2
8 - P05	6,0	135	4,5
9 - Kaolin	6,4	138	4,7
10 - Talc	4,5	112	4,0

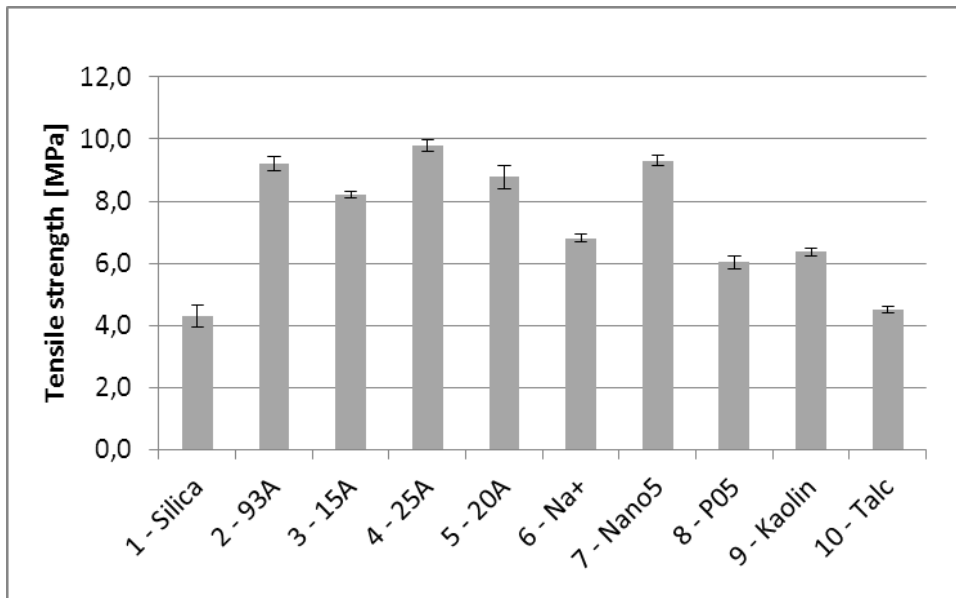


Figure 39: Comparison of tensile strength

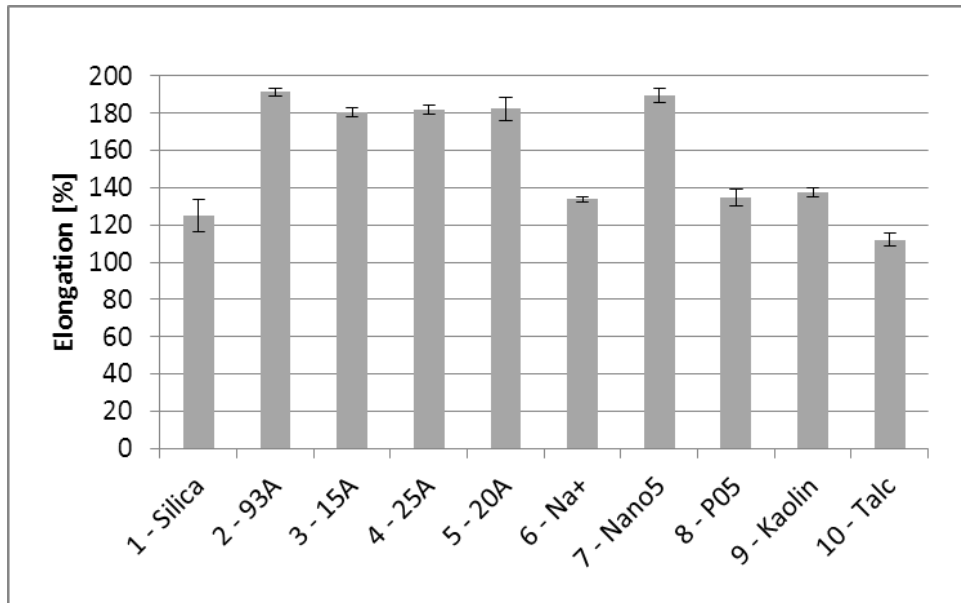


Figure 40: Comparison of elongation

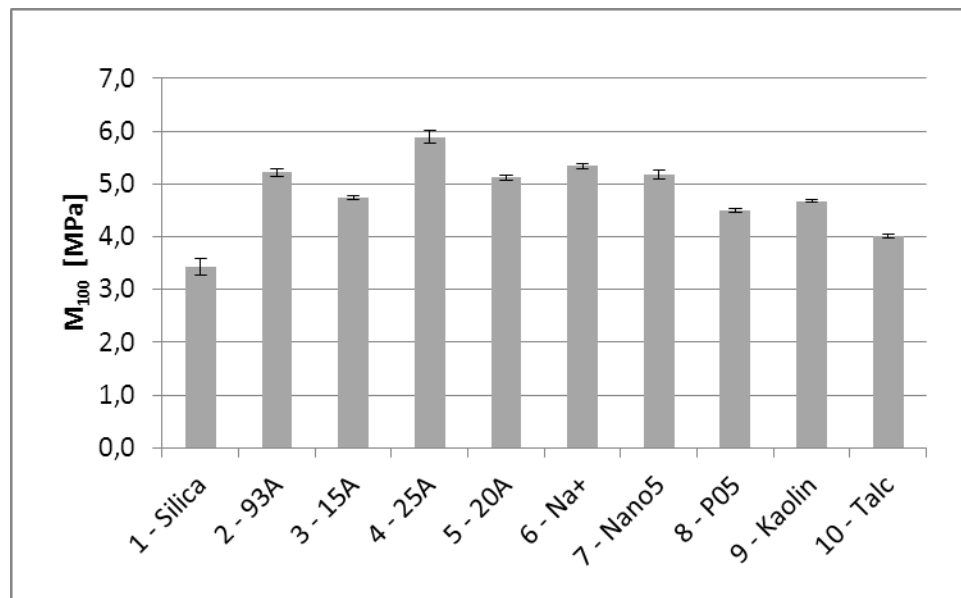


Figure 41: Comparison of modulus  $M_{100}$

Cloisite Na+ shows a lower reinforcing effect than the other nanoclays and results in a tensile strength and elongation similar to the kaolin addition. This is likely the result of a lack of exfoliation and distribution of Cloisite Na+ nanoclay during the mixing process. However, a significant improvement in tensile strength and elongation were achieved by other nanoclay fillers tested. Only the compounds filled by modified nanoclays meet the project targets for minimum tensile strength (8 MPa) and elongation (150 %). Figure 39 shows Cloisite 25A improves tensile strength by about 130 %, while Cloisite 93A and Nano5 improve strength by 115 %. Elongation is increased by approximately 70 % by Cloisite 93A and Nano5. Modulus  $M_{100}$  of compound with Cloisite 25A is improved by about 70 %. These improvements are

most likely the result of the higher aspect ratio of exfoliated nanoclays compared to lower aspect ratio of silica or common white fillers. These results demonstrate importance of achieving good exfoliation of the nanoclay during the mixing process.

#### 4.1.4 Tear strength

Results of tear strength are shown in Table 8 and Figure 42.

Table 8: Tear strength results

Compound	Tear strength [N/mm]
1 - Silica	1,8
2 - 93A	2,5
3 - 15A	2,3
4 - 25A	5,0
5 - 20A	2,0
6 - Na+	2,0
7 - Nano5	2,2
8 - P05	2,0
9 - Kaolin	1,2
10 - Talc	1,1

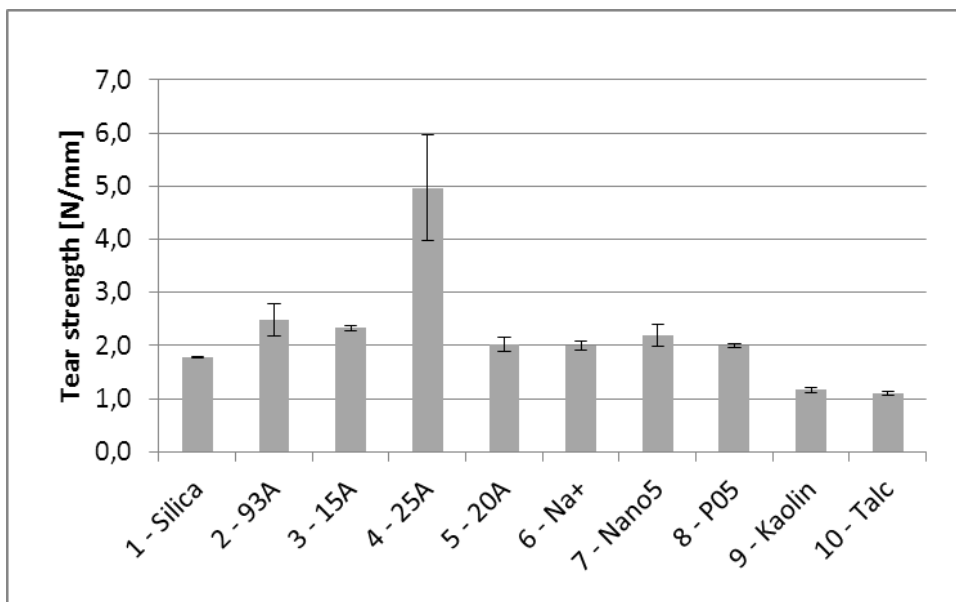


Figure 42: Comparison of tear strength

As was expected, compounds No. 9 and 10 with kaolin and talc show deterioration in tear strength due to the shape and size of plate like particles. Large particles initiate



or propagate cracks under these test conditions [35]. Larger improvements in tear strength were observed in compounds containing Cloisite 25A, which improved tear strength resistance by 180 %. This result correlates with tensile strength results suggesting good level of exfoliation of Cloisite 25A in the NBR matrix.

Compounds No. 4 (Cloisite 25A) and No. 2 (Cloisite 93A) meet the project target of a 2.5 N/mm for minimum tear.

#### 4.1.5 Compression set

Figure 43 shows results for compression set tested at temperature 110°C for 24 hrs. The highest increase in compression set was observed in compound No. 2 filled with Cloisite 93A and only this compound fails to meet the project target for a 20% maximum compression set. Compression set increased from 13% to 22% in comparison to base compound No. 1 filled by pure silica. Each type of nanoclay in this evaluation is modified by different modifier [2] and modifier type is the likely cause of increase in compression set of compound containing Cloisite 93A.

Compounds with nanoclays do not show better performance in this test in compared to compounds filled by kaolin or talc. Plate-like shape of particles does not improve properties as seen in tensile or hardness testing.

Table 9: Compression set results

Compound	Compression set [%]
1 - Silica	13
2 - 93A	22
3 - 15A	15
4 - 25A	17
5 - 20A	18
6 - Na+	15
7 - Nano5	15
8 - P05	16
9 - Kaolin	17
10 - Talc	14

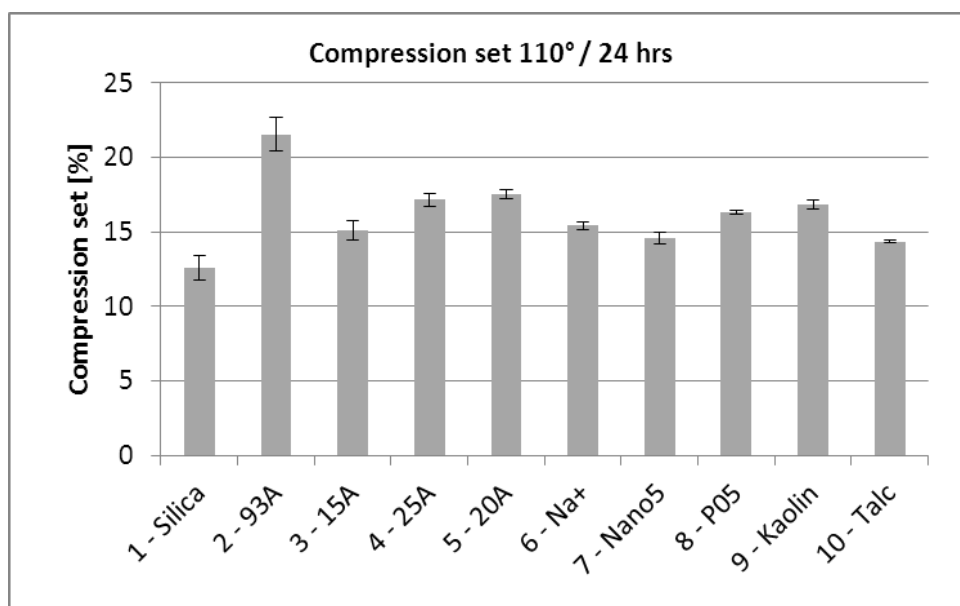


Figure 43: Compression set comparison

#### 4.1.6 Barrier properties

Figure 44 and Table 10 reveal that the addition of nanoclay significantly improves gas barrier properties which results in a reduction in permeation. As can be seen, the permeation of refrigerant R-134a decreased by 15-30 % after addition of nanoclays into compounds of NBR and silica. The reduction is probably caused by plate-like shape of exfoliated nanoclays. The plate-like fillers dispersed in the NBR matrix are able to reduce the permeation rate of molecules of R-134a through the elastomeric matrix by creating more tortuous pathways which the refrigerant molecules must travel to diffuse through the material. Exfoliated nanoclays should also reduce the diffusion coefficient by restriction of motion of NBR chains [58]. Recent research has shown that the higher aspect ratio fillers are the key factor to reduce gas permeation through nanocomposites [81], [82], [83] and the measured results agree with this conclusion.

Due to their laminar structure, a decrease of R-134a permeation was expected for compounds containing talc and kaolin. The difference between expected and obtained results may be explained by the random distribution of these particles in the NBR matrix. These randomly distributed particles then cannot create an effective tortuous path to resist the permeation of the R-134a refrigerant molecules.

The project target of a minimum 25 % reduction in R-134a permeation is met only by compound filled by Cloisite 25A. Compound with Cloisite 20A shows results which are very close to the project target.

Table 10: Permeation results

Compound	R-134a permeation [g/y]
1 - Silica	45,8
2 - 93A	37,3
3 - 15A	39,1
4 - 25A	33,2
5 - 20A	35,2
6 - Na+	43,2
7 - Nano5	39,1
8 - P05	46,4
9 - Kaolin	41,4
10 - Talc	45,3

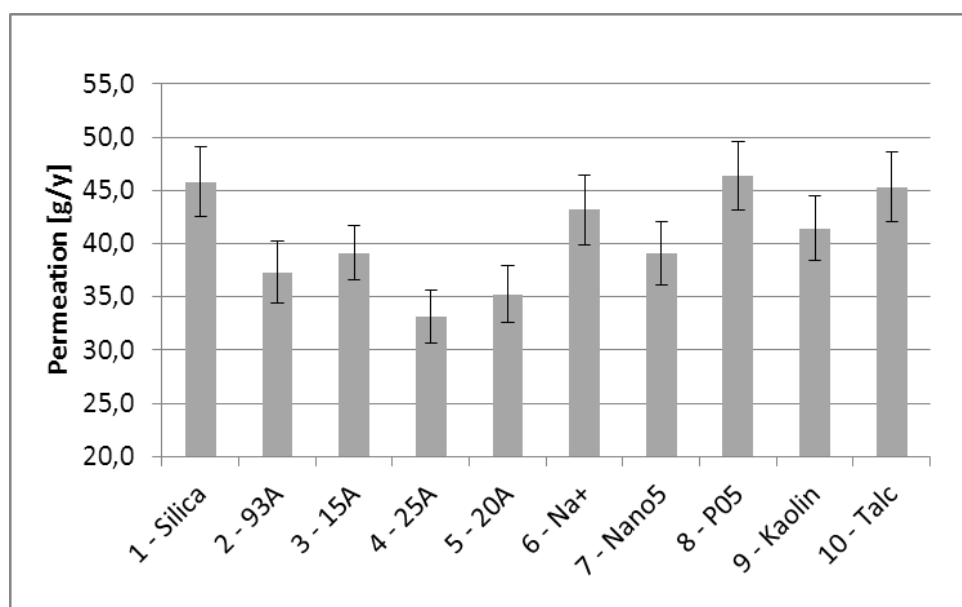


Figure 44: R-134a permeation comparison

#### 4.1.7 Dynamic-mechanical properties

Dynamic-mechanical properties of vulcanized rubbers were tested at temperatures of 40, 70 and 120°C in two different modes:

- 1) Mode 1 - constant strain amplitude of 1% with constant oscillation frequency 0,3 Hz
- 2) Mode 2 - constant oscillation frequency 0,1 Hz and strain amplitude from 0,5 to 250 %.

### ***Constant strain amplitude and constant oscillation frequency***

All vulcanized rubbers from compounds No. 1 to 10 were tested in mode 1 at constant strain amplitude and constant oscillation frequency at three different temperatures. The results in Figure 45 reveal dynamic storage modulus in shear ( $G'$ ) for compounds with nanoclays increases to temperatures of approximately  $70^{\circ}\text{C}$ , where  $G'$  begins to level off. It is possible that NBR chains are trapped in the filler network of silica and nanoclay and as the temperature increases above  $70^{\circ}\text{C}$ , these chains are released by breakdown of the particle structure. This figure shows a linear increase of dynamic modulus  $G'$  with temperature for compounds with silica, kaolin and talc, due to the different particle structure of the fillers. As shown in the figure, dynamic modulus  $G'$  of Cloisite  $\text{Na}^+$  is different from other nanoclay fillers and is very similar to kaolin. This behavior shows correlates with results seen for tensile strength and elongation and is probably the result of very low intercalation and distribution of Cloisite  $\text{Na}^+$  in the NBR matrix.

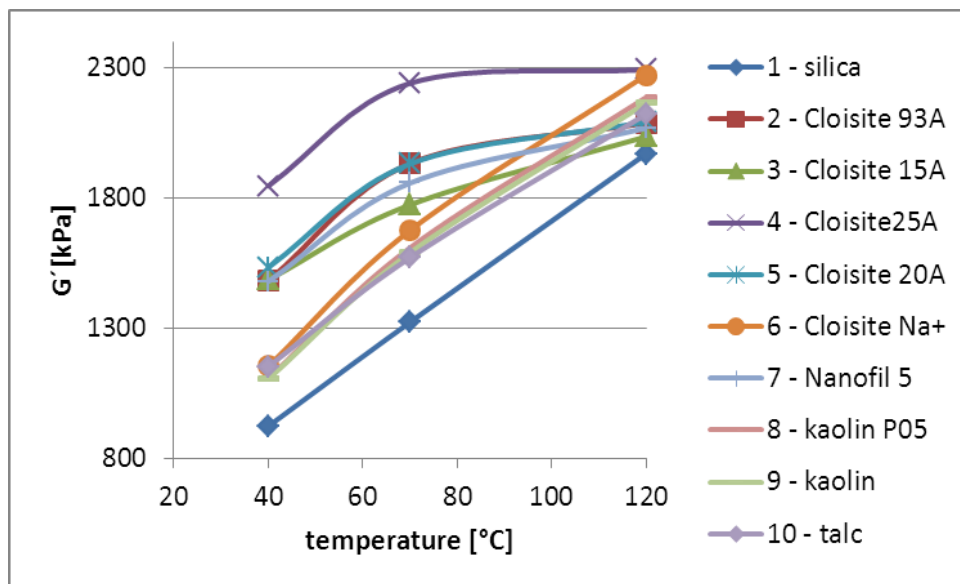


*Figure 45: Dependence of dynamic storage shear modulus  $G'$  on temperature at strain amplitude 1% and frequency 0,3 Hz*

As can be seen in Figure 46, loss factor ( $\tan \delta$ ) for compounds with nanoclays and with kaolin peak at a temperature of approximately  $60^{\circ}\text{C}$ , and then begins to decrease above this temperature. Increase of  $\tan \delta$  with temperature reveals increase in the filler particle network as well as restriction of polymer segments mobility by interaction polymer-filler [85]. The highest value of  $\tan \delta$ , and therefore the highest interaction with NBR matrix, is experienced by compound No. 4 filled by Cloisite 25A. Figure 49 shows a linear decrease of loss factor ( $\tan \delta$ ) with temperature for compounds with

silica and talcum, due to the different particle structure of the fillers in comparison to clays. As shown in the figure,  $\tan \delta$  of Cloisite Na<sup>+</sup> is different from other nanoclay fillers and is very similar to kaolin. This behavior was detected in previous tests also and indicates poor exfoliation and distribution of Cloisite Na<sup>+</sup> in the NBR matrix. Figure shows importance of modification of nanoclay for interaction with NBR matrix. As can be seen loss factor of all compounds with modified nanoclay is much higher than loss factor of compound with Cloisite Na<sup>+</sup> and therefore their interaction with NBR matrix is much better than interaction of unmodified Cloisite Na<sup>+</sup>.

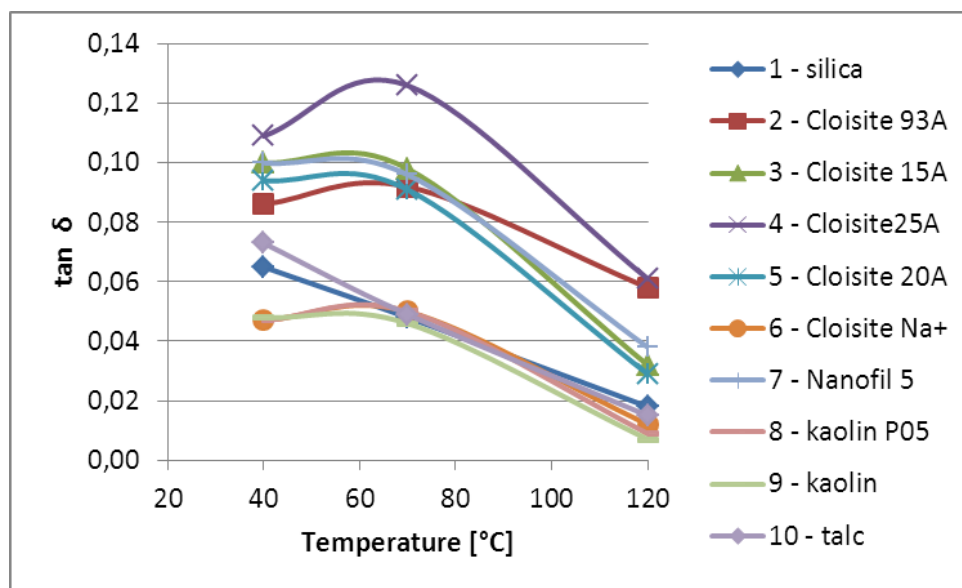


Figure 46: Dependence of loss factor  $\tan \delta$  on on temperature at strain amplitude 1% and frequency 0,3 Hz

### ***Constant oscillation frequency and various strain amplitude***

Compounds No. 1 with silica, No. 4 with Cloisite 25A and No. 8 with kaolin P05 were tested in mode 2 with a wide range of strain amplitudes. The purpose of this test was to compare behavior of the basic silica filled compound with the best nanoclay filler compound (No 4. - Cloiste 25A) and a compound with classic kaolin. The results in Figure 47 and Figure 48 illustrate decrease of  $G'$  of all tested compounds with increasing strain amplitude, showing a typical non-linear behavior called Payne affect. This is likely the result of the decay of particle network structures. Breakdown of the particle network by increasing strain amplitude releases trapped NBR chains from network and agglomerates of silica, silica / nanoclay, silica / kaolin and causes increase in the effective volume of polymer and therefore decrease of modulus  $G'$ . The compound with Cloisite 25A shows the highest values of  $G'$  over all range of measured deformations at temperatures of 40°C and 70°C, which indicates a stronger

particle networks as well as a stronger interaction with NBR matrix than in the case of silica and kaolin. These results correlate well with measured hardness and tensile strength values observed on the tested compounds.

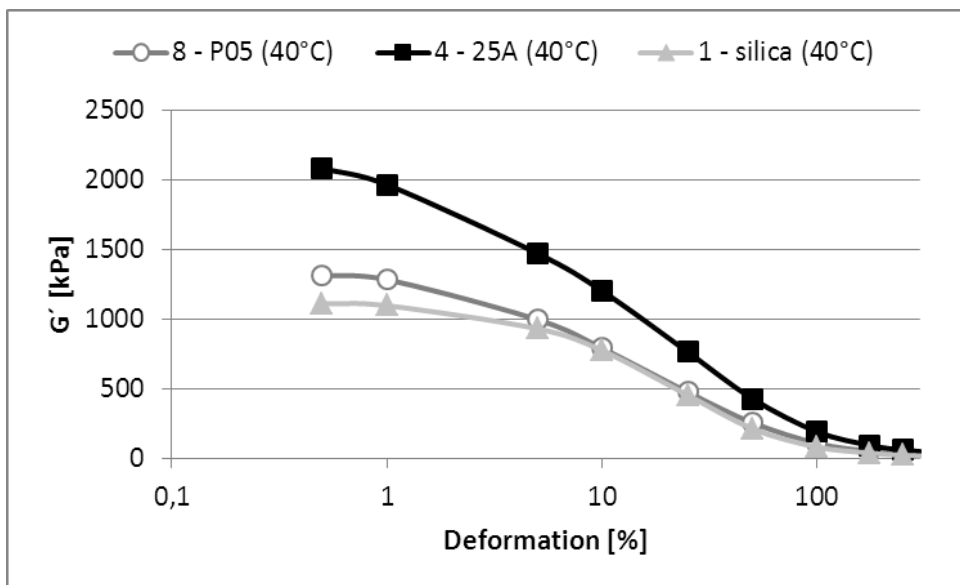


Figure 47: Dependence of real part of dynamic modulus  $G'$  on strain amplitude from 0,5 to 250 % at temperature 40 °C and oscillation frequency 0,1 Hz

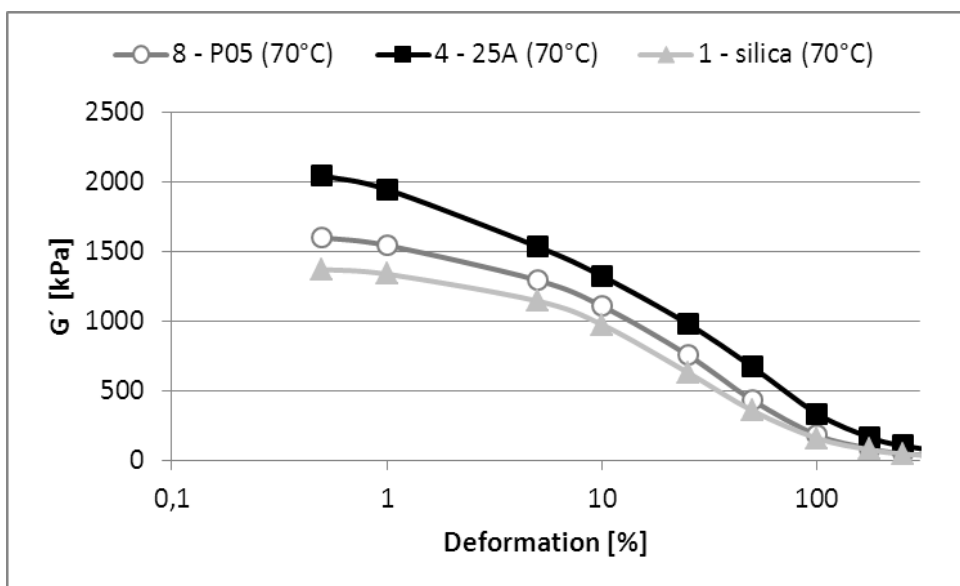


Figure 48: Dependence of real part of dynamic modulus  $G'$  on strain amplitude from 0,5 to 250 % at temperature 70 °C and oscillation frequency 0,1 Hz

Figure 49 shows decrease of  $G'$  of compound with Cloisite 25A is bigger at higher deformations in comparison to the base silica compound and the compound with kaolin. This result correlates with previous test with previous tests of  $G'$  at constant

strain amplitude. Stability of silica / nanoclay particle networks decreases with temperature and thus breakdown of this structure is higher. Temperature 120°C together with increasing strain amplitude accelerates release of trapped NBR elastomer from particle network and causes quick decrease of  $G'$  at higher deformations.

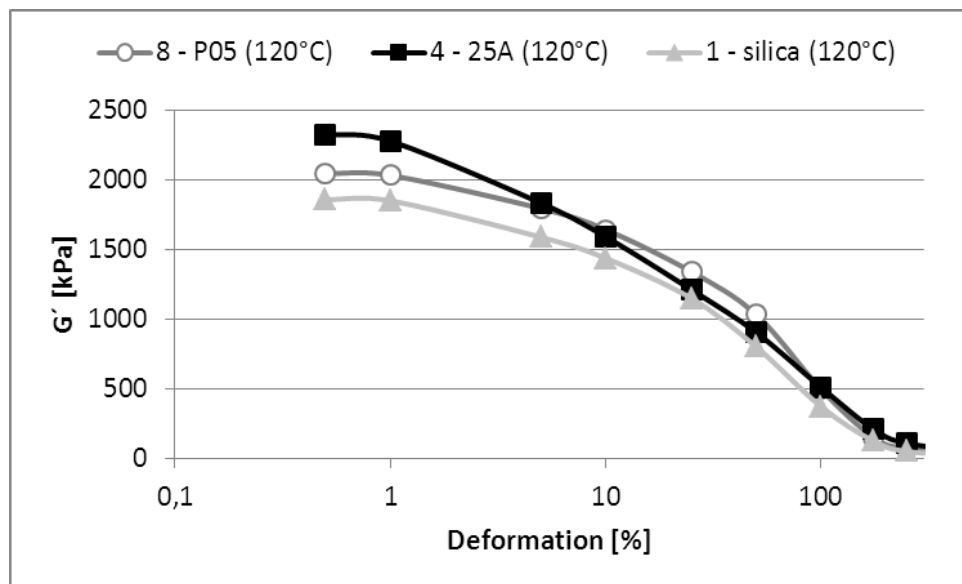


Figure 49: Dependence of real part of dynamic modulus  $G'$  on strain amplitude from 0,5 to 250 % at temperature 120 °C and oscillation frequency 0,1 Hz

Figure 50, Figure 51 and Figure 52 show dependence of loss dynamic shear modulus ( $G''$ ) on strain amplitude at constant oscillation frequency.  $G''$  shows maximum value at higher deformations in comparison to  $G'$  and after reaching of maximum rapidly decreases with increase of deformation. As shown in the figures, the loss modulus at low strain amplitudes is much larger for the Cloisite 25A compound than that observed for the other two tested compounds at all the tested temperatures. This could be a result of different behavior of particle networks present within the samples. Particle network of Cloisite 25A compound is more developed and stronger than network of kaolin and pure silica compounds. All three measured samples reach an initial peak at a strain amplitude of about 8 % at a temperature of 120°C, where the particle networks appear to begin to disintegrate. The compound filled by Cloisite 25A shows a weak peak at temperatures of 40°C and 70°C as well. The behavior of all three compounds appears to very similar at higher deformations above 50 %. The peaks at high deformations indicate destruction of the particle network. As can be seen in figures maximal peak is moved with temperature – while maximal  $G''$  at temperature 40°C is reached at strain amplitude 25 %, at temperature 70°C is peak moved to strain amplitude 50 % and at temperature 120°C to 100 %.

The increase of  $G''$  is influenced mainly by hydrodynamic effect, because unstrained particles of mineral fillers distributed in the NBR matrix increase viscosity of rubber compound [85]. Value of  $G''$  is influenced by the breakdown and reformation of the particle networks during dynamic strain [88].

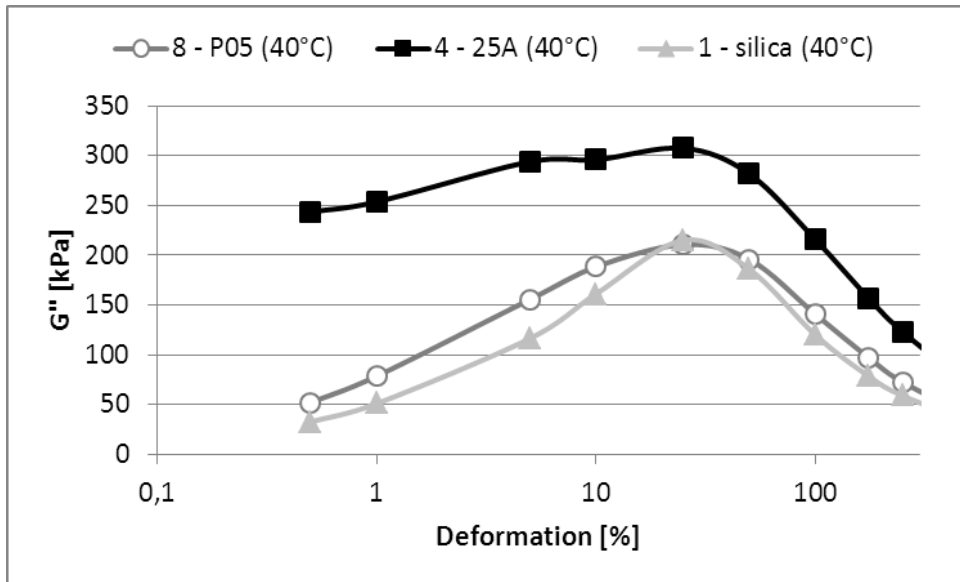


Figure 50: Dependence of loss dynamic modulus  $G''$  on strain amplitude from 0,5 to 250 % at temperature 40 °C and oscillation frequency 0,1 Hz

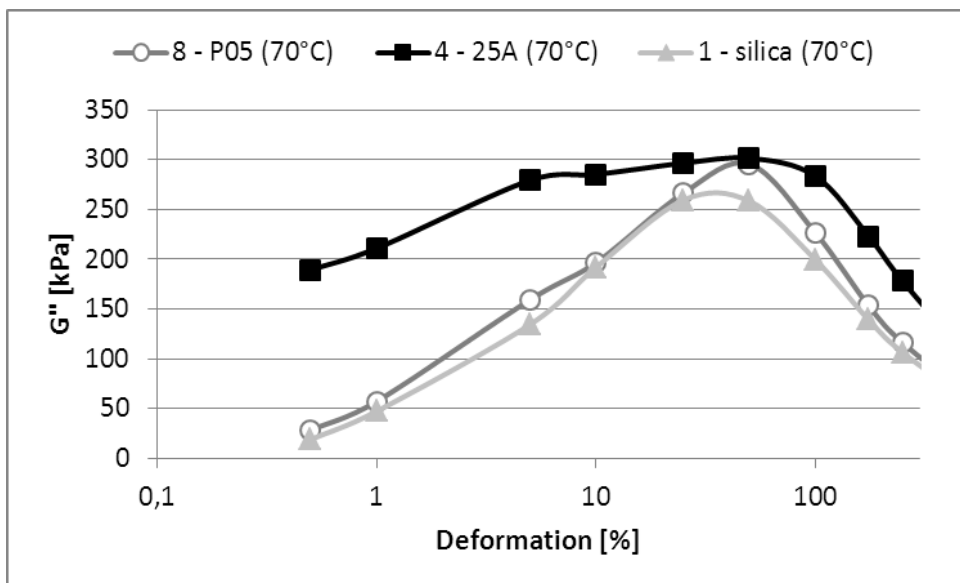


Figure 51: Dependence of loss dynamic modulus  $G''$  on strain amplitude from 0,5 to 250 % at temperature 70 °C and oscillation frequency 0,1 Hz



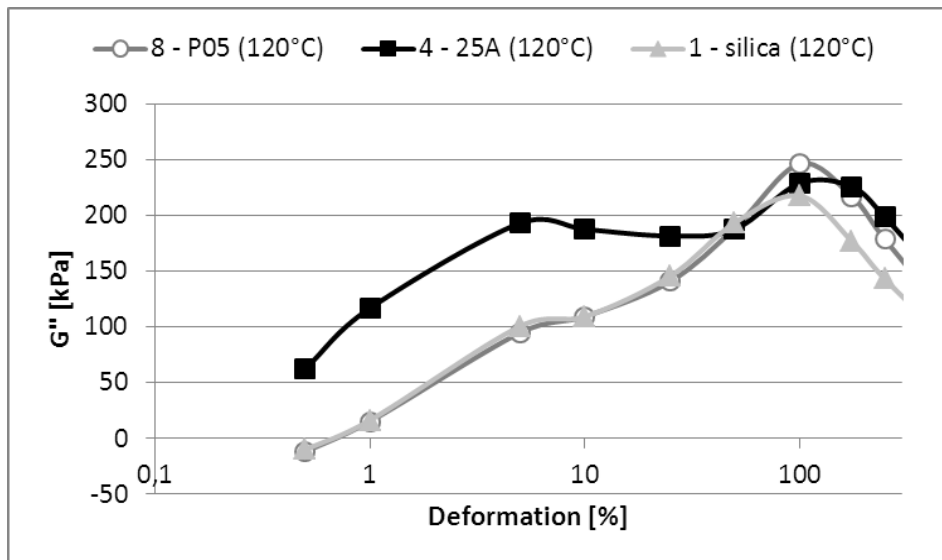


Figure 52: Dependence of loss dynamic modulus  $G''$  on strain amplitude from 0,5 to 25% at temperature 120 °C and oscillation frequency 0,1 Hz

The dependence of dynamic loss factor ( $\tan \delta$ ) on strain amplitude is shown in Figure 53, Figure 54 and Figure 55. Loss factor can be determined as ratio between broken down and reformed filler structures and filler structures unchanged during dynamic strain [18]. Figures confirm the theorized behavior of the particle network structure. The decay of this structure in compound No. 4, with nanoclay Cloisite 25A at low strain amplitudes, is likely not as rapid as for compounds with silica and kaolin due to the presence of a more stable particle network. The possibility exists that nanoclay fillers have a higher interaction with NBR matrix as result of combination of good exfoliation and high polymer-filler contact area which provides improved elastic behavior.

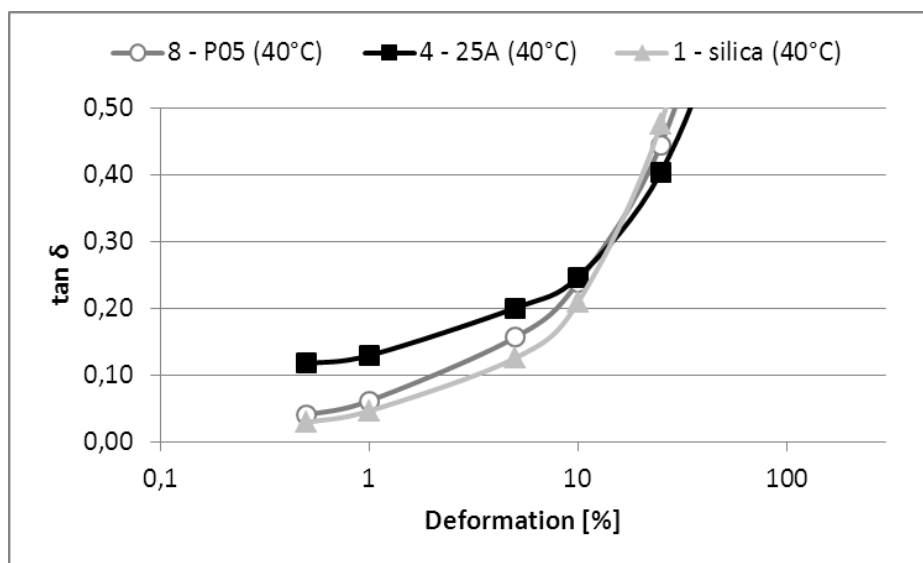


Figure 53: Dependence of loss factor  $\tan \delta$  on strain amplitude from 0,5 to 250 % at temperature 40 °C and oscillation frequency 0,1 Hz

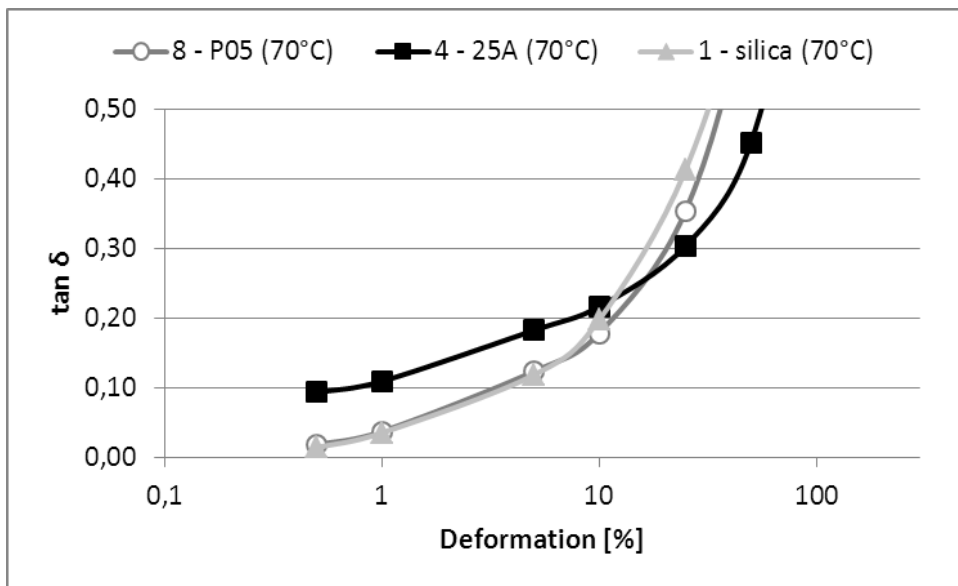


Figure 54: Dependence of loss factor  $\tan \delta$  on strain amplitude from 0,5 to 250 % at temperature 70 °C and oscillation frequency 0,1 Hz

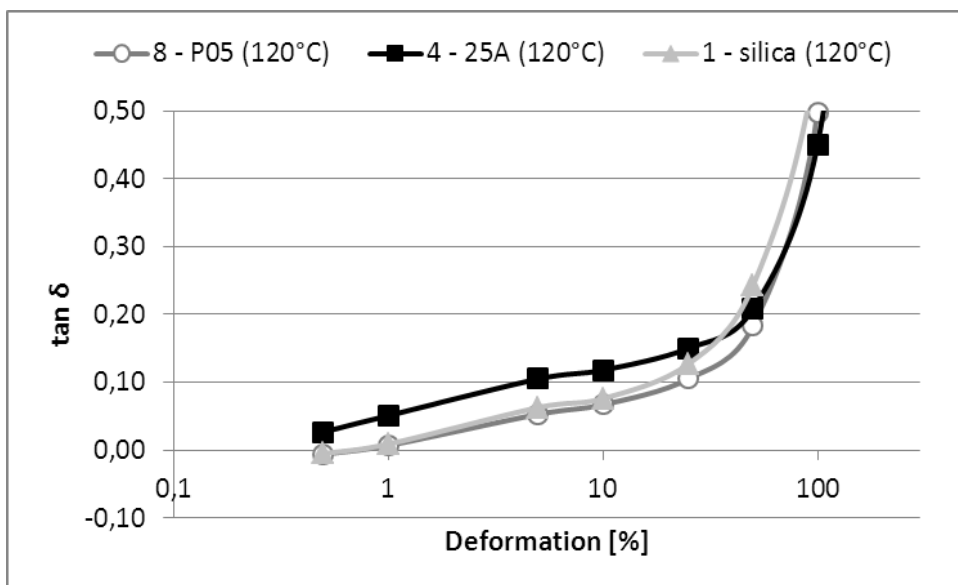


Figure 55: Dependence of loss factor  $\tan \delta$  on strain amplitude from 0,5 to 250 % at temperature 120 °C and oscillation frequency 0,1 Hz

#### 4.1.8 XRD analysis

The structural changes of tested fillers were investigated using X-Ray Diffraction (XRD) techniques to determine the atomic and molecular structure of NBR nanocomposites. Figure 56 describes structure of vulcanized compound No. 6 with Cloisite Na<sup>+</sup> in comparison to pure Cloisite Na<sup>+</sup> in powder form. As can be seen peak is slightly moved to the left and intensity is slightly decreased by weak changes of d-

spacing from 1.17 to 1.26 nm. This result does not indicate any exfoliation of Cloisite Na<sup>+</sup> in the NBR matrix. Cloisite Na<sup>+</sup> is not modified therefore exfoliation in the elastomer matrix is very difficult which is confirmed by the result of this study.

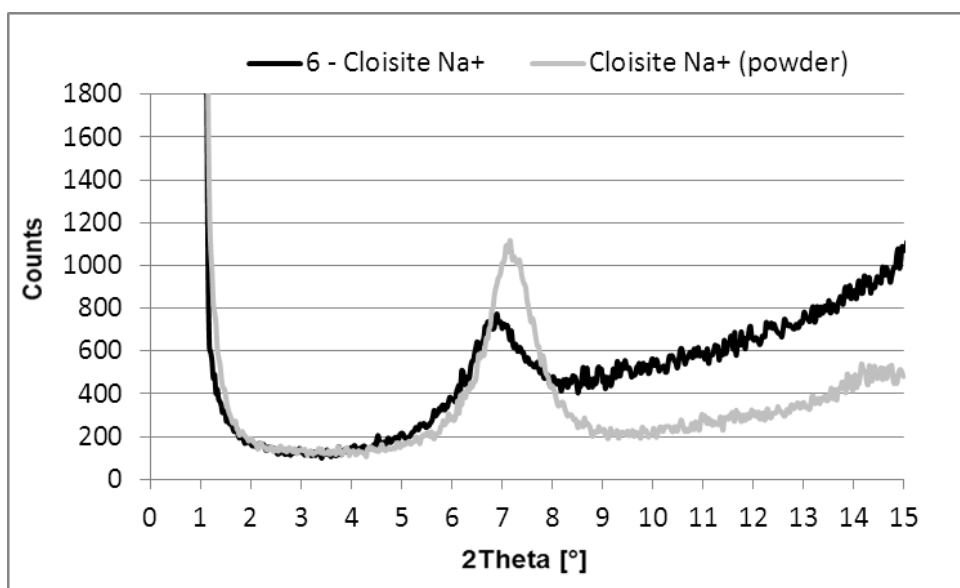


Figure 56: XRD pattern for compound No. 6 – Cloisite Na<sup>+</sup>

Compound No. 2 with Cloisite 93A and No. 5 with Cloisite 20A show better results. As can be seen in Figure 57 and Figure 58 movement of 2 Theta peak and a decrease in intensity is more apparent when compared to Cloisite Na<sup>+</sup>. Intercalation of NBR chains into structure of Cloisite 20A and of Cloisite 93A is expected based on this test results.

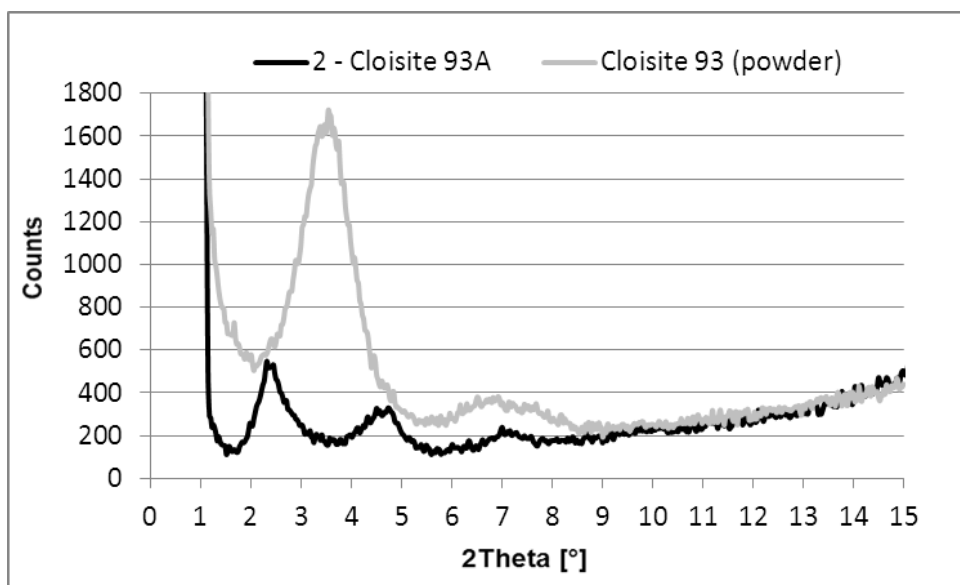


Figure 57: XRD pattern for compound No. 2 – Cloisite 93A

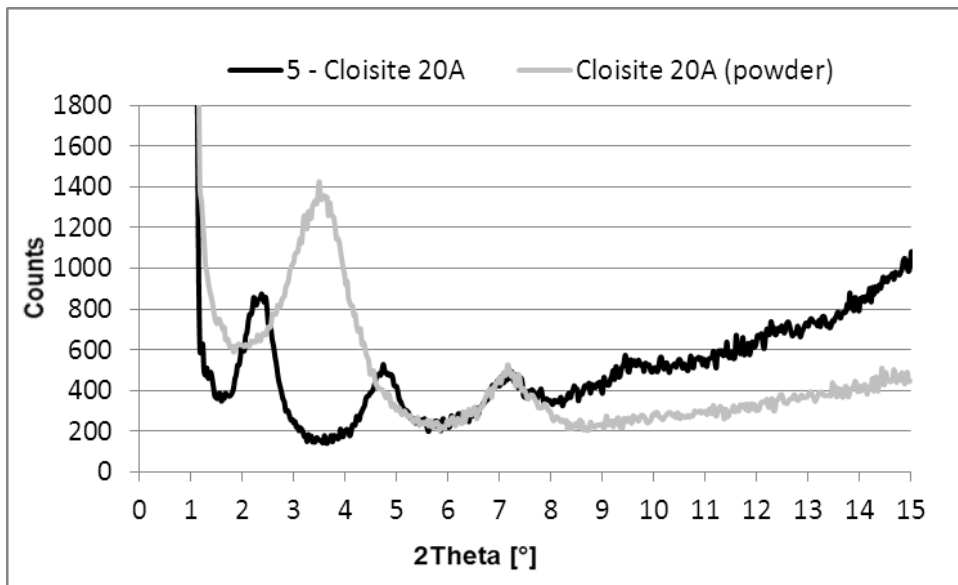


Figure 58: XRD pattern for compound No. 5 – Cloisite 20A

The best results show compound No. 4 filled by Cloisite 25A. As can be seen in Figure 59, the 2 Theta peak is moved from 5° to 2° and intensity is very low by increase of d-spacing from 1.86 to 2.97 nm. This result indicates good intercalation of Cloisite 25A in the NBR matrix and supports the results seen for the performance of compound No. 4 in previous tests.

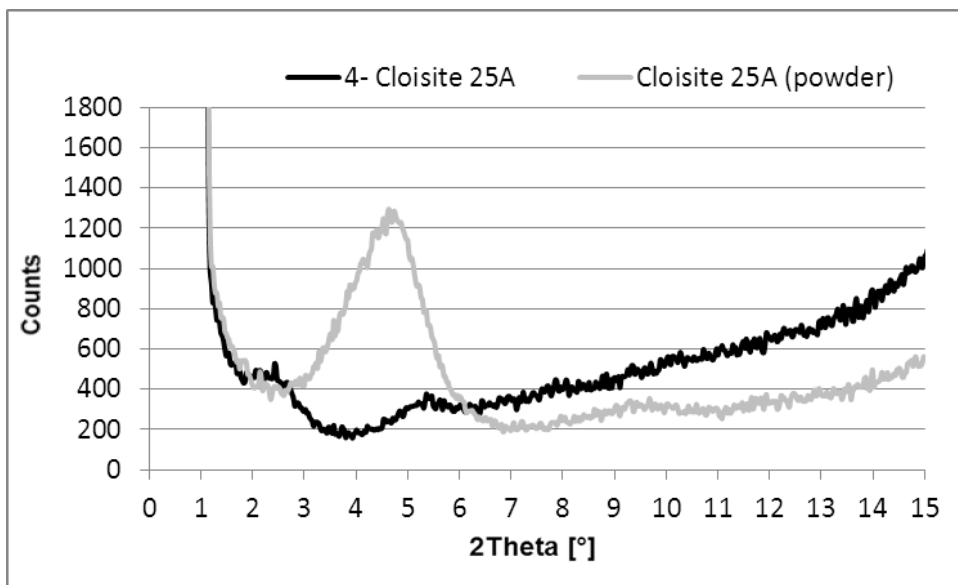


Figure 59: XRD pattern for compound No. 4 – Cloisite 25A

Figure 60 compares XRD patterns of compound No. 8 – Kaolin P05 with pure Kaolin. As can be seen, 2 Theta peak slightly decreases intensity, but d-spacing stays same – 0,71 nm. This observation indicates no change of original structure of kaolin in cured compound No. 8.

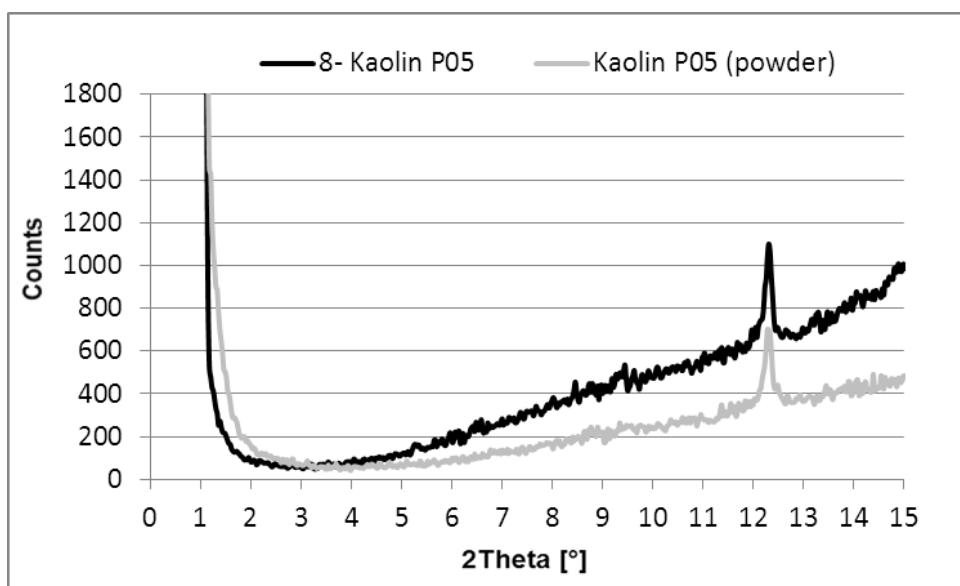


Figure 60: XRD pattern for compound No. 8 – Kaolin P05

XRD patterns of compound No. 1 silica and pure silica Perkasil KS 300 is shown in Figure 61. Base compound No. 1 does not show any change of original structure of silica. As can be seen XRD pattern does not shows any peak. It is due to spherical shape of particles of silica.

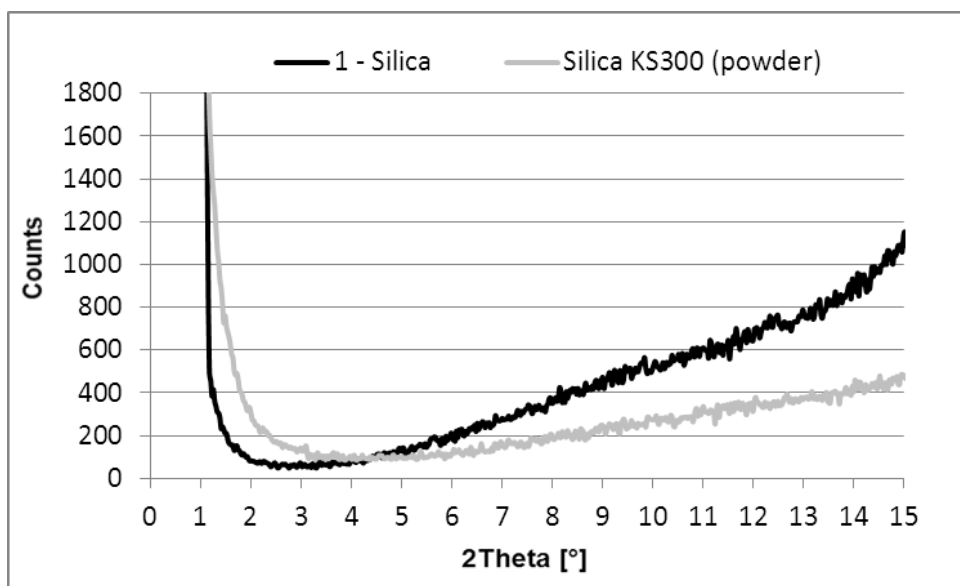


Figure 61: XRD pattern for compounds No.1 silica

#### 4.1.9 FT-IR analysis

Chemical changes of prepared compounds were studied by infrared spectroscopy, which is an important tool in the organic chemistry. Spectra for pure NBR and pure silica are shown in Figure 62 and for compounds No. 1 - Silica, No. 4 – Cloisite 25A, No. 6 – Cloisite Na<sup>+</sup> and No. 8 – Kaolin P05 in Figure 63 to Figure 65.

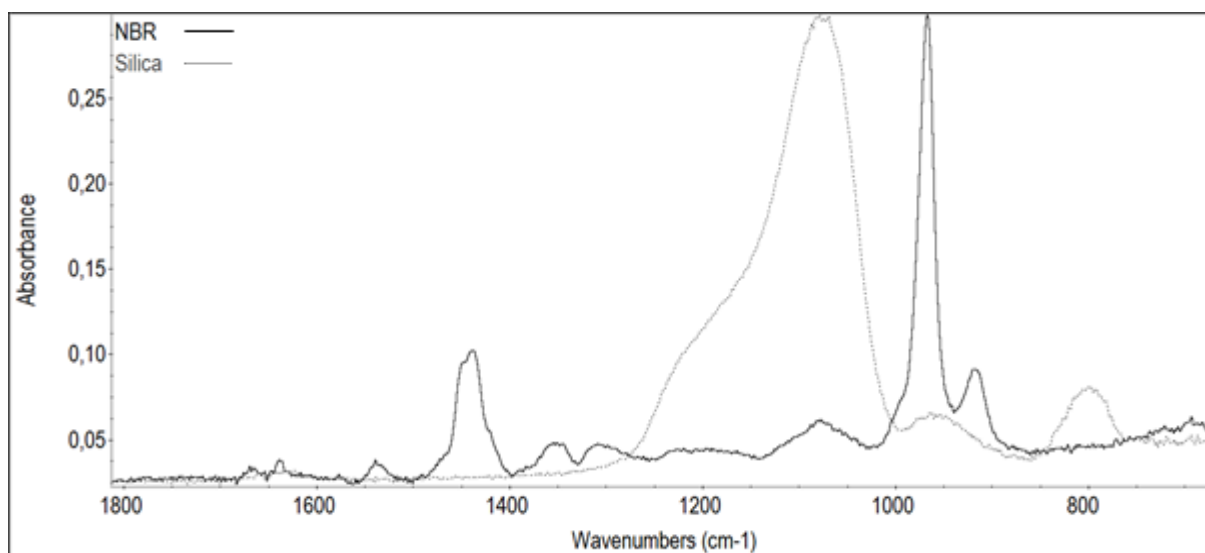


Figure 62: FTIR spectra for NBR and silica

As can be seen in the Figure 63, the maxima for silica and NBR stay in the same positions for compounds No. 4 and No. 6. The changes are observed for Si-O-Si bond originate from Cloisite for both presented compounds in Figure 63. There are no recorded peaks belong to the Cloisite Si-O-Si bond in the compounds No. 4 and 6, in spite of very strong absorption of this band. It is noted the shoulder in position  $1049\text{ cm}^{-1}$  for mixture No. 4 which is theorized to be a shift in the peak  $1009\text{ cm}^{-1}$  originating from Cloisite 25A. The maximum observed belongs to silica and changes the shape. Noted changes may be connected with chemical interaction of the Cloisite Si-O-Si bond. Composition No. 4 provides a large improvement when testing other properties, which may be connected with the chemical and structural changes. As shown in Figure 63 maxima for silica in the compound No. 6 is not changed, but the peak is broadened. This broadening may be connected with an increase in molecular weight.

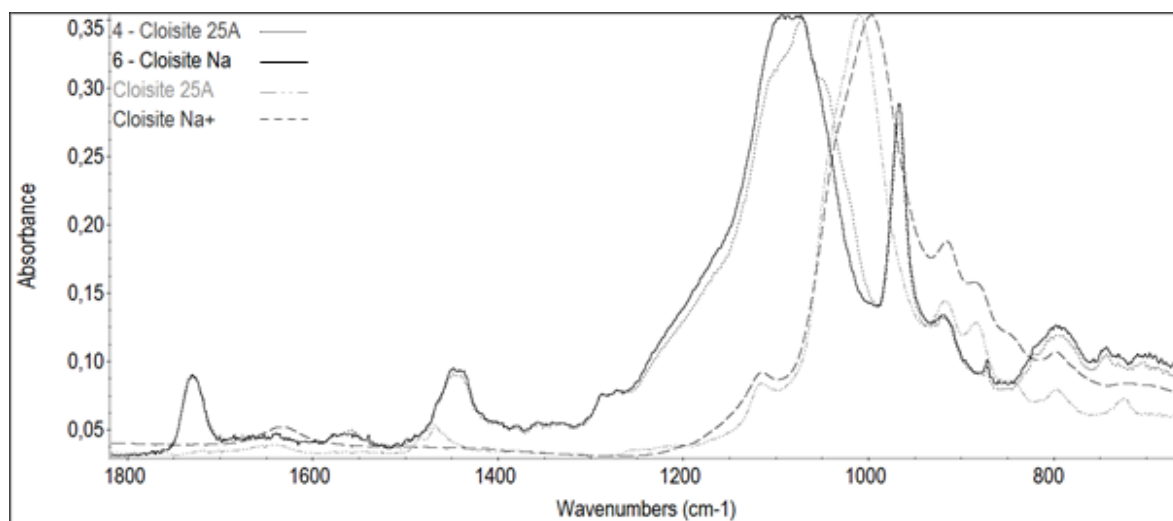


Figure 63: FTIR spectra for compounds No. 4 - Cloisite 25A and No. 6 - Cloisite Na+

Analysis of compound No. 8 does not show significant changes in the shape of silica Si-O-Si bond, as can be seen in Figure 64. The maximum for Si-O-Si bond coming from silica at  $1076\text{ cm}^{-1}$  was slightly shifted to  $1088\text{ cm}^{-1}$ . This may indicate some chemical interactions in the mixture with kaolin. Further the spectra of compound No. 1 (Figure 65) presented very small changes of silica Si-O-Si interactions. The shape obtained of the maximum and its position is approximately the same. The weak shift ( $10\text{ cm}^{-1}$ ) to higher wavenumbers in the Si-O-Si maximum was observed. The maximum at  $1730\text{ cm}^{-1}$  is connected with curing of rubber compounds.

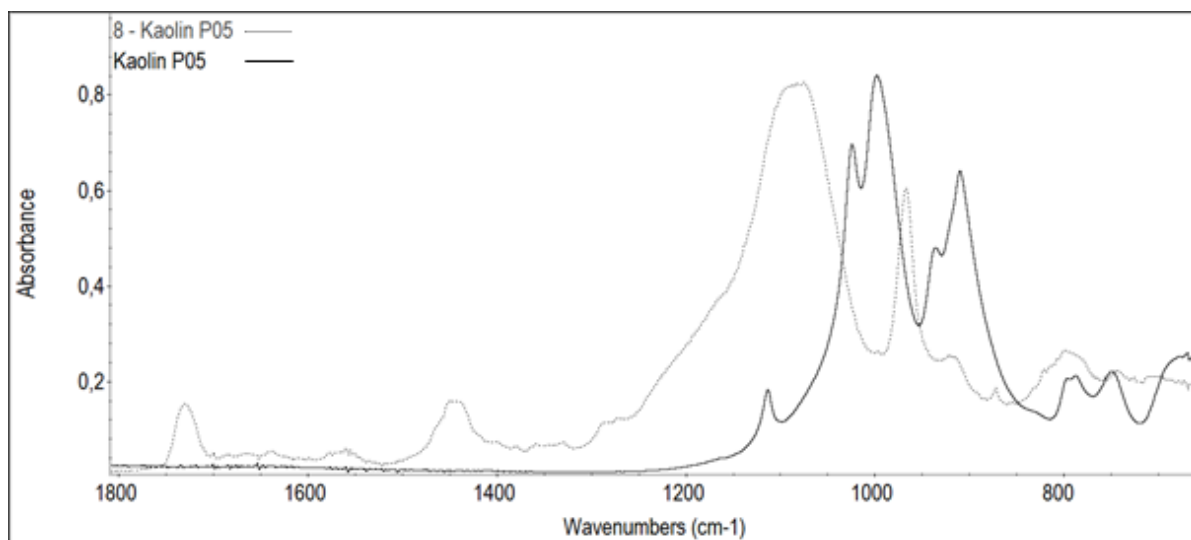


Figure 64: FTIR spectra for compound No. 8 – Kaolin P05

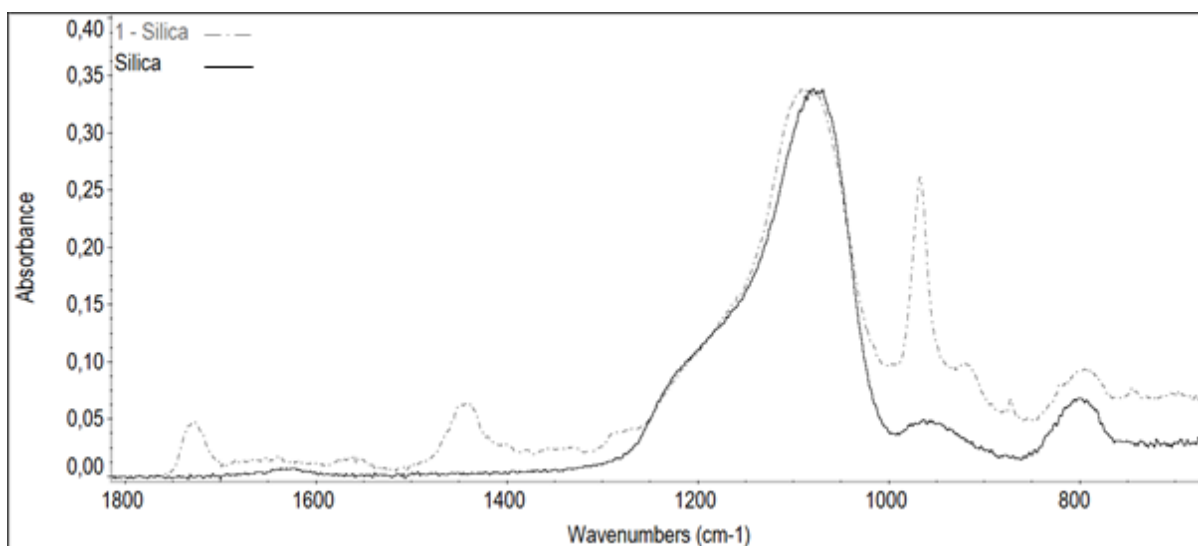
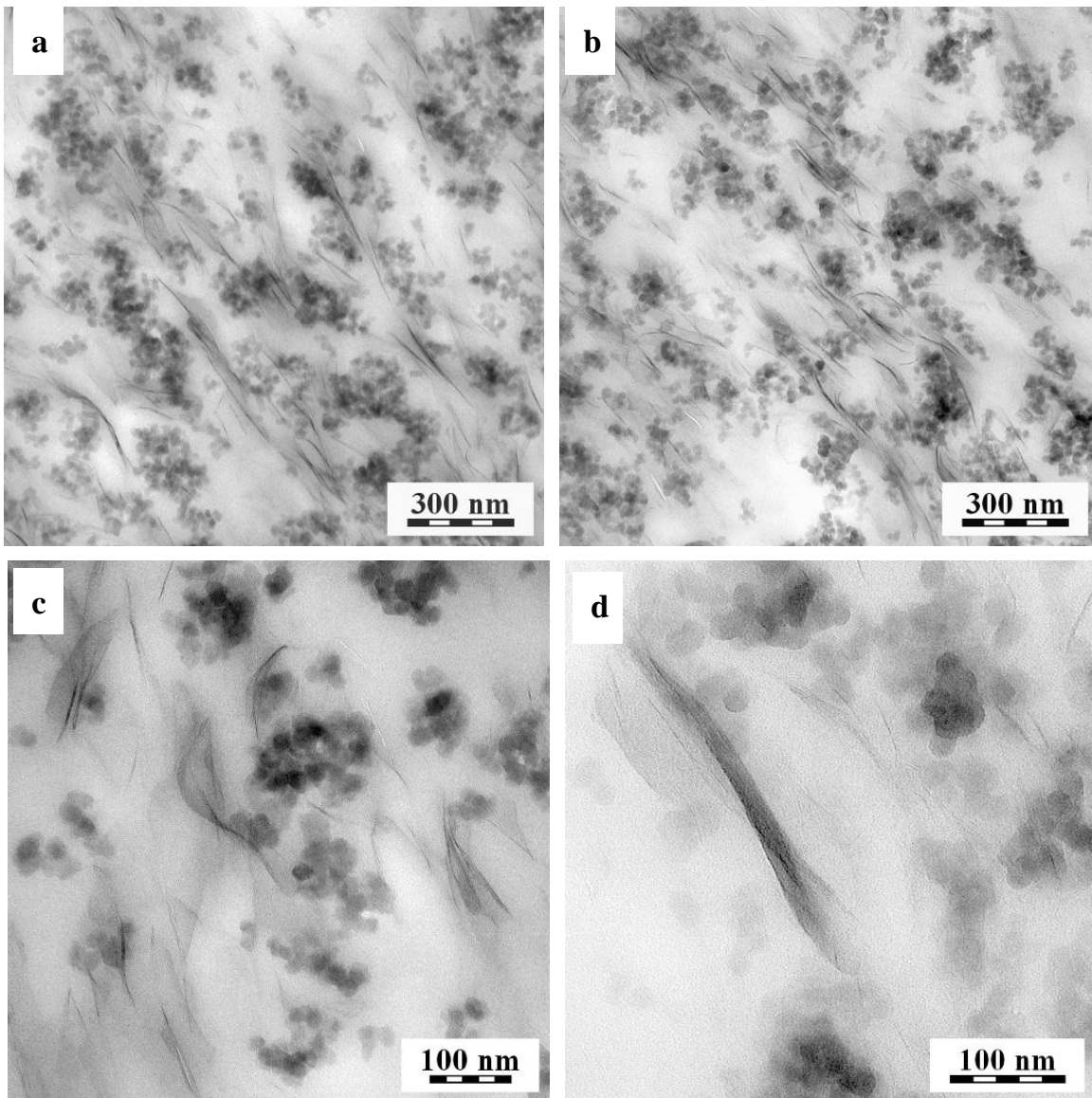


Figure 65: FTIR spektra for compound No. 1 - Silica

#### 4.1.10 TEM analysis

An additional test used for the investigation of the morphology of NBR nanocomposite was transmission electron microscopy (TEM). Figure 66 shows structure of compound No. 4 with Cloisite 25A. Nanoclay layers are homogeneously dispersed between aggregates of silica in the NBR matrix. As shown in figure, the exfoliated structure of nanoclay Cloisite 25A as well as some locations of intercalated structure of NBR / silica / clay nanocomposite can be observed. It appears that there is tendency of particles of silica to separate platelets of nanoclay and thus support and improve exfoliation of the nanoclay. Therefore a combination of silica with nanoclay seems to be optimal composition for polymer nanocomposites.





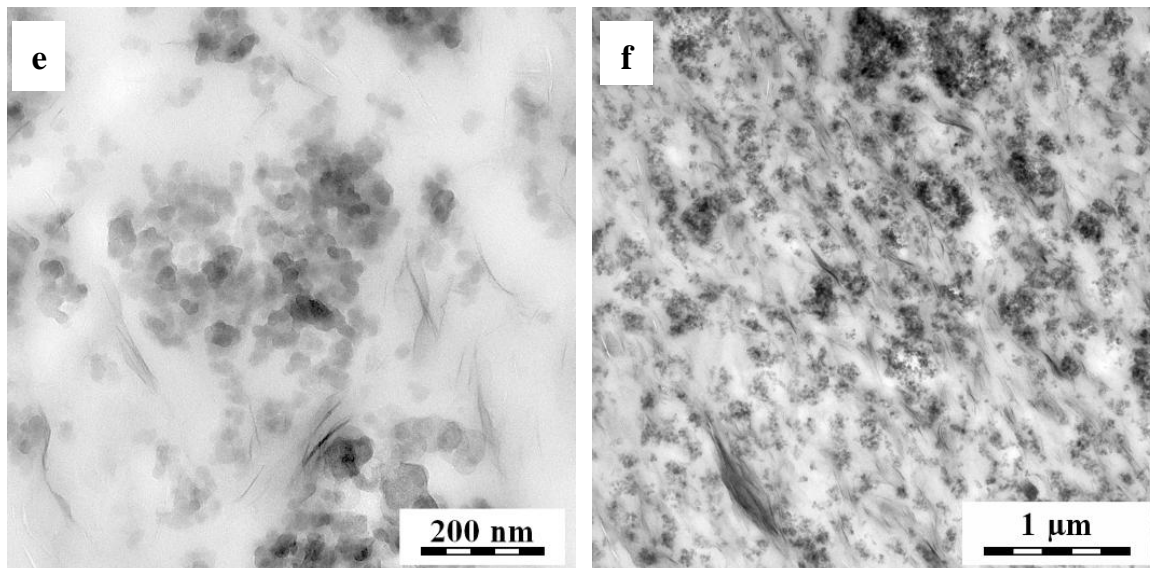


Figure 66: TEM analysis of compound No. 4 Cloisite 25A

#### 4.1.11 Summary

The objective of first stage of this study was to investigate combinations of silica and various nanoclay fillers added to an NBR matrix and identify combinations which optimize both mechanical properties and R-134a permeation resistance.

Nanoclay fillers mixed with silica provided a 30% reduction in permeation of refrigerant R-134a and improved mechanical properties. Enabling factors which were instrumental in providing these property improvements were adequate levels of intercalation and exfoliation of the nanoclay in the NBR matrix and polymer-silica-clay interactions. Intercalation, exfoliation and interaction were determined to be dependent on the type and amount of the nanofiller modifier. Cloisite Na<sup>+</sup> is an unmodified nanoclay and provides the NBR compound properties similar to common white fillers as talc and kaolin. On the other hand, Cloisite 20A and 15A contain the same modifier at different levels. The good performance of the Cloisite 20A with a higher modifier level led to better results than Cloisite 15A.

This investigation has shown surprisingly poor permeation resistance of compounds containing talc and kaolin. Their laminar structure has a good theoretical potential for reduction of gas diffusion; however, the actual reduction of permeation of R-134a in NBR compounds was not high. This poorer than expected performance was likely due to the low degree of orientation of particles in the NBR matrix when laminar particles did not represent a significant barrier to the permeation of refrigerant molecules.

The best results in this study were achieved with compound No. 4 filled by Cloisite 25A and Perkasil KS 300 silica. This compound obtained the best results in static-mechanical, dynamic-mechanical and permeation tests and met the project targets for

the tested parameters. These results were achieved by very good morphology of the NBR / Cloisite 25A / Perkasil KS300 nanocomposite. XRD and TEM analysis detected good distribution, intercalation and partial exfoliation of the nanoclay in the NBR matrix. Measurement by FTIR showed ability of silica and nanoclay to create particle network by Si-O-Si bonds. As expected, presence of silica in NBR compound improved exfoliation of nanoclay due to the increase of viscosity as well as by friction between particles of silica and platelets of nanoclay during the mixing process. Therefore the NBR nanocomposite seems to be optimal in combination with two mineral nano fillers – nanoclay and silica.

## 4.2 Nanoclay / silica mixture optimization

Finding the optimal mix ratio between nanoclay Cloisite<sup>®</sup> 25A and silica was the next step of this investigation. Two types of silica with different particle sizes were considered for study - Perkasil<sup>®</sup> KS 300 and Perkasil<sup>®</sup> KS 408. These fillers were used to investigate influence of different silica particle size on the nanoclay distribution in polymeric matrix.

The average particle size and surface area of Perkasil<sup>®</sup> KS 300 and Perkasil<sup>®</sup> KS 408 are shown in Table 11.

Table 11: Comparison of average particle size and surface area of silica

	Unit	KS 300	KS 408
Surface Area	m <sup>2</sup> /g	125	180
Average primary particle size	nm	20	18

### 4.2.1 Vulcanization characteristics

Vulcanization characteristics of the rubber compounds were determined by a rubber process analyzer (Alpha Technologies RPA 2000) at a temperature of 175°C.

Table 12: Vulcanization parameters

Content clay/silica [phr]	Cloisite 25A / Silica KS 408				Cloisite 25A / Silica KS 300			
	ML [dN.m]	MH [dN.m]	ts <sub>2</sub> [min]	t <sub>90</sub> [min]	ML [dN.m]	MH [dN.m]	ts <sub>2</sub> [min]	t <sub>90</sub> [min]
0/10	0,50	20,60	0,62	6,66	0,50	19,30	0,65	6,68
5/10	0,60	20,10	0,63	6,65	0,50	19,40	0,51	6,68
10/10	0,70	20,00	0,63	6,60	0,60	19,50	0,52	6,74
15/10	0,80	21,40	0,60	6,63	0,70	20,50	0,61	6,66
7,5/20	0,90	25,00	0,56	6,51	0,80	23,20	0,58	6,51
12,5/20	1,10	25,10	0,56	6,55	0,90	23,20	0,58	6,62
0/30	1,10	31,90	0,50	6,47	0,70	27,10	0,55	6,57
5/30	1,50	33,10	0,47	6,41	0,90	26,40	0,55	6,53
10/30	1,80	32,10	0,48	6,39	1,10	26,40	0,45	6,49
15/30	2,40	33,70	0,46	6,44	1,40	27,40	0,54	6,52

As shown in Table 12, vulcanization parameters  $t_{90}$  and  $ts_2$  are very similar for all tested compounds. Differences between value of ML and MH are caused by silica content and particle size. Loadings of 30 phr of the smaller Perkasil KS 408 particles increased ML and MH to the maximum values observed. Results show minimal influence of nanoclay to value of ML and MH.

#### 4.2.2 Hardness testing

As it is shown in Table 13 and Figure 67, the hardness increases with increasing levels of silica and nanoclay. The largest hardness increase was achieved with a 15 phr loading of nanoclay with an increase of 9 IRHD in the compound with 10 phr of silica and 8 IRHD in the compound with 30 phr of silica. These results indicate good distribution of nanoclay in NBR matrix and its exfoliation or intercalation. As can be seen in the results for KS 408 silica, reinforcing effects are higher in comparison to KS 300 silica. This could be caused by the higher surface area of KS 408 silica.

The project target for a hardness between 70 to 80 IRHD are met by all compounds filled by 30 phr of Perkasil KS 408 silica and compounds filled by a mixture of 30 phr of Perkasil KS 300 silica and minimum of 10 phr of nanoclay Cloisite 25A.

Table 13: Hardness results

Content clay/silica [phr]	Hardness [IRHD]	
	Cloisite 25A / Silica KS 408	Cloisite 25A / Silica KS 300
<b>0/10</b>	56	57
<b>5/10</b>	60	60
<b>10/10</b>	63	61
<b>15/10</b>	65	65
<b>7,5/20</b>	65	64
<b>12,5/20</b>	71	69
<b>0/30</b>	70	67
<b>5/30</b>	74	69
<b>10/30</b>	76	72
<b>15/30</b>	78	74

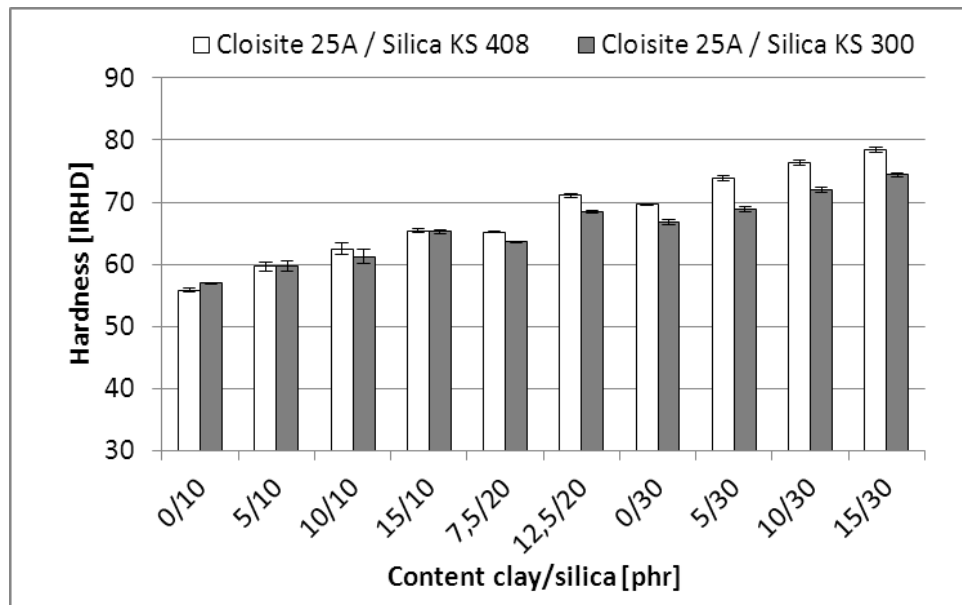


Figure 67: Comparison of hardness

#### 4.2.3 Tensile testing

Results of tensile strength, elongation and  $M_{100}$  are shown in Table 14 for both combinations of Cloisite 25A / silica KS 408 and Cloisite 25A / silica KS 300.

Table 14: Tensile strength, elongation and  $M_{100}$  results

Content clay/silica [phr]	Cloisite 25A / Silica KS 408			Cloisite 25A / Silica KS 300		
	Tensile strength [MPa]	Elongation [%]	$M_{100}$ [MPa]	Tensile strength [MPa]	Elongation [%]	$M_{100}$ [MPa]
<b>0/10</b>	3,0	94	-	2,5	94	-
<b>5/10</b>	3,4	127	2,7	3,3	122	2,8
<b>10/10</b>	4,6	152	3,4	4,6	153	3,1
<b>15/10</b>	5,9	155	3,9	5,4	142	3,9
<b>7,5/20</b>	5,8	144	4,1	5,3	140	3,9
<b>12,5/20</b>	7,5	152	5,0	6,7	154	4,4
<b>0/30</b>	4,9	119	3,9	3,8	101	3,7
<b>5/30</b>	6,2	141	4,5	5,5	136	4,0
<b>10/30</b>	7,9	159	5,2	7,6	169	4,7
<b>15/30</b>	10,2	168	6,4	9,4	182	5,5

The tensile strength value is influenced by increasing filling factor of silica and nanoclay. As can be seen in Figure 68, maximum reinforcing effect was achieved by compounds 15/30<sub>KS408</sub> and 15/30<sub>KS300</sub> with 15 phr or nanoclay and 30 phr of silica. Compounds with Perkasil KS 408 show higher value of tensile strength in comparison

to compounds with Perkasil KS 300. This is likely due to size and surface area differences between Perkasil KS 300 and KS 408.

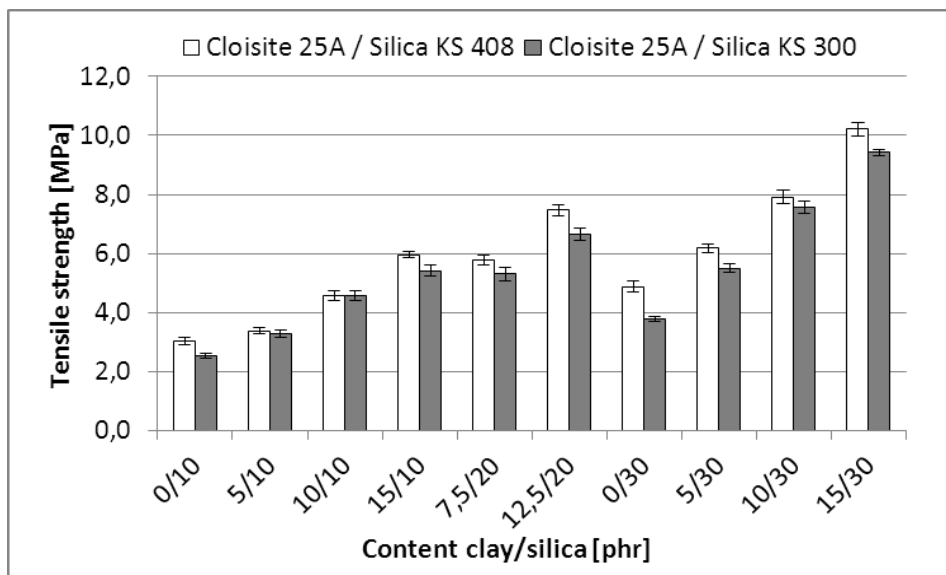


Figure 68: Comparison of tensile strength

As shown in Figure 69, maximal elongation was achieved by the compound labeled 15/30<sub>KS300</sub>. Perkasil KS 300 silica shows better results for maximal elongation at a filling factor 30 phr in comparison to Perkasil KS 408. As can be seen in the figures, differences in the size of silica particles influence the tensile strength and elongation by different amounts.

Compounds 15/30<sub>KS408</sub> and 15/30<sub>KS300</sub> with 15 phr or nanoclay and 30 phr of silica meet project targets for tensile strength (8 MPa min.) as well as for elongation (150 % min.).

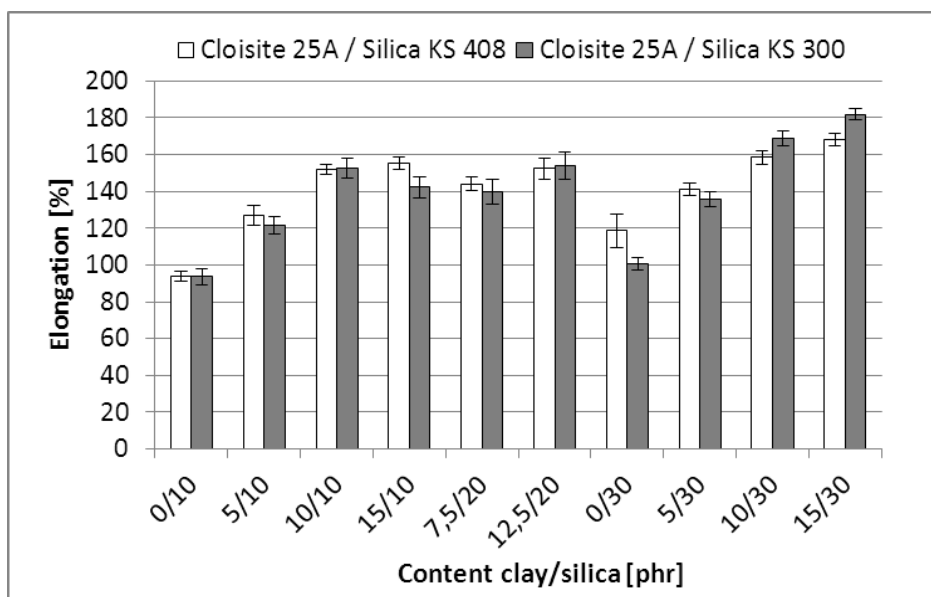


Figure 69: Comparison of elongation

The modulus  $M_{100}$  value is influenced by increasing filling factor of silica and nanoclay like tensile strength. Difference between reinforcing effect of silica Perkasil KS 300 and Perkasil KS 408 is shown in Figure 70. This behavior is caused by various particle size of silica.

As can be seen in Figure 70 the highest value of modulus  $M_{100}$  show compounds 15/30<sub>KS408</sub> and 15/30<sub>KS300</sub> with 15 phr or nanoclay and 30 phr of silica

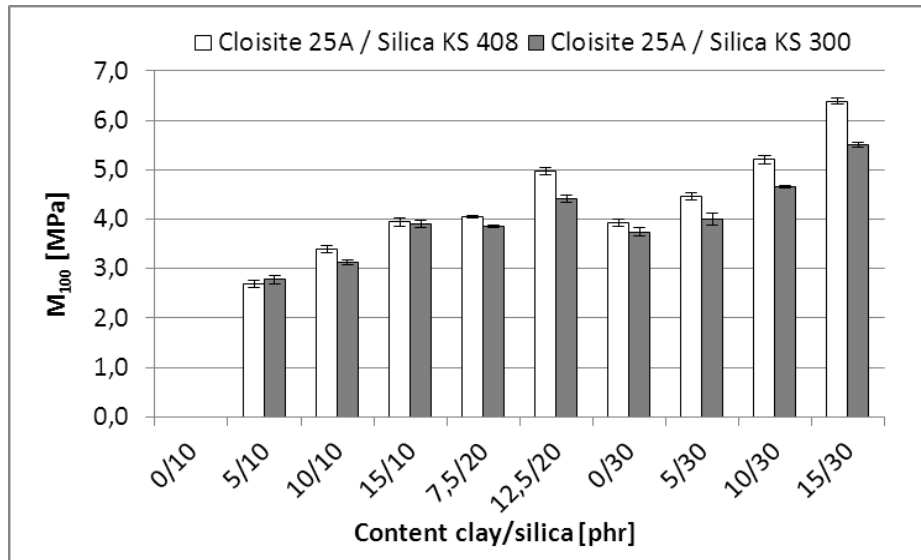


Figure 70: Comparison of modulus  $M_{100}$

#### 4.2.4 Tear strength

Results for tear strength are shown in Table 15 and Figure 71.

Table 15: Tear strength results

Content clay/silica [phr]	Tear strength [N/mm]	
	Cloisite 25A / silica KS 408	Cloisite 25A / silica KS 300
<b>0/10</b>	0,9	0,9
<b>5/10</b>	1,3	1,3
<b>10/10</b>	1,8	1,8
<b>15/10</b>	2,4	1,9
<b>7,5/20</b>	2,6	1,7
<b>12,5/20</b>	2,9	2,6
<b>0/30</b>	2,3	1,7
<b>5/30</b>	2,5	2,5
<b>10/30</b>	4,4	2,9
<b>15/30</b>	2,2	2,5

Maximum improvement in tear strength was achieved by the compounds denoted 10/30<sub>KS408</sub> and 10/30<sub>KS300</sub>. These compounds meet the project target of 2.5 N/mm together with compounds 5/30<sub>KS300</sub>, 5/30<sub>KS408</sub> and 15/30<sub>KS300</sub>. While previous mechanical property tests (hardness, tensile strength, and elongation) showed improvement and maximum results for compounds with 15 phr of nanoclay and 30 phr of silica, tear strength shows a significant deterioration at this filling ratio. The cause for this reduction in properties is likely the plate-like structure of Cloisite 25A. Sharp edges of platelets can initiate and facilitate crack propagation under the conditions tested.

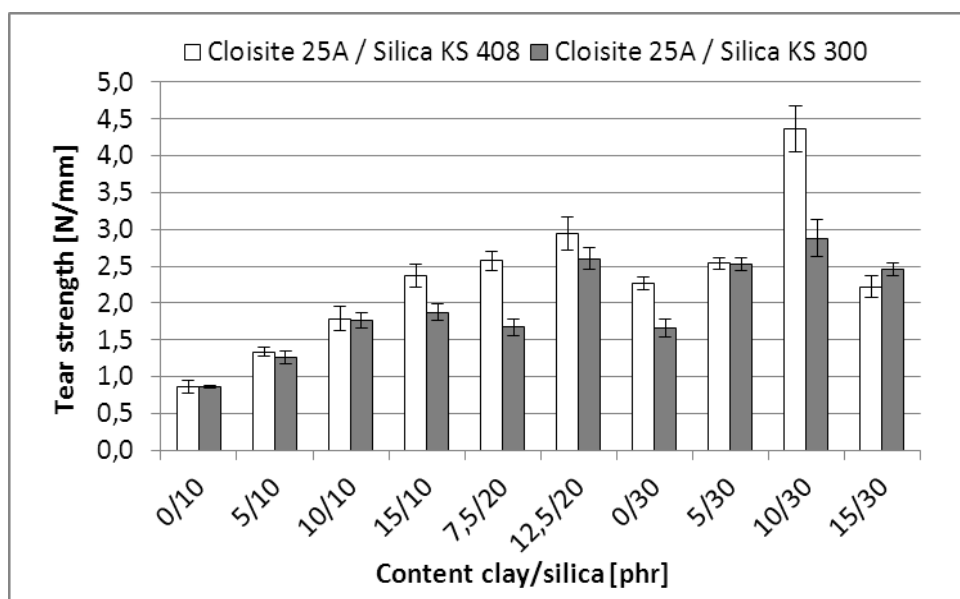


Figure 71: Comparison of tear strength

#### 4.2.5 Barrier properties

Permeation of all compounds tested is shown in Table 16 and Figure 72. Tests were performed with refrigerant R-134a. Compounds 10/30<sub>KS300</sub>, 15/30<sub>KS408</sub> and 15/30<sub>KS408</sub> decreased permeation approximately 30% to 35% and meet the project target for 25 % minimum reduction in R-134a permeation at a temperature of 70°C. The reduction of permeation is caused by the plate-like shape of exfoliated or intercalated nanoclays. The plate-like nanoclays in support of silica particles dispersed in the NBR matrix are able to reduce the diffusion of molecules of R-134a by creating more tortuous pathways for molecules of refrigerant R-134a to diffuse through. Key factors to reduce permeation in tested NBR nanocomposites were plate-like shape of the nanoclay and loading of 30 phr of silica (which probably supported exfoliation and intercalation of the nanoclay in the NBR matrix). This assumption is supported by the results of compounds with load of 10 phr of silica and compounds 5/30<sub>KS300</sub> and 5/30<sub>KS408</sub>. While permeation of compounds 5/10 and 5/30 is similar, permeation of compounds 10/10,



15/10 is much higher than 10/30, 15/30. Low loadings of silica are not able to improve and support intercalation and exfoliation of the nanoclay. Therefore optimal filling factor of NBR nanocomposite from a permeation point of view is 10 phr of nanoclay and 30 phr of silica.

Table 16: R-134a permeation results

Content clay/silica [phr]	R-134a permeation [g/y]	
	Cloisite 25A / Silica KS 408	Cloisite 25A / Silica KS 300
0/10	44,3	49,2
5/10	47,3	46,0
10/10	47,7	45,8
15/10	39,3	37,5
0/30	44,8	49,1
5/30	43,1	44,0
10/30	38,7	33,8
15/30	32,6	31,7

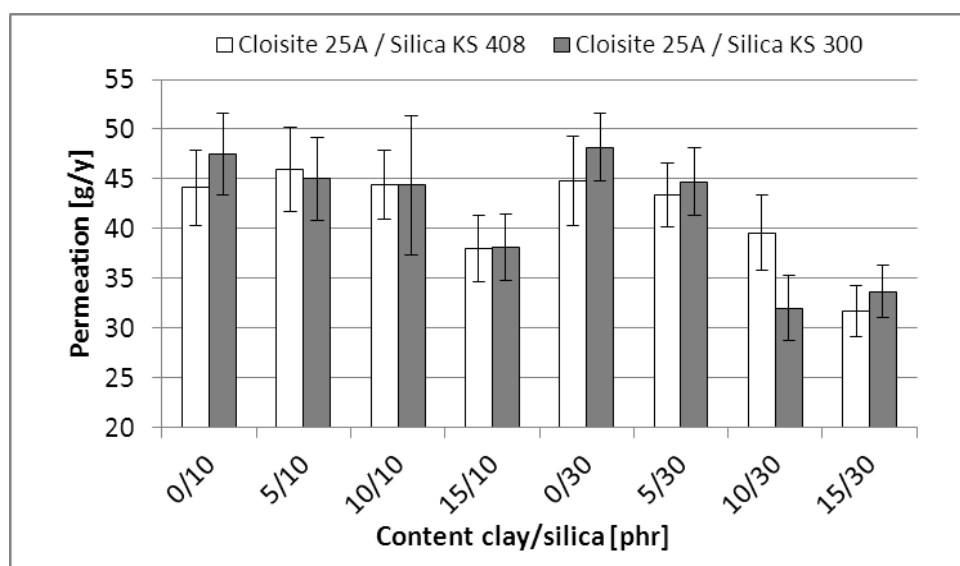


Figure 72: R-134a permeation comparison

#### 4.2.6 XRD analysis

Differences in morphology of NBR nanocomposites with various ratios of nanoclay and silica were investigated by XRD analysis. This investigation was done for all NBR compounds in this study with both types of silica – KS 300 and KS 408.

Figure 73 shows structure of NBR compounds with silica Perkasil KS 300. As can be seen in this figure, the first 2-Theta peak of all compounds is shifted to lower values in comparison to pure Cloisite 25A in powder form. This shift indicates intercalation of NBR chains between nanoclay platelets. Figure 73 reveals influence of different load of silica to intercalation of nanoclay. As can be seen in this figure, intensity of first peak of compounds filled by 10 phr of silica is higher than intensity of compounds with 30 phr of silica. Lower intensity assumes a less organized structure and better intercalation of Cloisite 25A in the NBR matrix. Better intercalation and exfoliation of nanoclay can be caused by the increased viscosity of the NBR compounds by silica incorporation and by collisions and friction between silica particles and nanoclay platelets during mixing process of rubber the compound. The assumption is that higher loadings of silica create more collisions with nanoclay and therefore silica can support better intercalation and exfoliation of the nanoclay platelets.

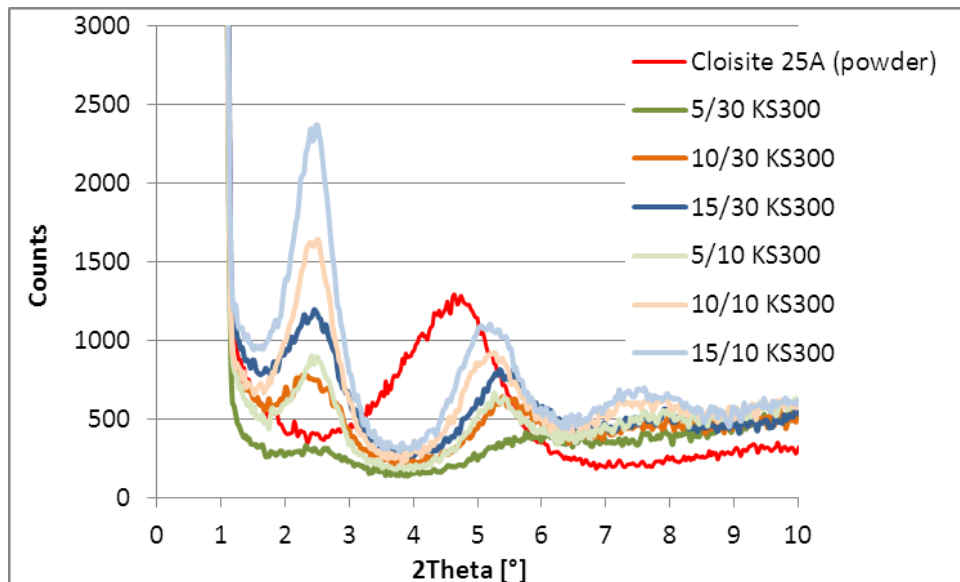


Figure 73: XRD pattern for compounds with Cloisite 25A / KS 300

Figure 74 reveals structure of nanocomposites with the alternate silica type - Perkasil KS 408. This figure shows similar influence of 10 phr and 30 phr loadings of Perkasil KS 408 silica to the intensity of 2-Theta peak as Perkasil KS 300 silica. Higher 30 phr loading of Perkasil KS 408 improved intercalation of nanoclay Cloisite 25A in compared to load of 10 phr of silica.

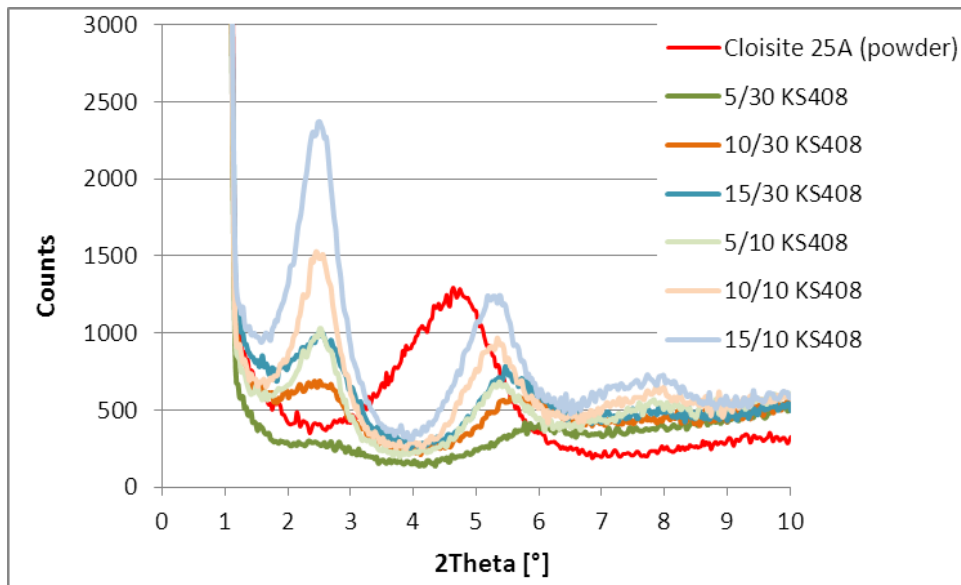


Figure 74: XRD pattern for compounds with Cloisite 25A / KS 408

Differences between both types of silica tested influence dispersion of the nanoclay in the NBR matrix are shown in Figure 75 and Figure 76. Figures compare same load of silica Perkasil KS 300 and Perkasil KS 408.

As shown in Figure 75 differences in position and intensity of 2-Theta peak at low loadings of 10 phr of silica are very small. Compounds with silica type Perkasil KS 408 shows slightly better results than compounds with Perkasil KS 300 silica.

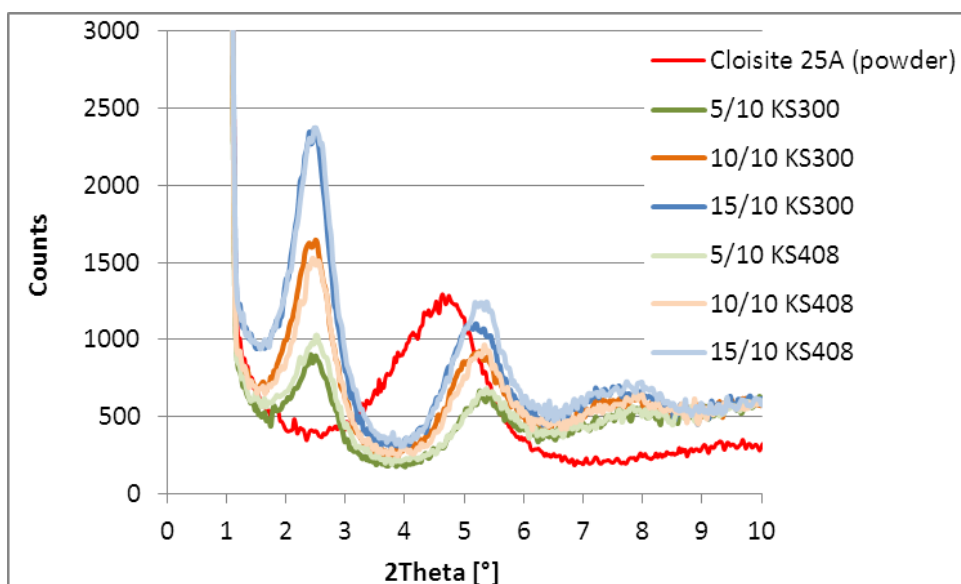


Figure 75: XRD pattern for compounds with 10 phr of silica

Larger difference between Perkasil KS 300 and KS 408 are revealed at higher loadings of silica. As can be seen in Figure 76, Perkasil KS 408 at 30 phr resulted in a lower intensity of the 2-Theta peak in comparison to those seen in Perkasil KS 300. Thus size of silica particle is one of the factors influences dispersion of nanoclay in the polymeric matrix.

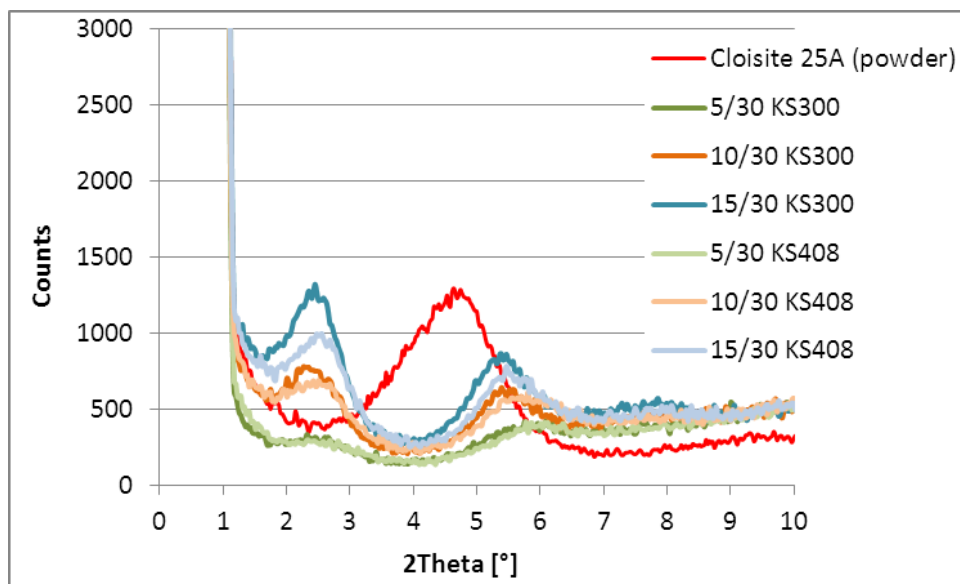
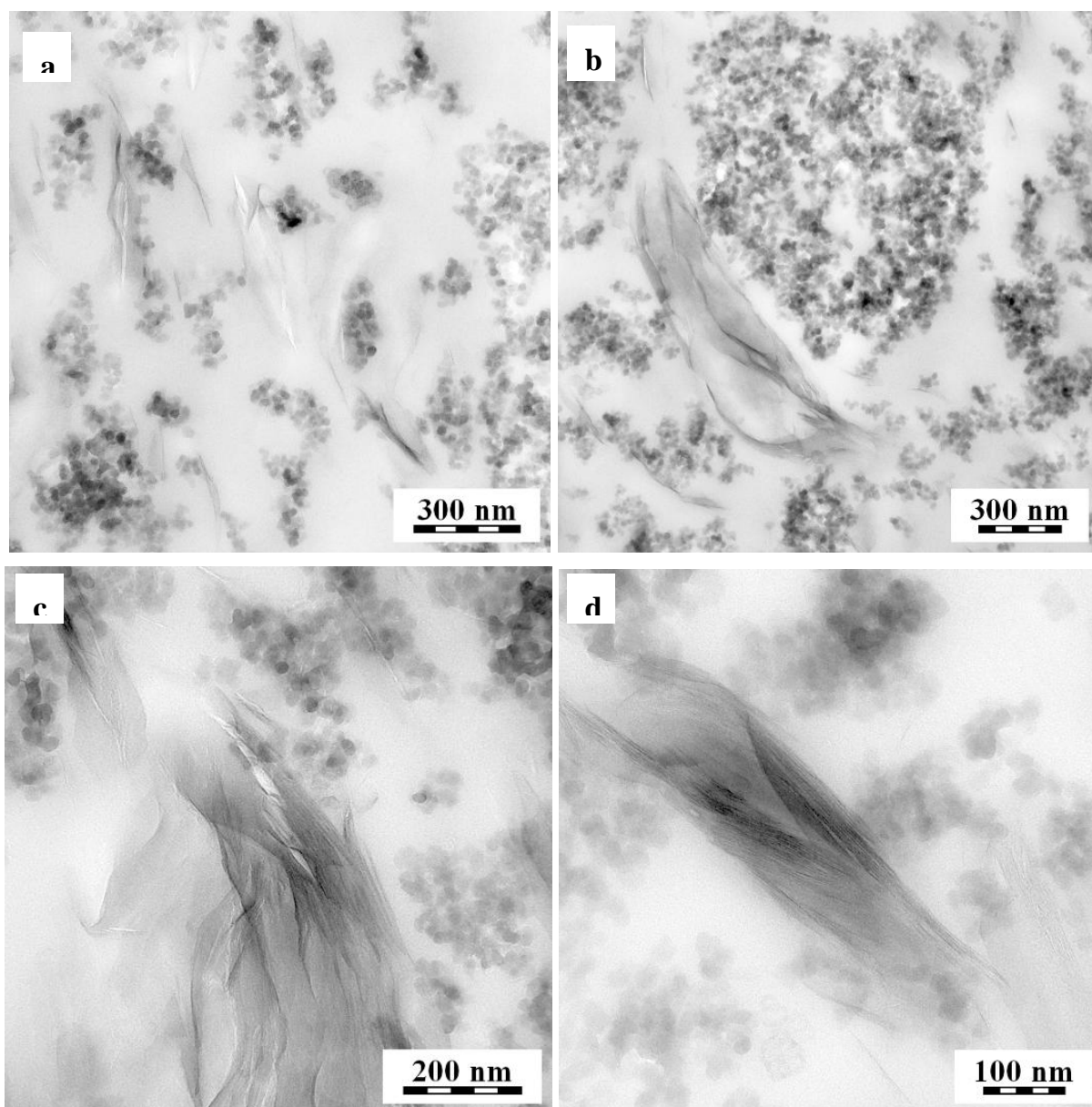


Figure 76: XRD pattern for compounds with 30 phr of silica

#### 4.2.7 TEM analysis

The NBR nanocomposite morphologies were investigated using TEM analysis to extend previous XRD analysis. TEM analysis was done for compounds filled by 30 phr of silica -10/30<sub>KS300</sub>, 5/30<sub>KS408</sub>, 10/30<sub>KS408</sub> and 15/30<sub>KS408</sub>.

Figure 77 shows the structure of compound 10/30<sub>KS300</sub> with silica Perkasil KS 300 and Cloisite 25A. The figures indicate the presence of intercalated structures of nanocomposite (figure b, c, d) as well as partial exfoliation of Cloisite 25A (figure a).



*Figure 77: TEM analysis - Cloisite 25A / KS 300 (10 phr / 30 phr)*

The morphology of compound 10/30<sub>KS408</sub> is shown in Figure 78. Intercalated structures (figure c, d) as well as partial exfoliation (figure a, b) are observed in this figure. This nanocomposite with KS 408 silica shows differences in structure in comparison to the previous nanocomposite with KS 300 silica from Figure 77. TEM analysis detects higher level of Cloisite 25A intercalation in compound 10/30<sub>KS408</sub> in comparison to the intercalation seen in compound 10/30<sub>KS300</sub>. This observation suggests the influence of silica particle size on the distribution and exfoliation of nanoclay in the polymeric matrix. This suggests smaller particles of silica improve distribution and intercalation of nanoclay. This correlates with the finding from the XRD analysis,

where intensity of the 2-Theta peak of compound 10/30<sub>KS408</sub> was lower than the peak seen with compound 10/30<sub>KS300</sub> (Figure 76).

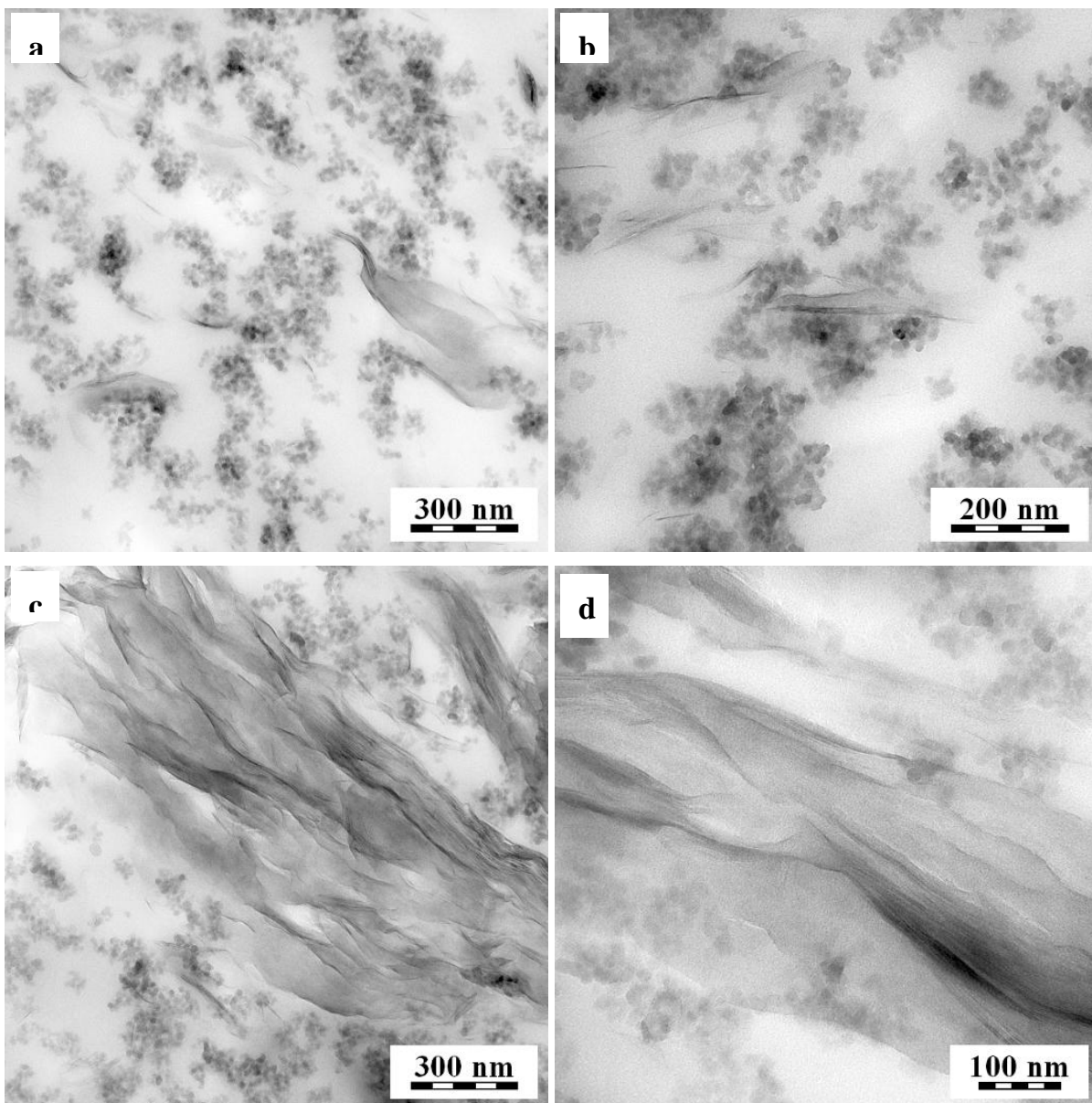


Figure 78: TEM analysis - Cloisite 25A / KS 408 (10 phr / 30 phr)

Compounds with low loadings (5 phr) of nanoclay exhibited the lowest intensity of 2-Theta peak in XRD analysis (Figure 76) and thus assumed very good distribution and exfoliation of nanoclay. But result of TEM analysis is different. Figure 79 shows intercalated structures only with no sections demonstrating exfoliation. The level of intercalation is the lowest when compared to the other compounds in TEM analysis.

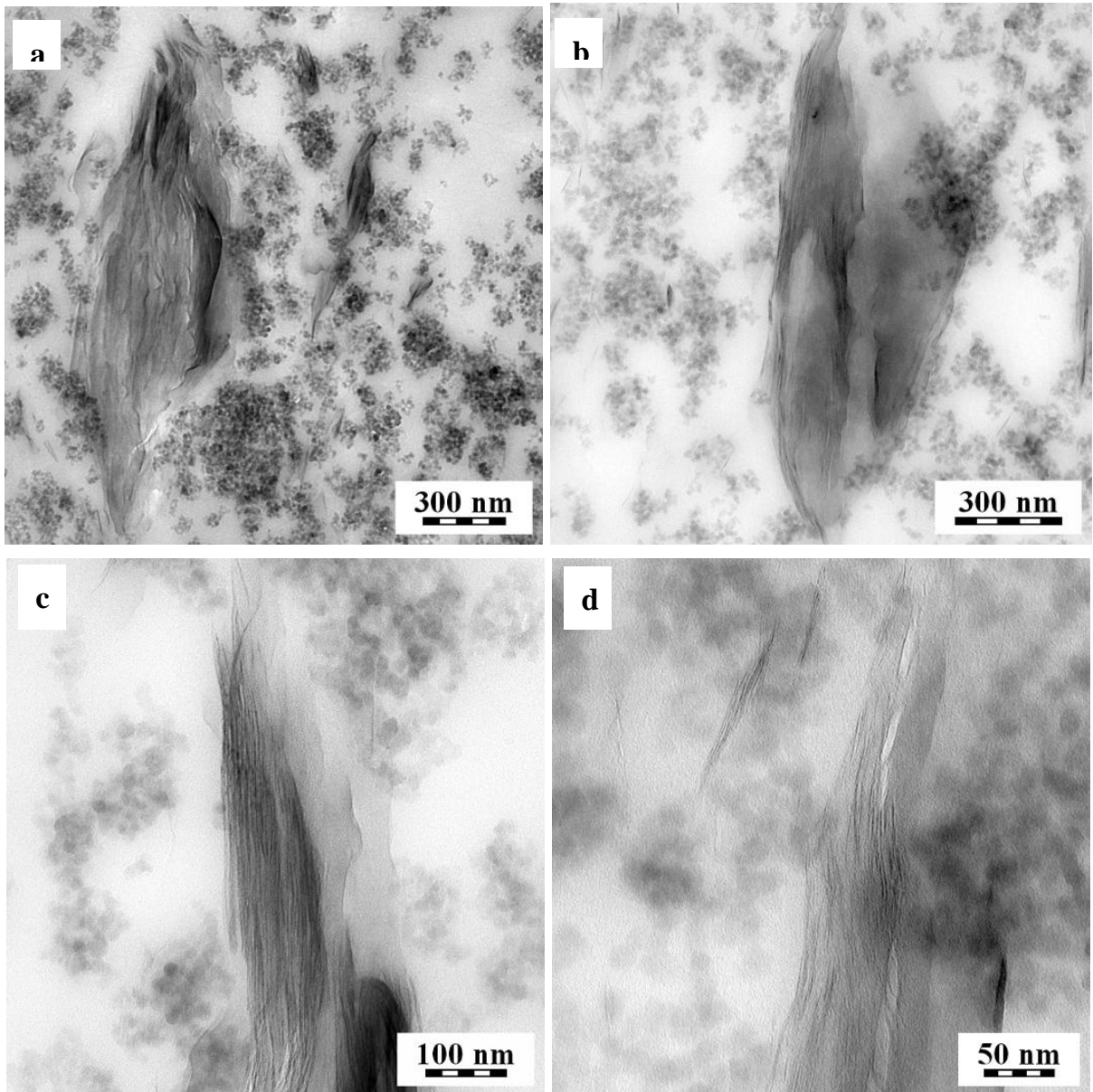


Figure 79: TEM analysis - Cloisite 25A / KS 408 (5 phr / 30 phr)

Figure 80 shows the morphology of compound 15/30<sub>KS408</sub>. Intercalation as well as partial exfoliation of nanoclay is seen in this figure. Figure 80b shows part of the intercalated platelets are separated and exfoliated in NBR matrix. Tendency of particles of silica to separate platelets of nanoclay and thus support and improve exfoliation of the nanoclay is observed in Figure 78c.

Direct observation in the TEM correlates with the results of XRD analysis, where intensity of the 2-Theta peak of compound 15/30<sub>KS408</sub> was higher than compound 15/30<sub>KS408</sub>.



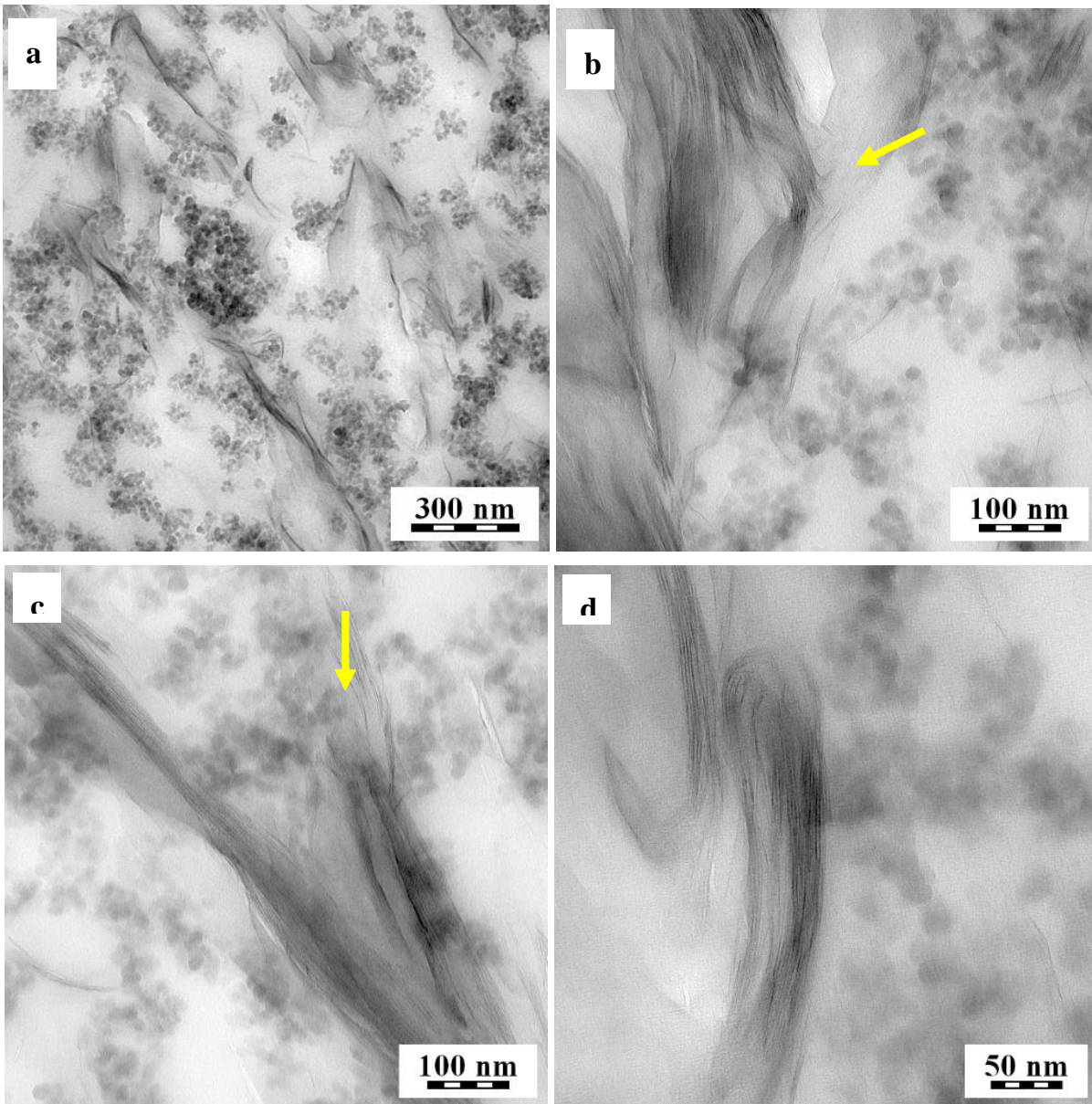


Figure 80: TEM analysis - Cloisite 25A / KS 408 (15 phr / 30 phr)

#### 4.2.8 Dynamic-mechanical properties

Dynamic-mechanical properties of vulcanized NBR nanocomposites were tested in two different modes:

1) Strain sweeps (mode 1) - constant oscillation frequency of 0,1 Hz and a strain amplitude from 0,5 to 25% at temperatures of 40 to 120°C

2) Temperature sweeps (mode 2) - constant strain amplitude of 1% with a constant oscillation of frequency 0,3 Hz at temperatures between 40 and 120°C



### *Strain sweeps*

All vulcanized NBR nanocomposites with various content of nanoclay and silica were tested at constant oscillation frequency with a wide range of strain amplitudes at temperatures of 40, 70 and 125°C.

Results of dynamic storage modulus in shear ( $G'$ ) for compounds with silica Perkasil KS 300 silica are shown in Figure 81 and for compounds with Perkasil KS 408 in Figure 82.

The results show decrease of  $G'$  for all the compounds tested with increasing strain amplitude, showing a Payne affect. This is likely the result of the decay of particle network structures. Breakdown of the particle network by increasing strain amplitude releases trapped NBR chains from network and agglomerates of silica / nanoclay and causes increase in the effective volume of NBR and therefore decrease of modulus  $G'$ . The compounds 15/30<sub>KS300</sub> and 15/30<sub>KS408</sub> show the highest values of  $G'$  over the full range of measured deformations. This assumes a stronger particle networks as well as stronger interaction with the NBR matrix than seen other mix ratio of nanoclay and silica. These results correlate well with measured hardness and tensile strength values observed on the tested compounds.

Figure 81 and Figure 82 show differences between the type and loading level of silica and nanoclay. Dynamic modulus is increasing with increasing silica and nanoclay contents. Higher value of  $G'$  of compounds with Perkasil KS 408 is likely caused by higher reinforcing effect by lower size of particles in compare to silica type Perkasil KS 300 and by better intercalation of the nanoclay. Benefits from the nanoclay are shown by results of compounds filled by only pure silica. As can be seen, values of  $G'$  of these pure silica compounds are the lowest for 30 phr loadings as well as for 10 phr. The biggest effect of nanoclay on  $G'$  is seen at the low deformations (up to 10%). At higher deformations, decay of nanoclay particle network structures is detected.

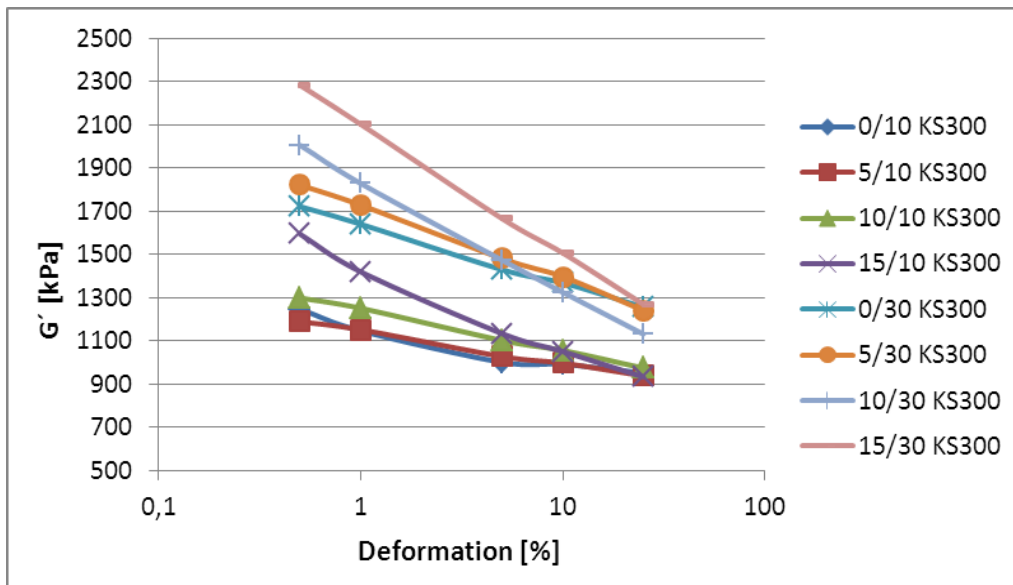


Figure 81: Dependence of dynamic storage shear modulus  $G'$  on strain amplitude at temperature  $70^{\circ}\text{C}$  - Cloisite 25A / Perkasil KS 300

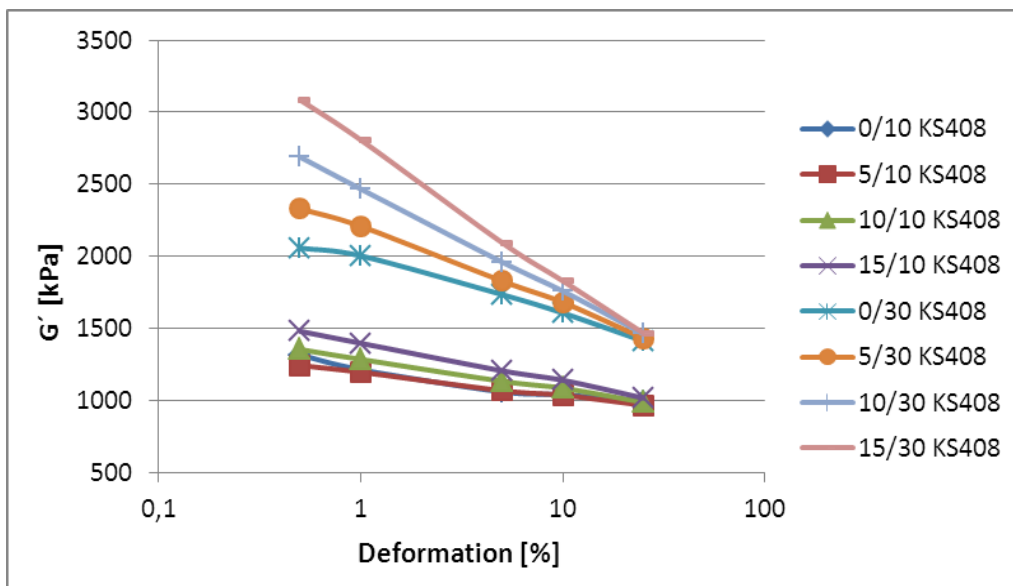


Figure 82: Dependence of dynamic storage shear modulus  $G'$  on strain amplitude at temperature  $70^{\circ}\text{C}$  - Cloisite 25A / Perkasil KS 408

Dependence of loss dynamic shear modulus ( $G''$ ) on strain amplitude at constant oscillation frequency is shown in Figure 83 for compounds containing Perkasil KS 300 and in Figure 84 for compounds with Perkasil KS 408. Value of  $G''$  is influenced by the breakdown and reformation of the particle networks during dynamic strain [88]. As shown in the figures, the loss modulus is much larger for compounds 15/30<sub>KS 408</sub> and 15/30<sub>KS 300</sub>, than that observed for the other compounds. This could be a result of

improved interaction between nanoclay and silica fillers and their ability to create strong particle networks. Almost all measured compounds were observed to reach initial peak at a strain amplitude about 8 % and main peak at amplitude about 5 %, where the particle networks appear to start to disintegrate. Ability of nanoclay and silica to create network between particles is probably caused by “-OH” groups on the silica and nanoclay particle surface.

Figure 83 and Figure 84 reveal different behavior between various particle sizes of silica. As can be seen compounds containing 30 phr of Perkasil KS 408 achieve higher value of  $G''$  than compounds with bigger silica particles KS 300. These results demonstrate stronger particle networks of nanocomposite with silica Perkasil KS 408 than with silica Perkasil KS 300. This could be caused by lower particle size of silica and thus higher amounts of -OH groups on the Perkasil KS 408. As can be seen in figures, values of  $G''$  of compounds containing 10 phr of silica are similar for both silica types - KS 300 as well as KS 408. These results show effect of higher load of silica to create stronger particle networks between particles of silica and nanoclay.

As shown in the figures, loss dynamic shear modulus is increasing with increasing loadings of silica and nanoclay and can be attributed to hydrodynamic effect as load of unstrained fillers [85]. A similar effect was observed in dynamic modulus testing.

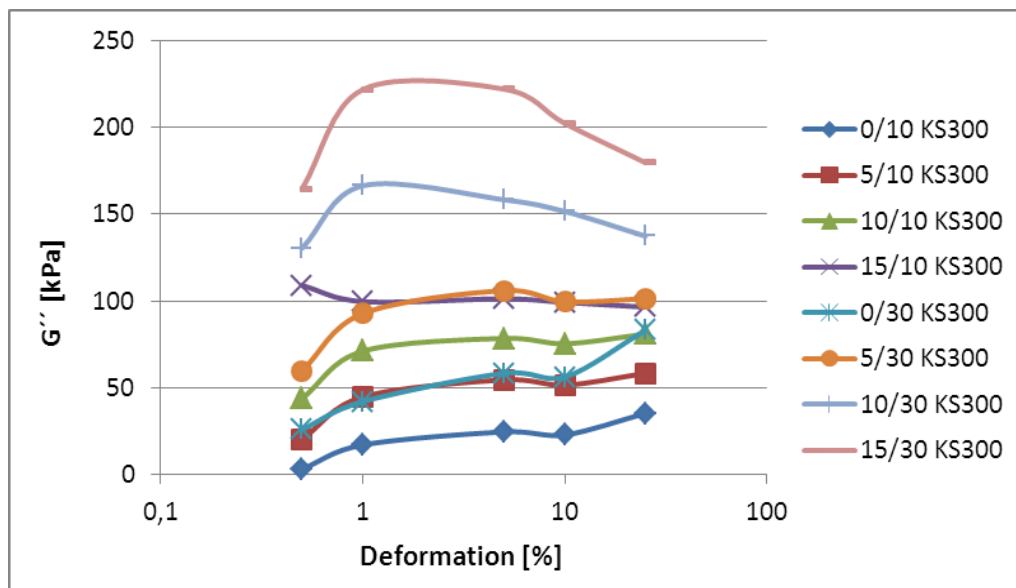


Figure 83: Dependence of loss dynamic modulus  $G''$  on strain amplitude at temperature 70°C - Cloisite 25A / Perkasil KS 300

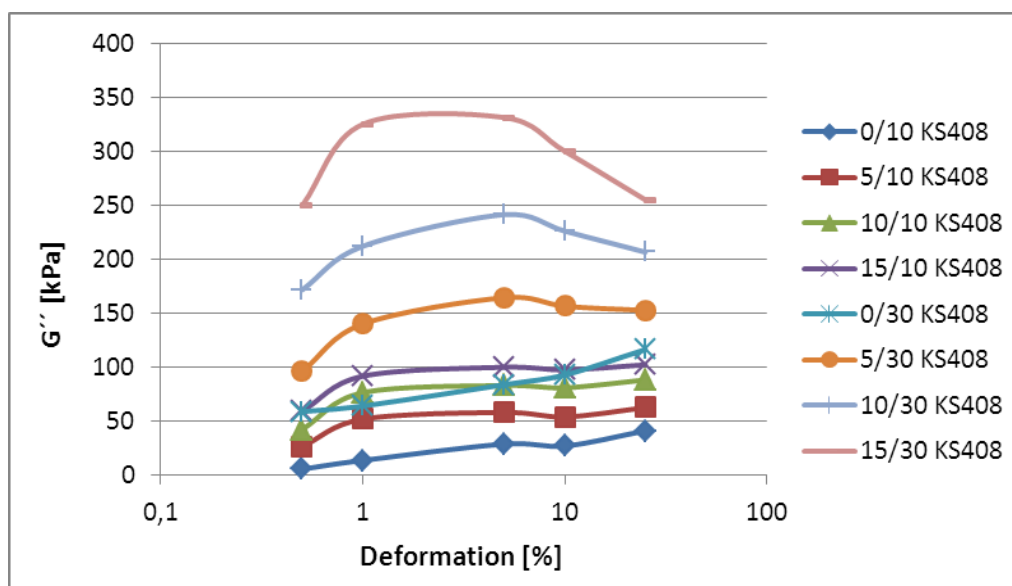


Figure 84: Dependence of loss dynamic modulus  $G''$  on strain amplitude at temperature  $70^{\circ}\text{C}$  - Cloisite 25A / Perkasil KS 408

The dependence of dynamic loss factor ( $\tan \delta$ ) on strain amplitude is shown in Figure 85 for compounds with Perkasil KS 300 and in Figure 86 for compounds with Perkasil KS 408. As can be seen compounds with nanoclay shows better results than compounds with both types of pure silica. Results show higher restriction of movement of polymer chains by nanoclay and therefore better reinforcing effect to NBR. Loss factor of compounds 15/30<sub>KS 300</sub>, 10/30<sub>KS 300</sub> and 15/10<sub>KS 300</sub> at very low deformation 0,5 % is very similar but increase of deformation shows better effect of higher load of nanoclay and silica. Filler network is very strong and cannot be break at low strain amplitude. This cause reduction of polymer fraction by trapped NBR chains in the silica / nanoclay particle structure and thus loss factor  $\tan \delta$  is the lower. Increase of strain deformation release trapped NBR chains by decay of particle structure and causes increase of  $\tan \delta$  [85].

The possibility exists that nanoclay fillers have a higher interaction with NBR matrix as result of combination of good exfoliation and high polymer-filler contact area which provides improved elastic behavior.

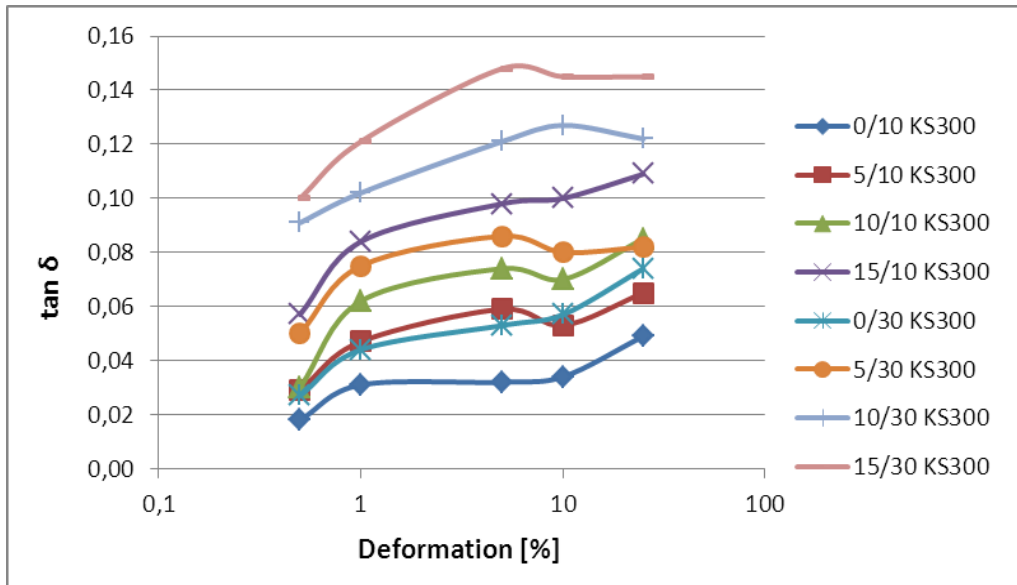


Figure 85: Dependence of loss factor  $\tan \delta$  on strain amplitude at temperature  $70^{\circ}\text{C}$  - Cloisite 25A / Perkasil KS 300

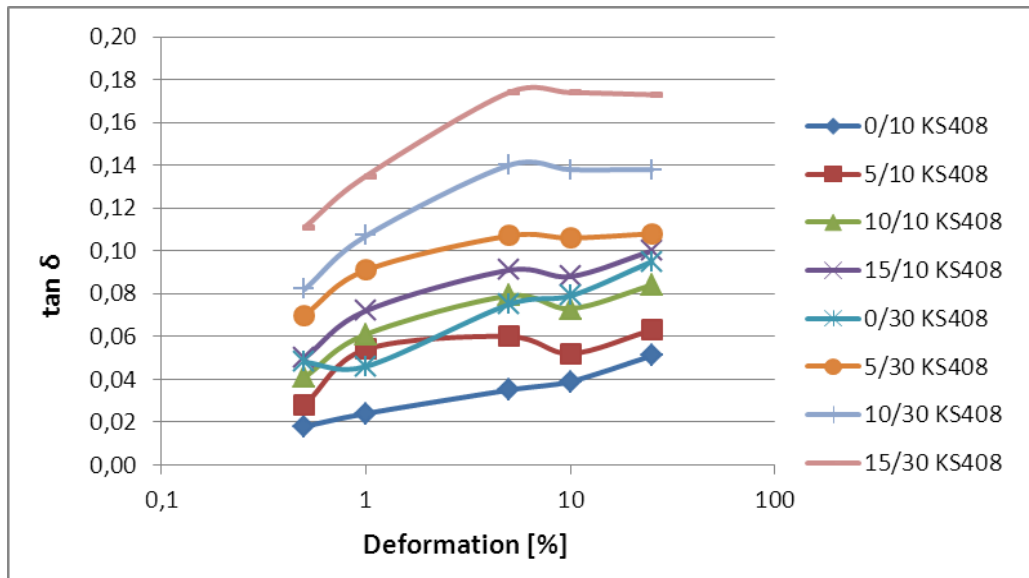


Figure 86: Dependence of loss factor  $\tan \delta$  on strain amplitude at temperature  $70^{\circ}\text{C}$  - Cloisite 25A / Perkasil KS 408

### Temperature sweeps

All vulcanized NBR nanocomposites with various content of nanoclay and silica were tested in temperature sweep (mode 2) at constant strain amplitude and constant oscillation frequency at temperatures between 40 and 120°C.

Results of dynamic storage modulus in shear ( $G'$ ) for compounds with Perkasil KS 300 silica are shown in Figure 87 and for compounds with Perkasil KS 408 in Figure 88.

These figures show an increasing of  $G'$  with higher filling factor of nanoclay and silica. A benefit from the nanoclay is shown by results of compounds filled by only pure silica. As can be seen, values of  $G'$  of these pure silica compounds are the lowest for 30 phr loadings as well as for 10 phr. Differences between loadings of 5, 10 or 15 phr of nanoclay are stronger with load of 30 phr of silica than with lower loadings of 10 phr of silica. These results support the hypothesis of improved of nanoclay intercalation by silica particles during mixing process.

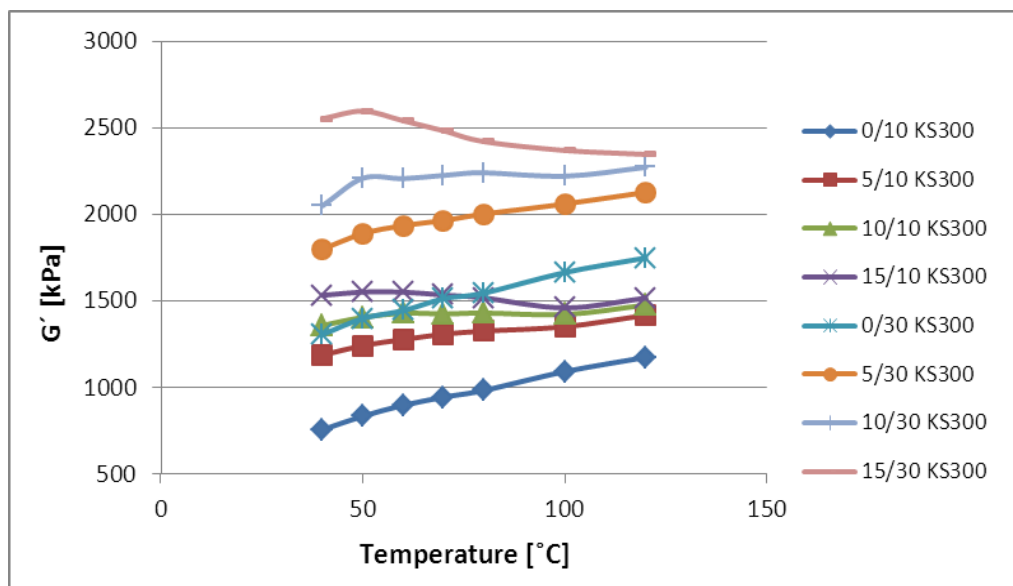


Figure 87: Dependence of dynamic storage shear modulus  $G'$  on temperature - Cloisite 25A / Perkasil KS 300

Figure 88 shows higher value of  $G'$  for compounds with Perkasil KS 408 than compounds with Perkasil KS 300. This is caused by the smaller size of silica KS 408 particles and thus higher reinforcing effect compared to Perkasil KS 300.

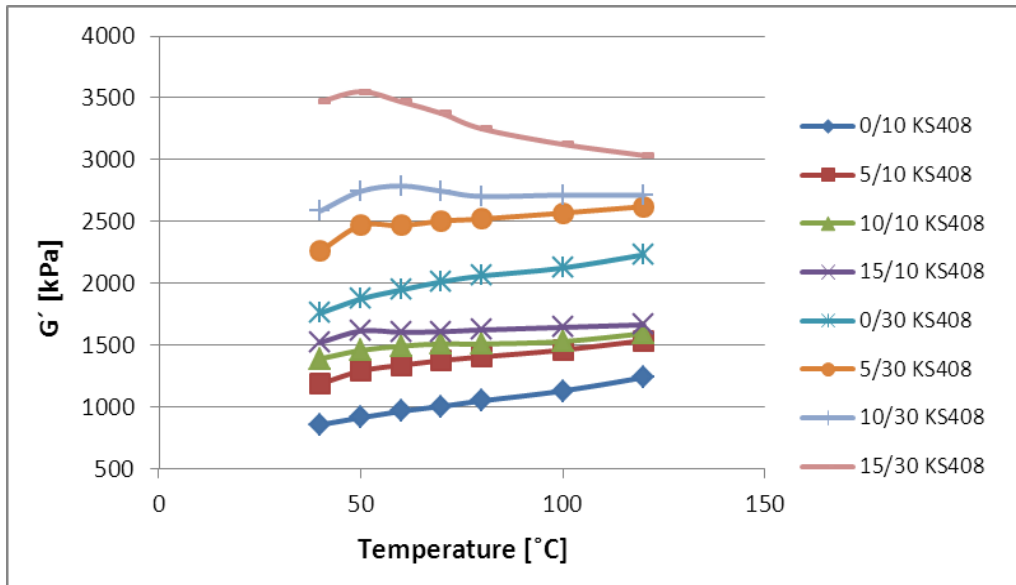


Figure 88: Dependence of dynamic storage shear modulus  $G'$  on temperature - Cloisite 25A / Perkasil KS 408

Results of dynamic loss factor ( $\tan \delta$ ) for compounds filled by Perkasil KS 300 silica are shown in Figure 89 and for compounds filled by Perkasil KS 408 in Figure 90. Compounds with same load of nanoclay show similar position of loss peak - compounds 10/30 and 10/10 at temperature  $60^\circ\text{C}$ , and compounds 5/30 and 5/10 at temperature  $50^\circ\text{C}$ . The figure also shows higher value of loss factor by higher load of silica. This could be caused by higher intercalation of nanoclay supported by silica and by reinforcing effect provided by the silica itself. The substantial decrease in loss factor after about  $60^\circ\text{C}$  can be caused by release of intercalated NBR chains from the nanoclay structure at higher temperatures.

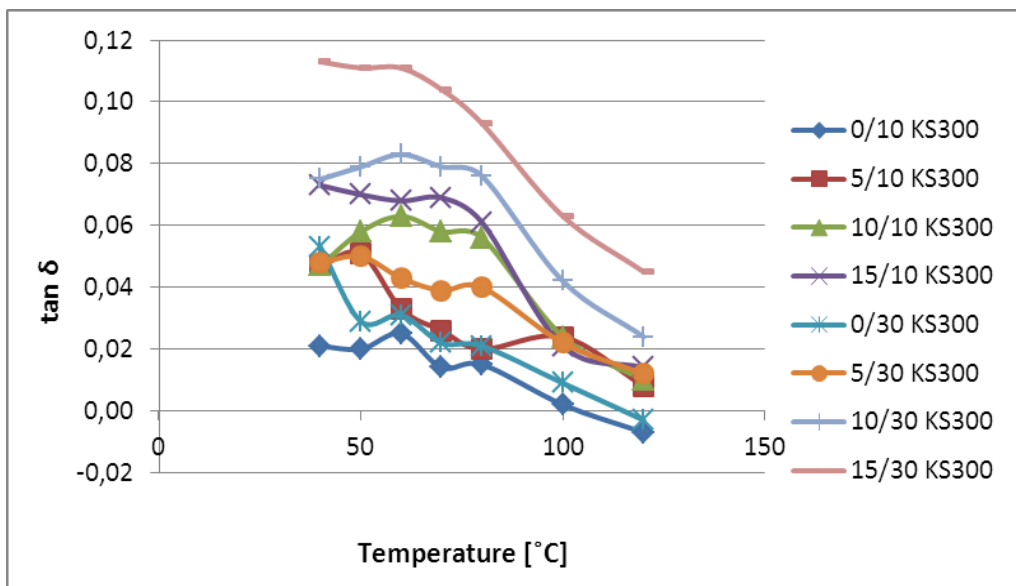


Figure 89: Dependence of loss factor  $\tan \delta$  on temperature - Cloisite 25A / Perkasil KS 300

Figure 90 shows the loss factor of compounds with Perkasil KS408 silica are higher than values of compounds with Perkasil KS 300 which confirms better reinforcing effect of smaller size particles found in the Perkasil KS 408. Also intercalation of nanoclay supported by this silica type could be better than what is provided by Perkasil KS 300 silica.

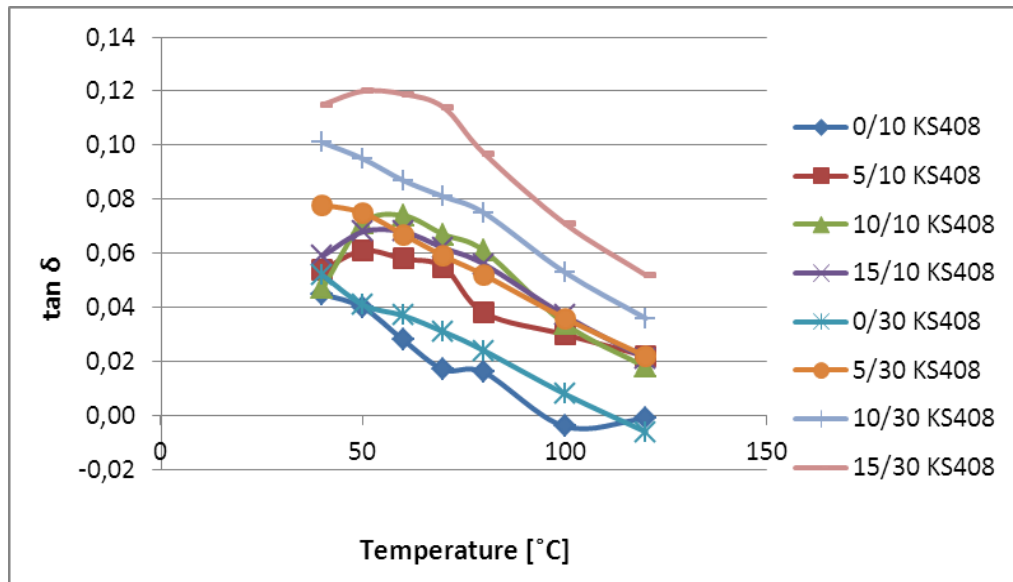


Figure 90: Dependence of loss factor  $\tan \delta$  on temperature - Cloisite 25A / Perkasil KS 408

Dependence of loss dynamic shear modulus ( $G''$ ) on the temperature at constant oscillation frequency is shown in Figure 91 for compounds with Perkasil KS 300 and in Figure 92 for compounds with Perkasil KS 408. Results reveal ability of nanoclay and silica to create network together between their particles. Connection is probably created by  $-OH$  groups, which silica and nanoclay contain on the surface. This can explain increasing of  $G''$  with increasing load of silica and nanoclay. Higher amount of silica and nanoclay creates more links between particles. Peaks on the curves show start of disintegration of particle network with increasing temperature.



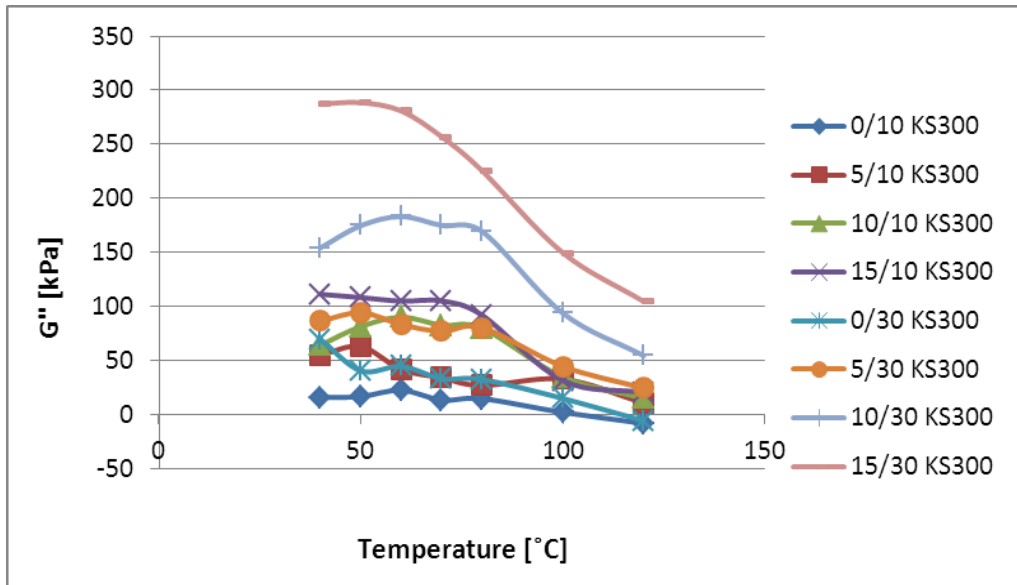


Figure 91: Dependence of loss dynamic modulus  $G''$  on temperature - Cloisite 25A / Perkasil KS 300

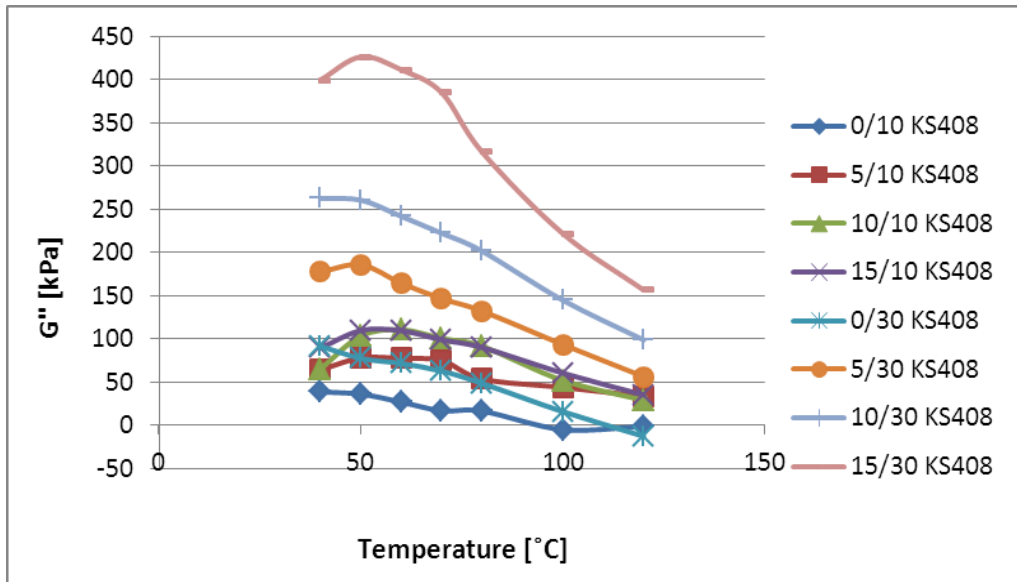


Figure 92: Dependence of loss dynamic modulus  $G''$  on temperature - Cloisite 25A / Perkasil KS 408

#### 4.2.9 Summary

The objective of the second part of this study was to investigate the influence silica has on the nanoclay distribution in the polymeric matrix and identify the optimal mix ratio of nanoclay Cloisite<sup>®</sup> 25A and silica.

XRD analysis revealed improvements in the nanoclay distribution with increasing loadings of silica. Morphology of NBR nanocomposites was much better with loadings of 30 phr of silica than lower loading 10 phr. In addition to these results, XRD analysis

detected the improved intercalation of nanoclay by smaller silica size particles - NBR nanocomposites with Perkasil KS 408 silica showed slightly better morphology than nanocomposites with Perkasil KS 300 silica.

Measurement by the rubber process analyzer showed the ability of silica and nanoclay to create a particle network, which depends on the loading of silica and nanoclay particles.

NBR compounds filled by 15 phr of Cloisite 25A and 30 phr of silica showed the best results in static-mechanical as well as in dynamic-mechanical testing and R-134a permeation testing. Results of these tests confirm importance of nanoclay intercalation influenced by silica.

Therefore, the presence of silica in NBR/clay nanocomposites is important to achieve a more optimal morphology. Exfoliation and intercalation of nanoclay is probably caused by increased compound viscosity as well as by friction and collisions between particles of silica and platelets of nanoclay during the mixing process.

Measured results show an optimal mix ratio of silica and nanoclay at 30 phr of silica and 15 phr of nanoclay. More effective exfoliation of nanoclay could decrease the loading to 10 phr of nanoclay.

### 4.3 Investigation of silica and influence of viscosity on nanoclay intercalation

Test results in chapters 4.1 and 4.2 revealed a positive effect of silica in distribution, intercalation and exfoliation of nanoclay in NBR matrix during the mixing process. The objective of the last investigation was to identify key factors which influence nanoclay intercalation and exfoliation – and to determine if these factors include higher viscosity of rubber compounds caused by loading of silica particles and/or collision and friction between particles of silica and nanoclay during mixing process.

#### 4.3.1 Rubber compound composition

The base recipe of rubber compounds (Table 4) was updated for this new investigation. Two NBR elastomers with different viscosities were utilized in this test – Europrene N33.45 with Mooney viscosity ML (1+4) 100°C = 45 and Krynac 49.75 with Mooney viscosity ML (1+4) 100°C = 75. Perkasil KS 408 silica was additionally added into Europrene N33.45 at various loading levels. Dioctyl adipate oil was removed from compounds to allow the mixing of compounds with only nanoclay. Loading of nanoclay Cloisite 25A was 10 phr in all compounds in this test.

Formulation of rubber compounds is shown in Table 17.

Table 17: Recipe of experimental compounds

	<b>N1/0</b>	<b>N1/15</b>	<b>N1/30</b>	<b>N1/45</b>	<b>N2/0</b>
<b>NBR Europrene N33.45</b>	100	100	100	100	-
<b>NBR Krynac 49.75</b>	-	-	-	-	100
<b>Silica KS 408</b>	-	15	30	45	-
<b>Cloisite 25A</b>	10	10	10	10	10
<b>Dioctyl adipate oil</b>	-	-	-	-	-
<b>Peroxide Norperox BIPB 40</b>	7	7	7	7	7
<b>Rhenofit TAC/GR 70</b>	2	2	2	2	2

Rubber compounds were prepared by two-roll mill. NBR, silica, nanoclay and the vulcanization system were mixed for 30 min at a temperature of about 40°C.

### 4.3.2 XRD analysis

Differences in the morphologies of NBR nanocomposites with various viscosity and loadings of silica was investigated by XRD analysis. This investigation was done for all five NBR compounds prepared.

As can be seen in Figure 93, the highest intensity of 2-Theta peaks is shown in compounds without silica – N1/0 and N2/0. Surprisingly compound N2/0 with the high viscosity NBR shows a higher intensity of 2 Theta peak than compound N1/0 with the medium viscosity NBR. These results show viscosity is not key factor for nanoclay distribution in polymeric matrix.

Compounds N1/15, N1/30 and N1/45 with various loading of silica / nanoclay show much lower intensity of 2-Theta peak than compounds N1/0 and N2/0 filled by nanoclay only. Figure shows a decreasing of peak intensity with increasing load of silica. These results reveal silica as key factor for the generation of morphology in the NBR / clay nanocomposite. Collisions and friction between particles of silica and nanoclay could support intercalation and exfoliation of nanoclay during mixing process.

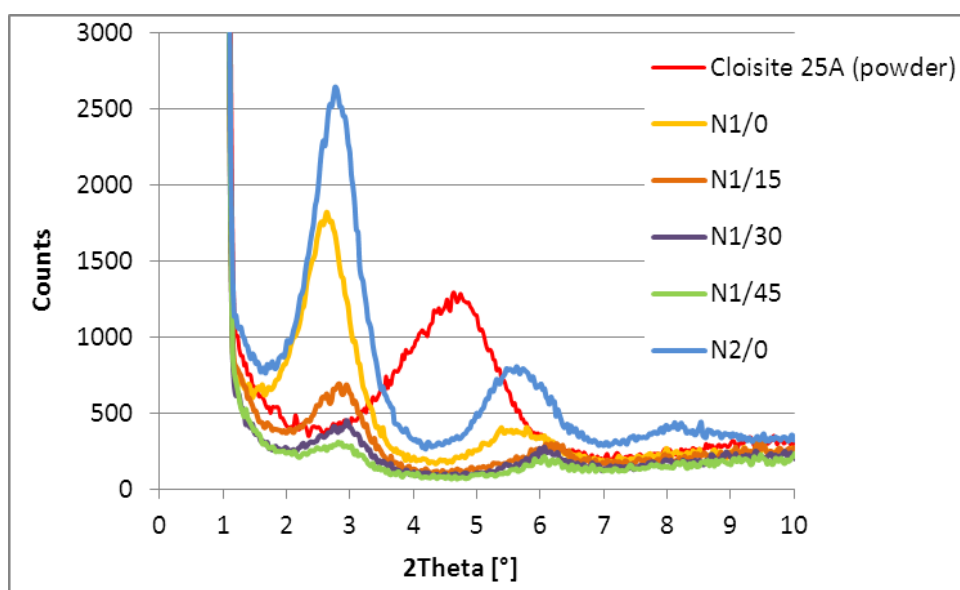


Figure 93: XRD pattern for compounds with various viscosity

### 4.3.3 Summary

The objective of the last stage of this study was to identify key factors which influence nanoclay intercalation and exfoliation in the compound with hybrid filler system silica / nanoclay.

This investigation reveals silica as key factor for the generation of morphology of NBR / clay nanocomposites. Collisions and friction between particles of silica and

nanoclay could support intercalation and exfoliation of nanoclay during mixing process. Higher viscosity of the raw NBR elastomer does not support optimal nanoclay intercalation in the compound without silica content.

## CONCLUSION

The objective of this study was to investigate the properties and behaviors of NBR rubber modified by hybrid filler systems and develop rubber compound with optimized morphology, mechanical properties, and reduced refrigerant R-134a permeation by using a suitable combination of fillers. Nanoclay fillers in combination with silica demonstrated the ability to provide a 30% reduction in R-134a permeation and while achieving improved mechanical properties. The key to obtaining these enhancements was adequate level of exfoliation or intercalation and polymer-filler interaction of the nanoclay fillers, confirmed by the measurements performed.

This exfoliation and interaction depends on several factors. The first factor is the type and amount of the nanofiller modifier. Cloisite Na<sup>+</sup> is an unmodified nanoclay and provides the NBR compound properties similar to common white fillers such as talc and kaolin. The best results seen in this study were observed with Cloisite 25A with a higher modifier level. Combinations of nanoclay with silica enhanced intercalation and exfoliation of the nanoclay during mixing of the compounds. Investigations revealed the presence of silica in NBR compounds as a key factor for intercalation and exfoliation of Cloisite 25A. This improved distribution of nanoclay in the NBR matrix is probably caused by an increase in viscosity as well as by friction and collisions between particles of silica and platelets of nanoclay during the mixing process. Smaller particle size of silica Perkasil KS 408 showed better support of nanoclay distribution in the NBR matrix than silica Perkasil KS 300 with higher particle size. Measured results show optimal mix ratio of silica and nanoclay to be 30 phr of silica and 15 phr of nanoclay.

Results of this study also demonstrated that high viscosity rubber compounds without silica do not provide enough nanoclay exfoliation in polymeric matrix. Therefore presence of silica in NBR/clay compound is very helpful to achieve a good level of exfoliation.

Use of nanoclay Cloisite 25A in combination with a silica filler has shown to produce a compound with higher permeation resistance to R-134a and improvement in tensile strength, elongation and dynamic modulus useful for sealing applications in the automotive A/C systems.

**Thesis contribution to science and industry application:**

- Completed study of the influence of various mixture of nanoclay and silica to mechanical properties, morphology and permeation reduction
- Detected a solution to reduce R-134a permeation of refrigerant by mixture of silica / nanoclay
- Identified a positive effect of silica to nanoclay intercalation and exfoliation
- Identified a cost effective hybrid mineral filler system silica / nanoclay as optimal solution for NBR nanocomposites

**Recommendation for future investigation:**

- Verify the results of this investigation using an HNBR elastomer (due to increasing requirements for high temperature resistance)
- Investigate optimization of mixing process by two roll mill and internal mixer
- Investigate behavior of hybrid mineral filler system silica / nanoclay in the other elastomers

## REFERENCES

- [1] DUCHÁČEK, V.: *Světlá plniva*, Česká společnost průmyslové chemie, Zlín 2010, ISBN 978-80-02-02203-9
- [2] ROCKWOOD ADITIVES: *Additives Reference Guide*, 2010
- [3] DIRECTIVE 2006/40/EC OF THE EUROPEAN PARLIAMENT AND OF THE COUNCIL *relating to emissions from air-conditioning systems in motor vehicles and amending Council Directive 70/156/EEC*, 17 May 2006
- [4] NIELSEN, O.J., JAVADI, M.S., SULBAEK ANDERSEN, M.P., HURLEY M.D., WALLINGTON T.J., SINGH R.: *Atmospheric chemistry of CF<sub>3</sub>CF@CH<sub>2</sub>: Kinetics and mechanisms of gas-phase reactions with Cl atoms, OH radicals, and O<sub>3</sub>*, Chemical Physics Letters 439, p. 18-22, 2007
- [5] SAE COOPERATIVE RESEARCH PROGRAM 1234-2: *Material compatibility of HFO-R1234yf (final report)*, 2008
- [6] YOON, P.J., GOSS, M., MCAFEE, C.: *Effects of Nanoclay Structure on the Mechanical Properties of EPDM*, Fall 170th Technical Meeting of the Rubber Division, American Chemical Society (presentation), 2006
- [7] GALIMBERTI, M., GIANNINI, L., D'ORIA, F., LOSTRITTO, A.: *Tailor made nanostructures for improved properties of tyre compounds*, 174th Technical Meeting, Rubber Division of American Chemical Society, Louisville, KY (USA), October 14-16, 2008
- [8] CATALDO, F.: *Preparation and properties of nanostructured rubber composites with montmorillonite*, Macromolecular Symposia. 247: p. 67-77, 2007
- [9] GALIMBERTI, M., GIUDICE, S., COOMBS, M., GIANNINI, L., BUTTAFAVA A., DONDI D., FAUCITANO A.: *Filler matrix interface characteristics and mechanical reinforcement in elastomeric, nanocomposites*, 178th Technical Meeting of the Rubber Division of the American Chemical Society, Inc. Milwaukee (WI) October 12-14, 2010
- [10] HRACHOVÁ, J., KOMADEL, P., JANIGOVÁ, I., ŠLOUF, M., CHODÁK, I.: *Properties of rubber filled with montmorillonite with various surface modifications*. Polymers for Advanced Technologies, 2012, vol. 23, p. 1414 – 1421
- [11] HRACHOVÁ, J., KOMADEL, P., JANIGOVÁ, I., ŠLOUF, M., CHODÁK, I.: *Effect of montmorillonite modification on mechanical properties of vulcanized natural rubber composites*. Journal of Materials Science, 2008, vol. 43, p. 2012 - 2017



- [12] GALIMBERTI, M., COOMBS, M., CIPOLLETTI, V., GIANNINI, L., CONZATTI, L., RICCÒ, T., MAURO, M., GUERRA, G. (2011) *Nano and nanostructured fillers and their synergistic behavior in rubber composites such as tyres*, 180th Technical Meeting of the Rubber Division of the American Chemical Society, Inc. Cleveland (OH) October 11-13, 2011
- [13] MAITI M., SADHU S., BHOWMICK A.K.: *Effect of carbon black on properties of rubber nanocomposites*, Journal of Applied Polymer Science 96: p. 443-451, 2005
- [14] PRAAVEN, S., CHATTOPADHYAY, P.K., ALBERT, P., DALVI, V.G., CHAKRABORTY, B.C., CHATTOPADHYAY, S.: *Synergistic effect of carbon black and nanoclay fillers in styrene butadiene rubber matrix: development of dual structure*, Composites: Part A. 40: p. 309-316, 2009
- [15] MALAS, A., DAS, C.K.: *Carbon black–clay hybrid nanocomposites based upon EPDM elastomer*, Journal of Material Science. 47: p. 2016–2024, 2012
- [16] ŠPAČEK, J.: *Technologie gumárenská a plastikářská II.*, Vysoké učení technické v Brně, 1980, ISBN 55-583-80
- [17] *Acrylonitrile-butadiene rubber (NBR)* [online]. [quot. 2013-15-07]. <[http://www.surplussales.com/rubber-plastic/pdf/rps-footrub-33\\_properties.pdf](http://www.surplussales.com/rubber-plastic/pdf/rps-footrub-33_properties.pdf) >
- [18] DICK, J.: *Rubber technology – compounding and testing for performance*, Hanser Gardner Publication, Inc. Cincinnati, 2001, ISBN 1-56990-278-X
- [19] DUCHÁČEK, V.: *Přírodní a syntetické kaučuky*, Česká společnost průmyslové chemie, Zlín 2006, ISBN 80-02-01784-6
- [20] CHOUDALAKIS, G., GOTSIS, A.D.: *Permeability of polymer/clay nanocomposites: A review*, European Polymer Journal 45, p. 967–984, 2009
- [21] SONEY, C.G., SABU, T.: *Transport phenomena through polymeric systems*, Progress in Polymer Science, 26, p. 985 – 1017, 2001
- [22] *Rubber materials used in sealing technology*. Presentation of Trelleborg company, 2008
- [23] FLACONNECHE B., MARTIN, J., KLOPFER M. H.: *Transport Properties of Gases in Polymers: Experimental Methods*, Oil & Gas Science and Technology, Vol. 56, p. 245-259, 2001
- [24] AUERBACH, J., MILLER, W.R., KURYLA, W.C., GEHMAN, S.D.: *A diffusivity approach for studying polymer structure*, Journal of Polymeric Science, vol. 28, p. 129-150, 1958

- [25] BARRER RM, SKIRROW G.: *Transport and equilibrium phenomena in gas–elastomer systems. I. Kinetic phenomena*, Journal of Polymeric Science, vol. 3, p. 549-563, 1948
- [26] VAN AMERONGEN, G.J.: *Influence of structure of elastomers on their permeability to gases*, Journal of Polymeric Science, vol. 5, p. 307-332, 1950
- [27] BRANDRUP, J., IMMERGUT, EDMUND H., GRULKE, ERIC A., ABE, AKIHIRO: *Polymer handbook (4<sup>th</sup> edition)*, 199, 2005 John Wiley a Sons, ISBN 978-0-471-16628-3
- [28] MASSEY, K.L.: *Permeability properties of plastics and elastomers*, Plastic Design library – William Andrew Publishing, 2003, ISBN 978-1-884207-97-6
- [29] CRANK, J., PARK, G.S.: *Diffusion in polymers*, Academic Press, London, 1968, ISBN 67-28001
- [30] BERENS, A.R., HOPFENBERG, H.B.: *Diffusion of organic vapors at low concentrations in glassy PVC, polystyrene, and PMMA*, Journal of Membrane Science, Vol. 10, p. 283-303, 1982
- [31] YI YAN, N., FELDER, R.M., KOROS, W.J.: *Selective permeation of hydrocarbon gases in poly(tetrafluoroethylene) and poly(fluoroethylene–propylene) copolymer*, Journal of Applied Polymer Science, vol. 25, p.1755–1774, 1980
- [32] NICHOLAS P. CHEREMISINOFF: *Handbook of Polymer Science and Technology: Composites and specialty applications*, CRC Press, 1989, ISBN 0-8247-8021-3
- [33] MAO, F.: *Permeation of hydrocarbons through polyvinyl chloride (PVC) and polyethylene (PE) pipes and pipe gaskets*, Dissertation thesis, Iowa State University. Civil, Construction, and Environmental Engineering, 2008
- [34] CIESIELSKI, A.: *An introduction to rubber technology*, Rapra technology limited, UK, 1999, ISBN 1-85957-150-6
- [35] *Vanderbilt rubber handbook*, [online]. [quot. 2011-29-11]. <<http://www.rtvanderbilt.com/rubber.htm>>
- [36] HEWITT, N: *Compounding precipitated silica in elastomers*, William Andrew Inc., 2007, ISBN 978-0-8155-1528-9
- [37] MILOSKOVSKA, E: *Structure-property relationships of rubber/silica nanocomposites via sol-gel reaction*, Dissertation, Eindhoven University of Technology, ISBN 978-90-386-3278-0, 2012

- [38] *Mineral Gallery* [online]. [quot. 2011-29-11].  
<<http://www.galleries.com/minerals/silicate/clays.htm>>
- [39] BERGAYA, F., THENG, G., LAGALY, G.: *Handbook of clay science*, Elsevier 2006, ISBN 978-0-08-044183-2
- [40] CIULLO, P.A.: *Industrial minerals and their used*, Noyes publication, 1996, ISBN 0-8155-1408-5
- [41] ASHTER, A.: *Elastomeric Nanocomposites: Quantifying the Effect of Modified Montmorillonite Clays on Styrene-Ethylene-Butadiene-Styrene (SEBS)*, University of Massachusetts, 2002
- [42] LIM JIAN ,W: *Development of layered silicates montmorillonite filled rubber-toughened polypropylene nanocomposites*, Dissertation, University teknologi Malaysia, 2006,
- [43] CHI MA, EGGLETON, R.A.: *Cation exchange capacity of kaolinite*, Clays and Clay Minerals, Vol. 47, No. 2, p. 174-180, 1999
- [44] BHATTACHARYA, N. S., KAMAL, M. R., GUPTA, R. K.: *Polymeric nanocomposites: theory and practice*, Carl Hansen Verlag, Munich, 2008, ISBN 978-156990-374-2
- [45] *Key properties of montmorillonite* [online]. [quot. 2011-29-11].  
<<http://www.nanoclay.com/keyproperties.asp>>
- [46] OKAMOTO, M.: *Polymer/layered silicate nanocomposites*, Rapra technology limited, UK, 2003, ISSN 0889-3144
- [47] KORNMANN, X: *Synthesis and Characterisation of Thermoset-Clay Nanocomposite*, Luleå University of Technology, ISSN 1402-1757, 1999
- [48] MERINSKA, D., MALAC, Z., POSPISIL, M. et al.: *Polymer/clay nanocomposites based on MMT/ODA intercalates*, Composite Interfaces, 9 (6), p. 529-540, 2002
- [49] MERINSKA, D.: *Polymer / clay nanocomposites*. Habilitační práce, UTB Zlín, Fakulta technologická, 2010
- [50] BEALL, G. W., KAMENA, K.: *A new family of intercalated clays for clay polymer nanocomposites*, ANNU. TECH. CONF. - SOC. PLAST. ENG., 57<sup>th</sup> (Vol. 3), p. 3973-3974, 1999
- [51] SINHA RAY, S, OKAMOTO, M: *Polymer/layered silicite nanocomposite: a reiew from preparation to processing*, Progress in Polymer Science 28, p. 1539–1641, 2003

- [52] GALIMBERTI, M.: *Rubber clay nanocomposites*. John Wiley & Sons, 2011, ISBN 978-0-470-56210-9
- [53] ODOM, I. E.: *Smectite clay Minerals: Properties and Uses*, Philosophical Transactions of the Royal Society of London. Series A, Mathematical and Physical Sciences, Volume 311, Issue 1517, p. 391-409
- [54] OKADA A, KAWASUMI M, USUKI A, KOJIMA Y, KURAUCHI T, KAMIGAITO O.: *Synthesis of nylon 6-clay hybrid*, *Journal of Materials Research*, vol. 8, p. 1179-1184, 1993
- [55] ALEXANDRE, M., DUBOIS, P.: *Polymer-layered silicate nanocomposites: preparation, properties and uses of a new class of materials*, *Materials Science and Engineering Report 28*, p.1–283, 2000
- [56] HITZKY, E.R., VAN MEERBEEK, A.: *Clay mineral and organoclay polymer nanocomposite*, *Handbook of Clay Science*, p. 583 - 621, 2006
- [57] SABU T., RANIMOL S.: *Rubber Nanocomposites: Preparation, Properties and Applications*, John Wiley and sons, 2010, ISBN 978-0-470-85345-3
- [58] LIANG, Y, WANG, Y., WU, Y., LU, Y., ZHANG, H., ZHANG, L.: *Preparation and properties of isobutylene–isoprene rubber (IIR)/clay nanocomposites*, *Polymer Testing 24*, p. 12-17, 2005
- [59] WANGA, Z.F., WANGA, B., QIA, N., ZHANGB, H.F., ZHANGB, L.Q.: *Influence of fillers on free volume and gas barrier properties in styrene-butadiene rubber studied by positrons*, *Polymer* vol. 46, issue 3, 2005, p. 719-724, 2005
- [60] BHOWMICK, A.; MADHUCHHANDA; SADHU, SUSMITA: *Brominated poly(isobutylene-co-para-methylstyrene) (BIMS)-clay nanocomposites: Synthesis and characterization*, *Journal of Polymer Science, Part B: Polymer Physics*, 2004, 42, (24), 4489
- [61] BEYER G.: *Nanocomposites as a new concept for flame retardancy of polymers*, presentation IRC 2005, Maastricht
- [62] KONEČNÝ P.: *Vlastnosti a chování kaučukových kompozitů s vrstevnými silikáty*, disertační práce, FT UTB, Zlín, 2007
- [63] BHARADWAJ RK.: *Modeling the barrier properties of polymer-layered silicate nanocomposites*, *Macromolecules* 2001; 34: p. 9189–92
- [64] ZHANGA, Y., LIUB, Q., ZHANGA, Q., LUA, Y.: *Gas barrier properties of natural rubber/kaolin composites prepared by melt blending*, *Applied Clay Science*, vol. 50, issue 2, October 2010, p. 255-259

- [65] LIANG, Y, CAO, W., LI, Z. et al.: *A new strategy to improve the gas barrier property of isobutylene–isoprene rubber/clay nanocomposites*, Polymer Testing 27, vol. 3, p. 270–276, 2008
- [66] STEPHEN, R., VARGHESE, S., JOSEPH, K., et al.: *Diffusion and transport through nanocomposites of natural rubber (NR), carboxylated styrene butadiene rubber (XSBR) and their blends*, Journal of Membrane Science 282, p. 162–170, 2006
- [67] TAKAHASHI, S., GOLDBERG, A., FEENEY, C.A. et al.: *Gas barrier properties of butyl rubber/vermiculite nanocomposite coatings*, Polymer 47, p. 3083–3093, 2006
- [68] KATO, M., USUKI, A., HASEGAWA, N., OKAMOTO, H., KAWASUMI, M.: *Development and applications of polyolefin– and rubber–clay nanocomposites*, Polymer Journal 43, p. 583-593, 2011
- [69] YANG, X., GIESE, U., SCHUSTER, R.H.: *Characterization of Permeability of Elastomers Part I HNBR*, Presentation at the Forschungsprojekte-Präsentationstag der DKG, 2008 in Fulda (Germany)
- [70] PHILIP CH YU: *Refrigerant Selection for Sustainable Future*, ASHRAE journal, p. 22-26, 2007 – 2008
- [71] NEUDER, CH., JANNICK, P.: *Material compatibility of elastomers with HFC- and HCFC-based refrigerants*, Solvay Flour und Derivate GmbH, product bulletin no. I/08.01/16/E, 1999
- [72] DICK, J., COUSINS, W.: *Effective Processability Measurements of Acrylonitrile Butadiene Rubber Using Rubber Process Analyzer Tests and Mooney Stress Relaxation*, Meeting of Rubber Division, American Chemical Society, Cleveland, 1997
- [73] *Die configuration of RPA 2000* [online]. [quot. 2013-17-07] < <http://www.alpha-technologies.com/rubber-process-analyzer-rpa-2000-dynamic-mechanical-rheological-tester>>
- [74] COMMISSION REGULATION (EC) No 706/2007 - laying down, pursuant to Directive 2006/40/EC of the European Parliament and of the Council, administrative provisions for the EC type-approval of vehicles, and a harmonised test for measuring leakages from certain air conditioning systems, 21 June 2007
- [75] PARKER HANNIFIN GmbH: Precision O-ring handbook, Catalogue 5705 E, 1997
- [76] D. V. BAGESHWAR, A. S. PAWAR, V. V. KHANVILKAR: *Photoacoustic Spectroscopy and its Applications*, Eurasian J. Anal. Chem. 5(2): p. 187-203, 2010

- [77] CZYŽ, P.: *Technická podpora měření úniků z klimatizačních komponent AC systémů*, bakalářská práce, VŠB - Technická univerzita Ostrava, Fakulta strojní, 2008
- [78] *Rentgenová spektroskopie a difrakce* [online]. [quot. 2013-28-06] <[http://physics.mff.cuni.cz/vyuka/zfp/txt\\_421.pdf](http://physics.mff.cuni.cz/vyuka/zfp/txt_421.pdf)>
- [79] *The Transmission Electron Microscope* [online]. [quot. 2013-28-06] <<http://www.nobelprize.org/educational/physics/microscopes/tem/index.html>>
- [80] CORISH, P. J.: *Concise Encyclopedia of Polymer Processing & Application*. Oxford: Pergamon Press, 1992, ISBN 0080370640
- [81] YANO, K., USUKI, A., OKADA, A.: *Synthesis and properties of polyimide-clay hybrid films*, Journal of Polymer Science: Part A: Polymer Chemistry 35, p. 2289–2294, 1997
- [82] LAN, T., KAVIRTANA, P.D., PINNAVAIA, T.J.: *On the Nature of Polyimide-Clay Hybrid Composites*, Chemical Materials 6, p. 573-575, 1994
- [83] MESSERSMITH, P.B., GIANNELIS, E.P.: *Synthesis and barrier properties of poly( $\epsilon$ -caprolactone)-layered silicate nanocomposites*, Journal of Polymer Science: Part A: Polymer Chemistry 33, p. 1047–1057, 1995
- [84] LUMASENSE TECHNOLOGIES: *Photoacoustic Multi-gas Monitor – INNOVA 1314*, P/N: 80-14502-02, 2007
- [85] WANG, M.: *The role of filler networking in dynamic properties of filled rubber*, Chemistry and technology 72, p. 430-448, 1999, Paper No. 48, Meeting of Rubber division, American chemical society, CRP-213-292, Indianapolis, 1998
- [86] PAYNE, A. R., WHITTAKER, R. E.: *Low Strain Dynamic Properties of Filled Rubbers*, Rubber Chemistry and Technology vol. 44, p. 440-478, 1971
- [87] PAYNE, A. R.: *The dynamic properties of carbon black-loaded natural rubber vulcanizates*, Journal of Applied Polymer Science, vol. 6, p. 57–63, 1962
- [88] PAYNE, A. R.: *The role of hysteresis in polymers*, Rubber Journal, 146, p. 36-49, 1964
- [89] Principles of Fourier Transfer Infrared Spectroscopy [online]. [quot. 2013-28-06] <[http://www.daham.org/basil/leedswww/ftir/ftir\\_principle.htm](http://www.daham.org/basil/leedswww/ftir/ftir_principle.htm)>

## **PUBLICATION**

### **Papers**

1. ZÁVORKA, Z, MALÁČ, J.: *Modification of Acrylonitrile-Butadiene Rubber Compound by nanoclay and silica*, 2013. Chemické listy 107, p. 200-202, 2013, ISSN 0009-2770.
2. ZÁVORKA, Z., MALÁČ, J., KALEDOVÁ, A.: *Nanoclay and Silica Modified Acrylonitrile-Butadiene Rubber Compounds with Improved Mechanical and Permeation Performance*, 2013. Submitted to Polymer Bulletin.
3. ZÁVORKA, Z, MALÁČ, J.: *Influence of silica to morphology of acrylonitrile-butadiene rubber / nanoclay nanocomposite*, in preparation.
4. ZÁVORKA, Z, MALÁČ, J.: *Influence of butadiene terpolymer to properties and behavior of acrylonitrile-butadiene rubber compound*, in preparation.

### **Poster**

1. ZÁVORKA, Z, MALÁČ, J.: *Modification of Acrylonitrile-Butadiene Rubber Compound by nanoclay and silica*, Slovak rubber conference, Bratislava, 2013

### **Supervisor of diploma work**

2. MENŠÍK, M: *Pryžová směs pro těsnící aplikace, diplomová práce*, UTB ve Zlíně, FT, UIP, 2010

## CURRICULUM VITAE

**First name:** Zdeněk  
**Surname:** Závorka  
**Academical degree:** Ing.  
**Date of birth:** November 17, 1975  
**Marital status:** married  
**Present address:** Dolní Bečva 552, 756 55  
**Telephone:** 604 656 427  
**E-mail:** [z.zavorka@seznam.cz](mailto:z.zavorka@seznam.cz)

### Education:

**University:** Technical University, Brno  
**Faculty:** Faculty of Technology, Zlin  
**Branch:** Technology and management  
**Specialization:** Rubber and plastic technology  
**Diploma work:** Study of properties of rubber compounds determining their electroconductivity

**Duration of study:** 1995 – 2000

**Post secondary study:** Private business school, Vsetín

**Trade:** Business  
**Specialization:** Management  
**Duration of study:** 1994 - 1995

**Secondary school:** Electrotechnical school, Rožnov pod Radhoštěm

**Trade:** Mechanic – electronic  
**Specialization:** Digital and control technology

**Duration of study:** 1990 – 1994

**Occupation:** May 2, 2002 till present  
Halla Visteon Autopal, s.r.o., Nový Jičín  
**Position:** Materials engineer (elastomers), Technical professional

September 1, 2000 – April 30, 2002

Gumárny Zubří, a.s.

**Position:** Technologist of rubber compounds